Chem Soc Rev

AIE Macromolecules: Syntheses, Structures and Functionalities

Journal:	*Chemical Society Reviews*
Manuscript ID:	CS-REV-01-2014-000044.R1
Article Type:	Review Article
Date Submitted by the Author:	07-Mar-2014
Complete List of Authors:	Hu, Rongrong; The Hong Kong University of Science and Technology, Chemistry Leung, Nelson; The Hong Kong University of Science and Technology, Chemistry Tang, Ben Zhong; The Hong Kong University of Science and Technology, Department of Chemistry

Journal Name

RSCPublishing

ARTICLE

AIE Macromolecules: Syntheses, Structures and Functionalities

Cite this: DOI: 10.1039/x0xx00000x

Rongrong Hu,[ab] Nelson L. C. Leung[b] and Ben Zhong Tang*[abc]

Received 00th January 2012,
Accepted 00th January 2012

DOI: 10.1039/x0xx00000x

www.rsc.org/

Macromolecules with aggregation-induced emission (AIE) attributes are a class of luminescent materials that display enhanced emission when they are aggregated. They have attracted much attention because of their good solubility, processability, high emission efficiency in the aggregated states, etc. A large variety of AIE macromolecules have been developed, showing exponential growth of research interest in this field. This review summarizes the design principles and recent synthetic advancements, topological structures, as well as the frontiers of functionalities and potential applications of AIE macromolecules, especially fluorescent sensing, biological and optoelectronic applications, with the emphasis on the recent progress. New luminogenic systems without conventional chromophores displaying aggregated state emission are discussed. The highly dense clusters of heteroatoms with lone pair electrons in these systems may serve as the chromophore and are cited as "heterodox clusters". It is expected that the mechanistic insights into the AIE phenomena, based on the restriction of intramolecular motions and structure rigidification, can guide the future design of AIE materials with fascinating structures and functionalities.

1. Introduction

Luminescent materials with great fundamental and technological implications represent a rapidly developing area and have attracted great academic and industrial interest.[1] Most of the fundamental studies of luminescent materials are conducted in solutions with considerable intermolecular interactions with solvent molecules, but minimal interactions between the dyes.[2] However, in real cases, the dyes are often utilized in the aggregated states with intimate contact among themselves. For example, the hydrophobic luminogens for chemosensors and biological applications are used in aqueous media and materials made for devices are used in their solid states.[3] The study of aggregated state emission of the luminescent materials is thus of great fundamental importance. Just as significant are their numerous potential applications such as fluorescent chemo/biosensors,[4] bio-imaging,[5] organic light-emitting diodes (OLEDs),[6] as well as other optoelectronic devices.[7]

Generally, aggregation of luminophores will lead to two different effects on photoluminescence (PL): aggregation-caused quenching (ACQ) and aggregation-induced emission (AIE).[8] The ACQ and AIE effect will compete in most luminogens, depending on the molecular structures as well as the intermolecular packing. For example, the *J*-aggregate is widely studied among various aggregates as its highly ordered intermolecular packing results in enhanced emission with both red-shifted absorption and emission.[9] When aggregation plays a destructive role in the luminescence, it's called ACQ with a typical example of *N*,*N*-dicyclohexyl-1,7-dibromo-3,4,9,10-perylenetetracarboxylic diimide (DDPD).[10] As shown in Fig. 1A, the dye emits brightly in the THF solution. When its poor solvent, water, is added, the hydrophobic dyes tend to aggregate which dramatically quenches the fluorescence. The ACQ effect has been a great obstacle to the development of the luminescent materials and has limited the application scope of the materials. A large number of endeavours have been devoted to mitigate this harmful effect to luminescence.[11] On the other hand, AIE provides a constructive effect on luminescence.[12] Fig. 1B shows the typical AIE phenomenon of hexaphenylsilole (HPS): in its THF solution, it's completely non-emissive, but when it aggregates due to the addition of water, its poor solvent, the emission dramatically increases and becomes bright after a large amount of water has been added. With their high emission quantum efficiency in the aggregated state, AIE materials provide a promising solution to the obstacles in this field. One typical difference between ACQ and AIE systems is that the former generally possesses large conjugated coplanar molecular structures which result in strong intermolecular interactions such as π–π stacking interactions, while the latter possess twisted propeller-shaped molecular structures. In the aggregate state, ACQ dyes normally experience red-shifted and weakened emission, while emission intensity of the AIE dyes is greatly boosted without significantly shifted emission.

In the recent decade, many scientists all over the world have been working in the area since the report of AIE phenomenon.[13] Thanks to their enthusiastic research, a large variety of AIE molecules has been developed with great structural diversity.[14] Luminogens with AIE characteristics, referred to "AIEgen" in this review, share the common feature of propeller-shaped structures and free-rotatable periphery aromatic moieties. A few typical examples such as tetraphenylethene (TPE), hexaphenylsilole (HPS) and distyreneanthracene (DSA) are shown in Chart 1.

Mechanistic studies suggest that in the solution, the free rotations of such periphery phenyl rings consume the excited state energy by nonradiative decay, thus quenching the emission.[15] In other words, energy loss of the excited state is related to structural flexibility. When the molecules are aggregated, such free rotations are hindered because of the short distances among the crowded molecules. The nonradiative energy consuming pathway is thus blocked and strong emission is vitalized. The fluorescent enhancement from the solution state to the aggregated state is defined by the AIE factor (α_{AIE}): $\alpha_{AIE,I} = I_{aggr}/I_{soln}$, or $\alpha_{AIE,\Phi} = \Phi_{aggr}/\Phi_{soln}$, where I_{aggr} and I_{soln} are the fluorescence intensity of the aggregates and solution, and Φ_{aggr} and

Φ_{soln} are the fluorescence quantum efficiency of the aggregates and solution, respectively. The α_{AIE} values can be as large as several thousand, depending on the structures of AIE dyes, allowing us to compare the fluorescence enhancement of each dye. When the AIEgens were incorporated into the polymer chains, the long-chain segments of AIE polymers should inherently impose steric hindrance on the free rotation of the embedded luminogenic units. As such, molecular rotations are more easily restricted in polymer systems than in small molecules, resulting in a relatively more emissive solution state for the polymers.[16] Based on the principles of restriction of intramolecular motions (RIMs) and the structural rigidification (SR), AIE systems have been designed and developed. As a result of their unique fluorescent behaviours in the aggregated states, these luminescent materials are utilized in various different practical applications such as fluorescent sensing, bio-imaging, and optical devices.[17] Several review papers have summarized the development of AIE materials in the past decade with the emphasis on the structure, mechanism and application point of view.[18]

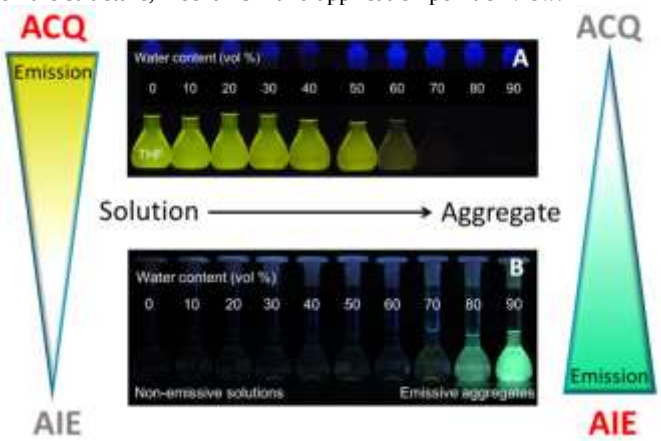

Fig. 1 Fluorescence photographs of solutions/suspensions of (A) DDPD and (B) HPS in THF/water mixtures with different water contents. Adapted with permission from Ref. 10. Copyright 2011 The Royal Society of Chemistry.

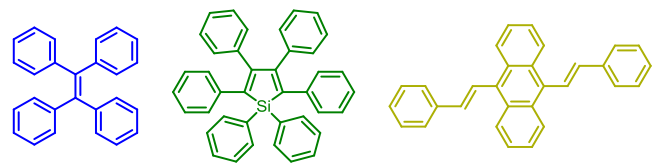

Chart 1 Typical AIE luminogens TPE, HPS and DSA.

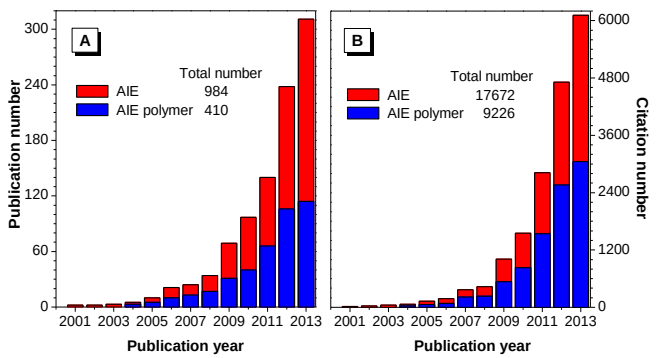

Fig. 2 Histograms showing the annual numbers of publications and citations on the topic of "aggregation-induced emission" and "aggregation-induced emission polymer" from 2001 to present (data obtained from Web of Science on 6 January 2014).

Much progress has been achieved regarding small molecular AIE dyes. On the other hand, AIE polymers and other macromolecules have been less explored.[19] In fact, polymer materials have many advantages over small molecule materials. There are numerous opportunities to tune the polymer structure, topology and morphology, as well as functionalities which are difficult to achieve in small molecule materials.[20] Hence, it provides a much larger platform for material manipulation. Up to date, many polymers possessing AIE characteristics have been reported, such as polyacetylenes, polyphenylenes, polytriazoles, and poly(phenyleneethylene)s.[21] Recently, even non-conjugated nitrogen/oxygen-rich polymers with multiple lone pair electrons were also found to be AIE-active. By combining the AIE property with polymer characteristic, attractive materials can be generated with unique properties. For example, in conjugated AIE polymer systems, the molecules have extended exciton transfer pathways, thus resulting in high sensitivity upon fluorescent sensing process. Furthermore, owing to their unique structures, the AIE characteristic can combine with those polymer properties to give emission response towards external stimuli such as light, heat, chemicals, etc.[22] They also possess good processability and can be fabricated into large-area thin solid films and devices by simple, cheap, energy saving processes which greatly simplify the fabrication of optical devices. With the advantages endowed by the polymer behaviours, it is an exciting area to explore AIE macromolecules with their potential applications and a few review papers have summarized the early progress of AIE polymers.[23]

Research interests are exponentially growing in this young field as shown in Fig. 2. In this review, we will summarize most of the research efforts directed to AIE macromolecules with the emphasis on the most up to date progress. The review will cover the design and syntheses, structures and topologies, as well as functionalities and applications of AIE macromolecules. AIE polymers with AIEgens in the side-chains, main-chains, polymer centres/terminals are synthesized by various chain and step polymerizations. Thanks to the enthusiastic devotion of scientists all over the world, a large variety of AIE polymers with linear and nonlinear structures have been prepared. Mechanistic insights into the RIMs and SR of the molecular structures will be discussed in some typical examples. New luminogenic systems based on "heterodox clusters" (HC) have been introduced as nonconventional luminogens.[24] Last but not least, AIE macromolecules show various valuable properties and have found a series of high-tech applications. From the discussion of this review, we hope to gain more insight for design strategy and structural-property relationship of AIE macromolecules to guide future work in this field.

2. Design and syntheses

AIE macromolecules can be constructed through various synthetic strategies. The core principle is to incorporate typical AIEgens, such as TPE, HPS and DSA, into the polymer structures. Scheme 1 illustrates the typical methods. Firstly, directly linking the AIEgen-containing monomers (Scheme 1A) or copolymerizing AIEgens with other monomers (Scheme 1B) can both generate AIE polymers with AIEgens embedded in the polymer main chain. AIE-inactive precursors can also polymerize and react to generate AIEgen core structures in the polymer main chain (Scheme 1C). In addition, AIEgens can also be attached on the polymer as side chains. In Scheme 1D and 1E, an AIEgen was attached on a polymerizable monomer, which then undergoes homopolymerization or copolymerization to afford linear polymers with AIEgens as side chains. Another interesting design is to use AIEgen-containing

initiators to initiate a polymerization and result in linear polymers with AIEgens on the terminal of the polymers (Scheme 1F).

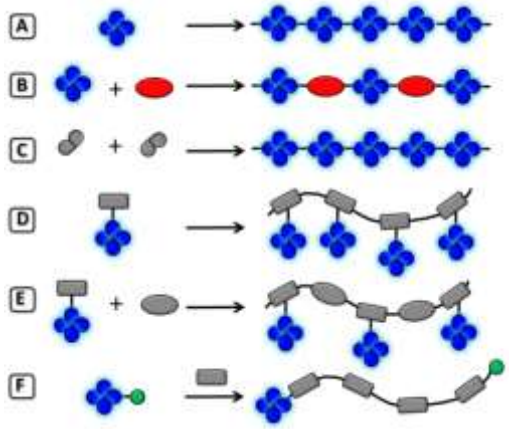

Scheme 1 Polymerization strategies towards AIE polymers.

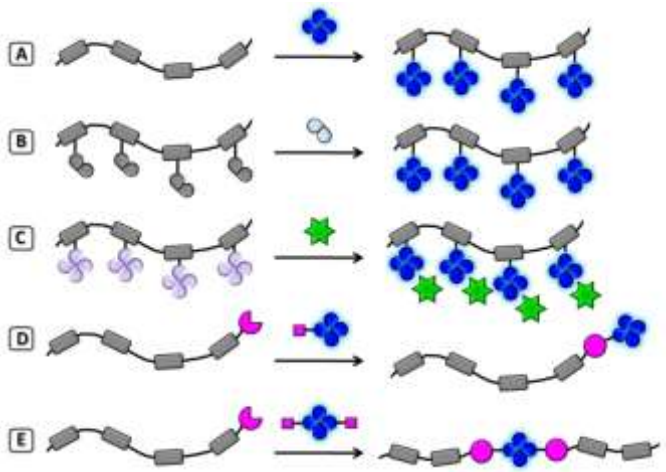

Scheme 2 Polymer reaction strategies towards AIE polymers.

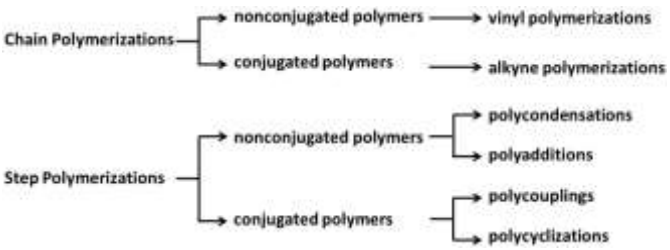

Scheme 3 Synthetic methods for the construction of AIE polymers.

Besides direct polymerizations, AIE-inactive polymers can also be modified to generate AIE polymers through polymer reactions. One method is to directly attach AIEgens to the polymers (Scheme 2A). An alternative way is to construct new AIEgens directly through polymer reactions of AIE-inactive polymers and small molecular precursors (Scheme 2B). There are also reports that show AIE-inactive polymers becoming AIE polymers through interactions with bulky compounds (Scheme 2C). The free rotations of the fluorophores can be controlled by adding bulky additives. Furthermore, if the polymer has functional groups on the end, it can directly react with AIEgens with one or two reaction sites to generate AIE polymers with AIEgen on the terminal or the centre of the polymer, respectively (Scheme 2D and 2E). Although only examples for linear polymers are shown here for simplicity, such strategies can also be applied to nonlinear polymers.

Various polymerization reactions have been adopted to realize the aforementioned strategies as shown in Scheme 3. The two main categories of the polymerization methods used to prepare AIE polymers are chain polymerizations and step polymerizations. Under each category, nonconjugated and conjugated AIE polymers are synthesized through different polymerization reactions. For example, vinyl polymerizations, including homopolymerization, copolymerization, and polymer reactions have been adopted to furnish nonconjugated AIE-active vinyl polymers. Alkyne polymerizations are used to construct conjugated AIE-active polyacetylenes. Through chain polymerizations, polymers with AIEgens attached on the side chains are obtained. On the other hand, step polymerizations are more widely adopted to construct AIE polymers with AIEgens built onto the polymer main chains. For instance, polycondensations and polyadditions are used to synthesize nonconjugated polymers, while polycouplings and polycyclizations are utilized to synthesize conjugated polymers. In this part, each of the synthetic approaches in Scheme 3 as well as the AIE property of the polymers will be discussed.

2.1 Free radical polymerization

Free radical initiated chain polymerization was used to transfer AIE-active alkene monomers to polymers bearing AIEgens on their side chains. For example, an AIE-active polyethene **2** was obtained by radical polymerization initiated with azobisisobutyronitrile (AIBN) from carbazolyl-substituted triphenylethene-containing AIE-active monomer **1** (Scheme 4A).[25] Although polymer **2** contains many rigid aromatic rings, it still shows excellent solubility in common organic solvents such as dichloromethane, toluene, THF, etc. Meanwhile, it has high thermal stability with 5% weight loss temperature of 467 ^{o}C. The emission maximum of the solution and solid state of **2** is 466 and 482 nm, respectively. In a THF/water mixed solvent system, the emission intensity gradually increases with increasing water content. Later, Dong et. al. reported an AIE-active styrene derivative **3** with a phosphaphenanthrene side-group.[26] The free-radical polymerization of **3** initiated by AIBN was carried out for 12 h in THF solution to obtain **4** in 80% yield (Scheme 4B). Both solutions of **3** and **4** possess an emission maximum at 355 nm. However, the intramolecular rotation of phosphaphenanthrene groups in **4** is restricted by the polymer chain to some extent, its emission intensity in solution is 4.2 times as much as that of the monomer. When more than 70 vol % water, a poor solvent of the polymer, was added to the THF solution of **4**, the hydrogen bonding among a water molecule and two phosphaphenanthrene groups greatly restrict the intramolecular rotation of the polymer. A new shoulder at 450 nm emerges and the PL intensity increases with more water content, suggesting AIE characteristic.

The atom transfer radical polymerization (ATRP) technique was also used to prepare AIE polymers. Lu et. al. reported that pyrazoline-containing monomer **5** with a diethylamino electron donor and a 1,8-naphthalimide electron acceptor was polymerized by ATRP using the CuBr/*N*,*N*,*N*',*N*'',*N*''-pentamethyldiethylene-triamine (PMDETA) catalytic system to afford polymer **6** (Scheme 5).[27] The emission maximum of **6** in THF solution is 551 nm. When ethanol was added as a poor solvent, λ_{em} was red-shifted and the PL intensity decreased with the increase of ethanol fraction from 0 to 50 vol %. This can be attributed to the intramolecular charge transfer (ICT) effect caused by increased solvent polarity. The emission was then revitalized when a large amount of ethanol (> 60 vol %) was added, owing to the restriction of rotations and the rigidified chain segments. The PL intensity of **6** in the THF/ethanol mixture with 99 vol % ethanol is 2.83-fold higher than that of THF solution. In a similar DMF/ethanol mixture, the PL enhancement is 4.12-fold.

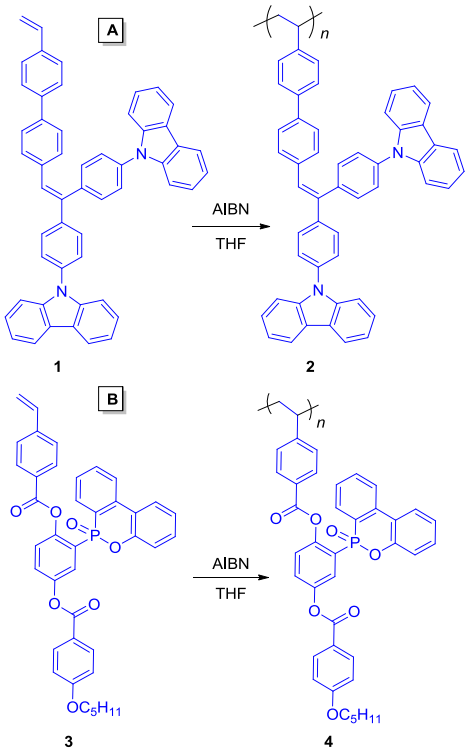

Scheme 4 Synthetic routes of (A) carbazolyl triphenylethene-containing polystyrene **2** and (B) phosphaphenanthrene-containing polystyrene **4** through free radical polymerization.

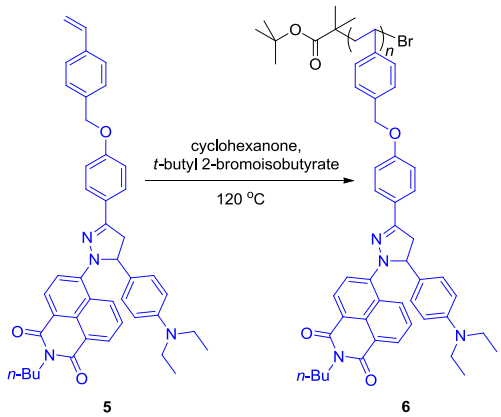

Scheme 5 Synthetic route of polymer **6** through ATRP.

Another design from the same group is to use an AIE-active initiator for ATRP to prepare AIE polymers.[28] An ICT and AIE dual active initiator **7** with pyrazoline, 1,8-naphthalimide and dimethylamino moieties was designed and synthesized. When **7** was used as an ATRP initiator, typical vinyl monomers such as styrene **8**, methyl methacrylate **9**, and 2-hydroxylethyl methacrylate **10** can be polymerized under moderate conditions to afford polymers **11**–**13** (Scheme 6). In pure DMF solutions, both **11** and **12** emitted weakly at about 545 nm, while DMF solution of **13** exhibited a weak emission at 570 nm which was similar to that of the initiator **7**. The fluorescent enhancement after aggregation is 155- (**11**), 65- (**12**), and 10-fold (**13**), respectively. Acidification of the DMF/water mixture of **13** further increases the PL intensity about 7-fold.

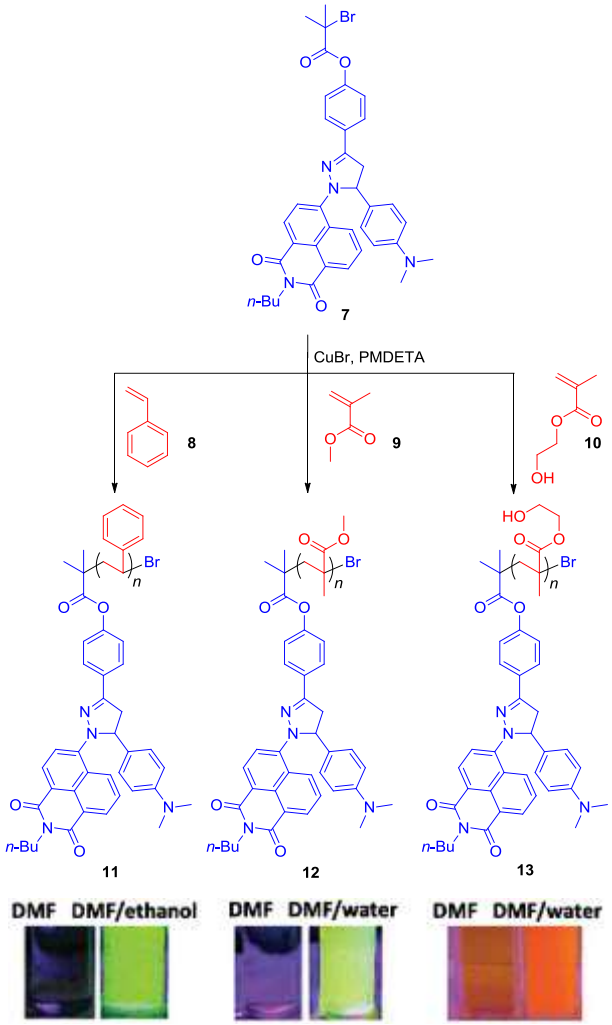

Scheme 6 Synthetic routes of polymers **11–13** through AIEgen-containing dye-initiated ATRP and their fluorescence photographs of solutions and aggregates. Adapted with permission from Ref. 28. Copyright 2012 The Royal Society of Chemistry.

2.2 Copolymerization

Copolymerization of vinyl monomers with AIEgens is a popular method to integrate multiple building blocks and various functionalities into a single AIE polymer. For example, a poly(*N*-isopropylacrylamide) (PNIPAM) **16** labelled with a TPE fluorogen was achieved by direct copolymerization of monomer **14** and **15** through AIBN-initiated free radical polymerization (Scheme 7A).[29] Since the TPE fluorogen is a sensitive AIEgen, incorporating a small amount of AIEgen is effective to turn PNIPAM into an AIE polymer while maintaining the original properties of PNIPAM. The labelling degree of AIEgen in polymer **16** is small and can be tuned from 0.27% to 1.12%. The TPE label served as a fluorogenic probe that reveals fine details of the thermal transitions in the aqueous solution of the polymer. By tuning the labelling degree of the polymer, the working mode was readily changed between non-monotonic and monotonic.

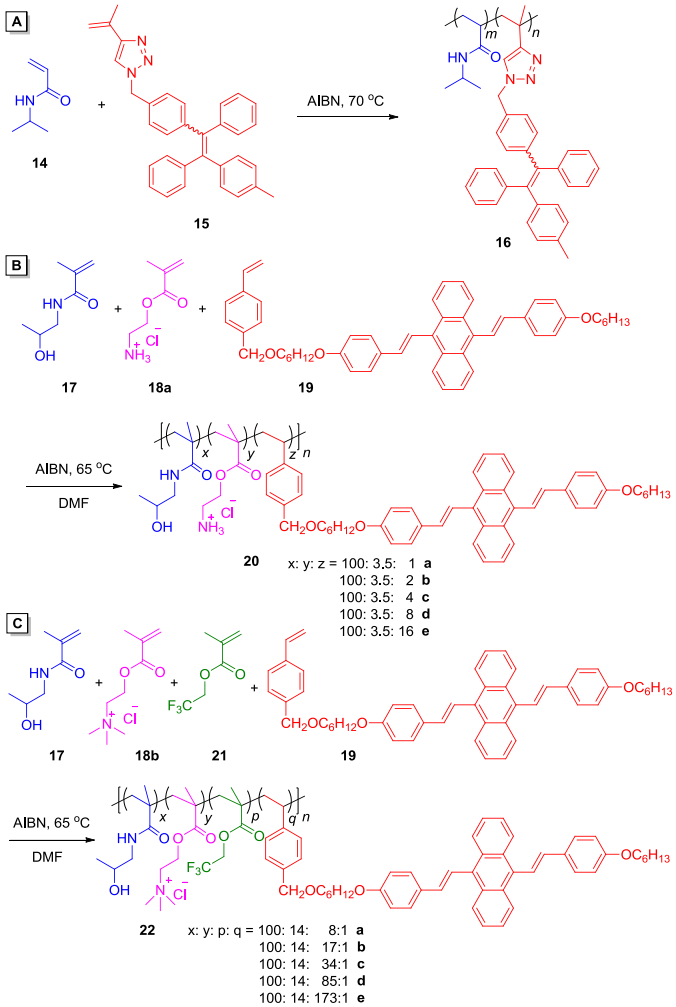

Scheme 7 Synthetic routes of AIEgen-containing amphiphilic copolymers through free radical copolymerization.

Multicomponent copolymerization has also been reported to construct AIE polymers with multiple building blocks as well as functionalities. A series of poly[*N*-(2-hydroxypropyl)methacrylamide]-based amphiphilic random copolymers **20a–e** were synthesized through a radical copolymerization (Scheme 7B).[30] A hydrophobic monomer **19** possessing AIEgen was used to copolymerize with *N*-(2-hydroxypropyl)methacrylamide (HPMA) **17** and 2-aminoethyl methacrylate (AEMA) **18a** under the normal radical polymerization condition at 65 °C for 20 hours using AIBN as a thermal initiator to form a series of copolymers. Besides AIE-active monomer **19**, **17** is chosen because poly[*N*-(2-hydroxypropyl) methacrylamide] (PHPMA) is a non-toxic biopolymer and has been widely used for drug delivery. Furthermore, by incorporating positively charged monomer **18**, cellular uptake of the polymers can be enhanced. The molar ratio of **17** to **18** was fixed at 100:3.5 and the influence of molar ratio of **19** on the photophysical properties was investigated by tuning the molar ratio of **19** to the sum of **17** and **18**, from 1:103.5 to 16:103.5. The increase of the molar fractions of **19** results in higher quantum efficiencies of the AIE copolymers. The DMSO solution of **20c** has almost no emission with quantum efficiency Φ_F of 0.08%, while the Φ_F of **20c** in DMSO/water (2:98 v/v) increased to 7.9%, which is 98-fold higher than that of the DMSO solution. These amphiphilic polymers were confirmed to form small micelles with average diameters of around 10 nm in their aqueous solutions.

The hydrophobic environment in the copolymers can facilitate the aggregation of the AIEgens to achieve high Φ_F, thus an additional hydrophobic monomer 2,2,2-trifluoroethyl methacrylate (TFEMA) **21** was incorporated into this copolymerization to synthesize amphiphilic copolymers **22a–e** through four-component copolymerization of **17**, [2-(methacryloyloxy)ethyl]trimethyl-ammonium chloride (MATMA) **18b**, **21** and AIE-active monomer **19** (Scheme 7C).[31] AIBN was used as an initiator for the free radical polymerization to obtain four-component random copolymers **22a–e** through a fixed molar ratio of **17, 18b** and **19** while only tuning **21**. As an example, the emission spectra of **22d** in DMSO had a weak emission at 520 nm with a Φ_F of 0.02%, while the Φ_F of its DMSO/H_2O (2:98 v/v) suspension increased to 38%, which is 1900 times as much as that in pure DMSO. The increase of the molar ratios of the hydrophobic monomers **19** and **21** results in high Φ_F of up to 40% in the aqueous solutions.

Amphiphilic block copolymers with AIE characteristics can be prepared through ATRP as well. For example, the amphiphilic diblock copolymers **25a-c** were obtained by ATRP of styrene **8** and pentaphenyl-substituted silole-containing monomer **24** simultaneously via using α-(2-bromo-2-methylpropoyloxy)]-poly(ethylene glycol) **23** as a macroinitiator and CuBr/PMDETA as catalysts (Scheme 8A).[32] By tuning the feeding molar ratio of AIE monomer **24** to macroinitiator **23**, copolymers **25a–c** with different pentaphenylsilole compositions (weight fractions of 3%, 6%, and 17%, respectively) were prepared. The amphiphilic block copolymers can self-assemble to form fluorescent micelles which show uniform nanostructure and AIE feature. The THF solutions of **25a–c** showed almost no emission, while intense fluorescence was observed from the self-assembled micelles of **25a–c** with the emission peak at 503 nm. Typically, the fluorescence Φ_F of the micelles of **25b** are up to 13.8%, which is attributed to the hydrophobic core of the micelles that shield AIEgens from interacting with polar solvent molecules.

Similarly, reversible addition fragmentation chain transfer polymerization (RAFT) method was adopted to prepare AIE copolymers. Copolymerization of **26** with the equivalent amount of styrene **8** led to the random polymer **27** by using EDMAT and AIBN as the free chain transfer agent and the radical initiator, respectively (Scheme 8B).[33] Further copolymerization of **27** with 150 equiv. of 4-vinylpyridine **28** yielded polymer **29** by employing a similar RAFT approach. The block amphiphilic copolymer **30** was then obtained by reaction of polymer **29** with excess amount of iodomethane in DMSO. According to the ^{1}H NMR result, the average numbers of styrene, TPE, 4-vinylpyridine and methylated 4-vinylpyridine moieties in copolymer **30** were estimated to be 15, 15, 28, and 102, respectively. The amphiphilic polymer can self-assemble to form fluorescent micelles by slow addition of deionized water into the DMF solution of **30** under vigorous stirring and dialyzing for 72 hours. The DMF solution and DMSO/H_2O (5: 95 v/v) mixtures are only weakly emissive, however, the fluorescent intensity of the polymeric micelles in aqueous solution at 480 nm was 4 times as much as that in DMSO/H_2O mixtures. The TPE moieties in the hydrophobic core of the micelles of **30** aggregate and restrict the intramolecular free rotation more than in DMF solution and DMSO/H_2O mixtures, thus causing the micelles to have a stronger emission with a Φ_F of 12%.

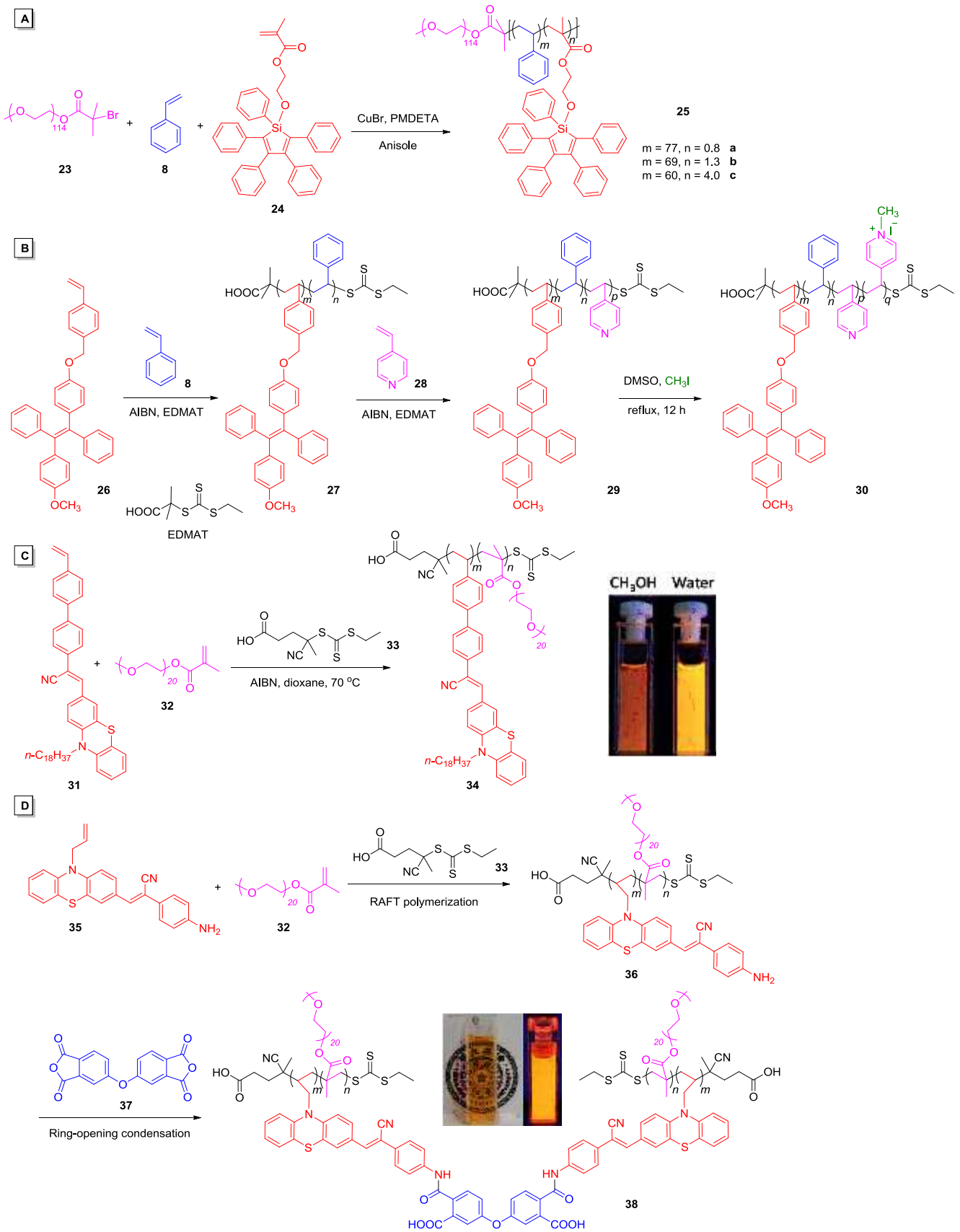

Scheme 8 Synthetic routes of polymers **25a–c**, **30**, **34**, and **38** through ATRP or RAFT copolymerizations. Insets: (C) methanol and water solutions of **34** and (D) **38** in water under daylight and UV irradiation, respectively. Adapted with permission from Ref. 34 and 35. Copyright 2014 The Royal Society of Chemistry.

The AIE polymer **34** was prepared via a RAFT polymerization method using a polymerizable AIE dye **31** and hydrophilic macromolecule **32** as monomers with a feed molar ratio of 1:10 (Scheme 8C).[34] The hydrophobic nature of **31** and hydrophilic nature of **32** enable polymer **34** to form fluorescent organic nanoparticles with uniform size. The hydrophobic region aggregates and serves as the core, leading to strong fluorescence, while the polyethylene glycol segments cover the core as a hydrophilic shell, resulting in high water dispersibility and excellent biocompatibility. The emission peak of **34** in water is located at 582 nm and it red-shifted to 597 nm when the polymer was dispersed in methanol which is a good solvent for **31** (Scheme 8C, inset photo). The possible reason for such bathochromic shift is reported that two different kinds of nanoparticles, crystal particles and amorphous particles, could have formed in water and methanol, respectively. Moreover, the fluorescent intensity of **34** in water is about 3 times of that in methanol. Similarly, another hydrophobic AIE dye **35** with vinyl and amino end-groups was copolymerized with hydrophilic monomer **32** via RAFT polymerization to afford copolymer **36** with the ratio of **35** to **32** at 1:9.[35] Polymer **36** then underwent subsequent room temperature ring-opening condensation with 4,4'-oxydiphthalic anhydride **37** in air to furnish the targeted cross-linked amphiphilic copolymer **38**. As shown in the inset photo of Scheme 8D, strong orange fluorescence was observed from the nanoparticles of **38** in water and the emission maximum is located at 552 nm. In addition to the strong fluorescence, the nanoparticles also possess uniform size, high water dispersibility, and excellent biocompatibility.

2.3 Post-functionalization

The existing macromolecules can be modified through polymer reactions as another strategy to achieve AIE polymers as discussed in Scheme 2. Two commonly adopted approaches are introduced here as examples: one is to construct AIEgens in situ via polymer reactions, another is to attach AIEgens onto the polymers as side chains.

For instance, poly(4-acetyl styrene) **39** and 2-aminobenzophenone **40** can undergo Friedländer condensation to afford polymer **41** with quinoline moiety (Scheme 9A).[36] The THF solution of **41** is weakly emissive at 400 nm with a Φ_F of 2.1%, which increased to 3.7% in THF/H_2O (1:9 v/v) mixtures. Complexing bulky camphorsulfonic acid (CSA) to the quinoline moieties of **41** can further hinder the intramolecular motions, in particular, the free rotations of the aromatic rings. As such, equivalent mol of CSA, relative to the repeating units of **41**, was reacted with **41** to obtain **42**. When compared to **41**, the inherently hampered molecular rotations of **42** result in enhanced emissions at 500 nm with a Φ_F of 11.6%, which further increased to 38.1% in 90% aqueous mixtures. Analysis of the solid state Φ_F values of **41** (4.3%) and **42** (66.7%) provides additional evidence that CSA complexation enlarges Φ_F in such structures. As well, by lowering the temperature, both the molecular rotations of **41** and **42** are further restricted, thus enhancing emission. This work demonstrates that the addition of poor solvent, complexation with CSA and reducing the temperature are three effective approaches to enhance fluorescence of AIE polymers.

In another work, amino-containing TPE derivative **44** was directly linked onto poly(acrylic acid) (PAA) **43** through amidation to obtain partially substituted PAA polymer **45** (Scheme 9B).[37] The acid functional groups and hydrophobic TPE pendants of **45** endow the polymer pH-responsiveness and AIE features, respectively.

A similar strategy was adopted to prepare amphiphilic AIE polymer with multiple components through the quaternization reactions (Scheme 9C).[38] Cholesterol derivative **48** was first reacted with a toluene solution of poly(*N*-methyldietheneamine sebacate) **46**. Benzyl bromide TPE derivative **47** was then added to obtain polymer **49**. The DMF solution of **49** is non-emissive. With addition of water into the solution, an intense PL peak centred at 480 nm was recorded and the emission continuously intensified with gradual addition of water, which suggests the AIE nature of **49**. The polymer chains aggregate into particles in the aqueous mixtures and the sizes of the aggregates are tunable with the diameter ranges from 2 μm to 50 nm.

As the Click reaction is another popular method to modify polymers, it has also been used to functionalize them with AIE characteristics. A phosphaphenanthrene-containing 4-ethynylbenzonate grafted glycidyl azide polymer **52** was prepared by alkyne-azide click reaction between azide-containing polymer **50** and AIE-active precursor **51** using CuI as catalyst (Scheme 10A).[39] When the molecules of **52** aggregate in dichloromethane/hexane mixtures, the emission intensity increases. When the hexane fraction is < 70 vol %, the emission intensity at 368 nm rises with increasing hexane content. At the same time, a new PL peak appeared at 428 nm, which enhanced with increasing hexane content as well. When hexane fraction reaches 90%, both emission peaks blue-shifted and the PL intensity increased about 2.8- and 4.8-fold, respectively. The aggregate state of **52** based on the π–π stacking and polarity interaction of the molecules restricts the intramolecular rotation of phosphaphenanthrene groups and exhibits AIE property.

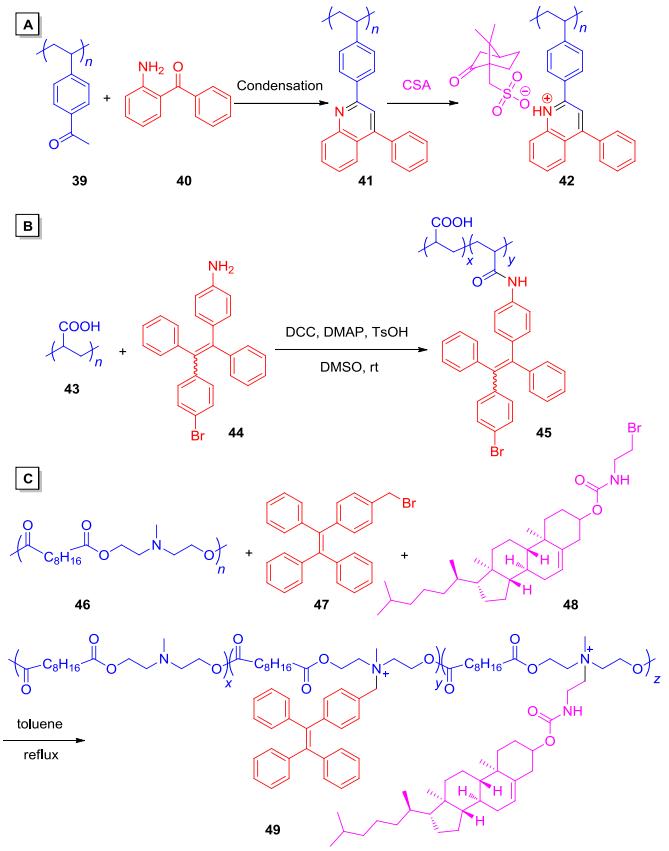

Scheme 9 Synthetic routes of polymers **42**, **45,** and **49** through polymer reactions.

The same strategy was used to prepare the vinyl polymers **55a** (M_w = 37 300) and **55b** (M_w = 525 400) with 2,4,6-triphenylpyridine pendant groups through reaction between the azide-functionalized **54** and the polymeric precursor **53** with acetylene pendant groups (Scheme 10B).[40] As shown in the inset photos, compound **54** is typical AIE-active: the THF solution does not emit, while the

THF/water mixture (1:9 v/v) shows blue emission. The solution of **55a** with relatively small Mw and short polymer chain shows weak emission, which gradually gains emission intensity when the water fraction (f_w) in the mixed solvents is increased. The fluorescent enhancement can be verified from the Φ_F enhancement (25–78%) of the aqueous mixtures with increasing f_w value of **55a**. Furthermore, a large extent of aggregation on the solid of **55a** led to an even higher Φ_F of 84%. The high M_w analogue **55b** with a relatively longer polymer chain, however, behaves differently. The THF solution is quite emissive and only a slight emission difference is observed among the aqueous mixtures with f_w of 0–60 vol %. The emission spectrum of the solid resembles that of the solution, indicating that the extent of aggregation in the aqueous suspensions and the solid are very similar. Indeed, the Φ_F of the aggregated states and the solid state of **55b** are both in the range of 82 to 84%. Moreover, little difference exists between the solid samples of **55a** and **55b**. Decreasing the temperature to −108 °C enhanced the PL intensity of **55a**. In contrast, **55b** does not experience any enhancement, because the long polymer chains of **55b** at room temperature already impose high energy barriers for the molecular rotations of the pendant triphenylpyridine fluorophores. Therefore, cooling does not have much effect on the rotational energy barrier or the emission of **55b**.

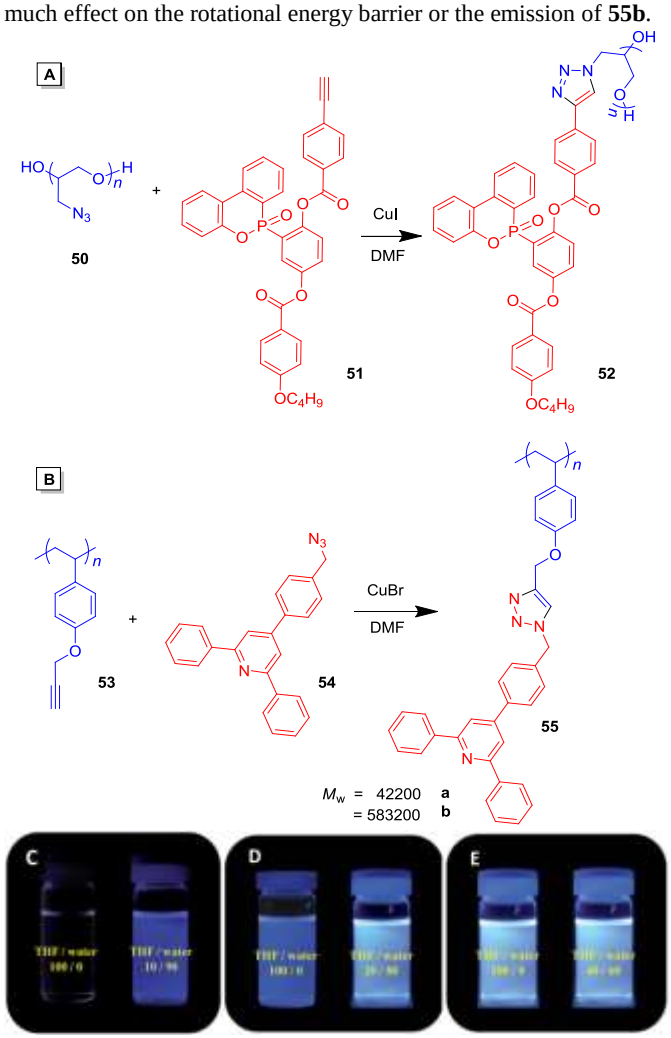

Scheme 10 Synthetic routes of grafting polymers (A) **52** and (B) **55a–b** based on click reaction of polymers. Photographs of (C) **54**, (D) **55a**, and (E) **55b** in pure THF and THF/water mixture with 90% water volume fractions under illumination with a 365 nm UV lamp. Adapted with permission from Ref. 40. Copyright 2012 The Royal Society of Chemistry.

2.4 Metathesis polymerization

The aforementioned AIE polymers all possess non-conjugated main chains, while a large variety of AIE polymers with conjugated main chains have also been reported in the past decade. Besides the vinylene polymerizations, metathesis polymerizations of monosubstituted and disubstituted AIEgen-containing acetylene monomers are also used to build AIE polymers with side chain AIEgens.

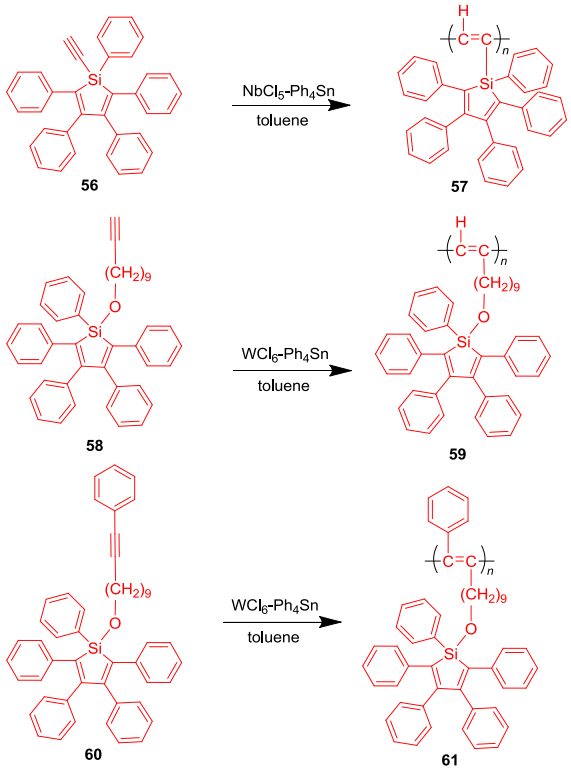

Scheme 11 Synthetic routes of three substituted polyacetylenes **57**, **59**, and **61** carrying 1,2,3,4,5-pentaphenylsilolyl pendants through metathesis polymerizations.

1,2,3,4,5-pentaphenylsilole-bearing monosubstituted acetylene **56** was first used to conduct the metathesis polymerization under the catalysis of $NbCl_5$–Ph_4Sn to afford polyacetylene **57** (Scheme 11).[41] However, this AIEgen-containing polymer turns out to be AIE-inactive, probably due to the short distance between the AIEgen and the polymer backbone which bring high rigidity of the luminogen. A long alkyl chain spacer was then inserted in between the acetylene and AIEgen functional groups to furnish monosubstituted acetylene **58** and disubstituted acetylene **60**, which then underwent polymerization using WCl_6–Ph_4Sn as catalysts to afford polyacetylenes **59** and **61**, respectively. The Φ_F of chloroform solution of **59** is 0.15% while it rose to 2.95% when 90% methanol was added with an $\alpha_{AIE,\Phi}$ value of 20. The emission efficiency of aggregation of **61** is 9.25% and the $\alpha_{AIE,\Phi}$ value is 46.

When the catalyst was changed from sensitive $NbCl_5$/WCl_6–Ph_4Sn to functional group-tolerable organorhodium complexes, the polymerization proceeds smoothly even with aminated TPE and ester-containing acetylene monomer **62** (Scheme 12A).[42] Although Rh-catalyzed polymerizations normally yield *Z*-rich polyacetylenes, the polymerization of **62** using $[Rh(nbd)Cl]_2$ as catalyst selectively yields polymer **63** with an *E* conformation. The polymer backbone and the TPE pendants are separated by flexible alkyl spacers and **63** thus shows typical AIE behavior. The THF

solution of **63** is nonluminescent and its emission intensity at 558 nm gradually increases with increasing water content in THF/water mixtures. The $\alpha_{AIE,I}$ value reaches 56 in the polymer nanoaggregates. Monomer **65** was then designed by removing the ester spacer from **62**. Its polymerization under the catalysis of $[Rh(nbd)Cl]_2$ yields polyacetylene **66**, which is faintly luminescent in THF solution with an emission maximum at 613 nm. The λ_{em} of **66** redshifted about 113 nm compared with its parent form of poly(phenylacetylene), suggesting that the polyacetylene backbone has conjugated with the TPE pendants. When water is added, the emission intensity of **66** starts to increase from 20% water content and the $\alpha_{AIE,I}$ value is 2.8. Both **63** and **66** can be transformed to conjugated polyelectrolytes **64** and **67** for further applications via ionization by hydrochloric acid, respectively. In addition, TPE-containing disubstituted acetylene **68a–b** can be polymerized under the catalysis of WCl_6–Ph_4Sn to obtain polyacetylenes **69a–b** (Scheme 12B).[37] Both polymers were weakly emissive in solution. The light emission of **69a** was enhanced when aggregated in poor solvents or solid state, however, the emission of **69b** was quenched in the aggregated states. This demonstrates that the photophysical properties of polyacetylenes could be readily tuned by molecular engineering endeavours.

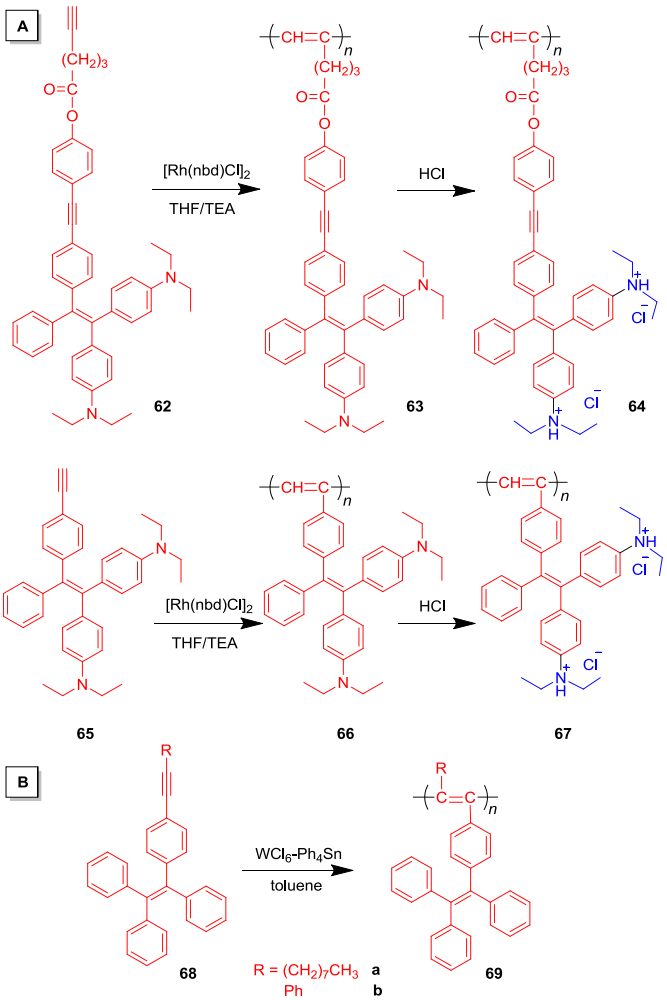

Scheme 12 Synthetic routes of substituted polyacetylenes carrying TPE pendants.

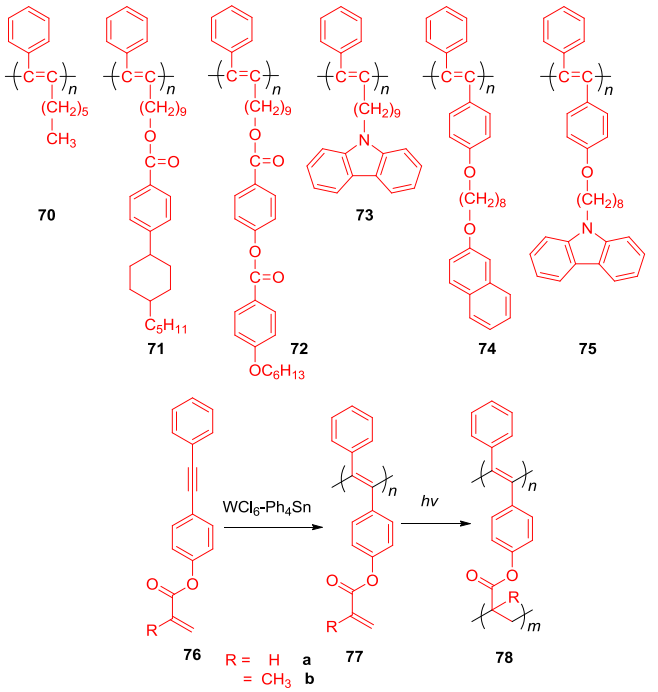

Scheme 13 Chemical structures and typical synthetic routes of disubstituted polyacetylenes without AIEgens.

Even when no AIEgen was involved in the monomer structure, AIE polyacetylenes can still be obtained through polymerization. Polyacetylenes **70–75** were prepared in high yields by $TaCl_5$– or WCl_6–Ph_4Sn catalysts in toluene at elevated temperatures under nitrogen (Scheme 13).[43] All the polymers possess high M_w, predominately *trans*-configurations and good solubility. Upon excitation, **70–75** emit at 458–506 nm in dilute THF solution with Φ_F ranging from 14.8–22.4%. The fluorescence intensity of such polyacetylenes is generally boosted about 2-fold when their chains are induced to aggregate by adding water into their THF solutions. AIE effect is a general characteristic for all the disubstitute polyacetylenes in this work, regardless of their pendant groups. Conformational simulations suggest that the polymer chains containing n = 3 repeat units can facilitate the formation of intramolecular excimers. According to "n = 3 rule", molecules with phenyl rings spatially separated by 3 carbon atoms can form intramolecular excimers that emit in the redder spectral regions, compared to their "monomer" emissions.[44]

Last but not least, since the most widely used $TaCl_5$ and $NbCl_5$ catalysts for the polymerizations of disubstituted acetylenes are intolerant to functional groups, WCl_6–Ph_4Sn catalyst was used to polymerize diphenylacetylene monomers **76a–b** functionalized with photopolymerizable vinyl and ester groups to form their corresponding disubstituted polyacetylenes **77a–b** with the (meth)acrylic functionality intact (Scheme 13).[45] The solutions of **77a–b** emit green light upon photoexcitation with Φ_F of 41% and 47%, respectively. When the polymer chains are aggregated, their Φ_F are increased, up to 88%, showing AIE feature. The remaining (meth)acrylic groups can further undergo photopolymerization to form **78a–b**, which bestow photosensitivity onto the polymers for potential applications in fluorescent photoresist patterns to be discussed in section 4.8.

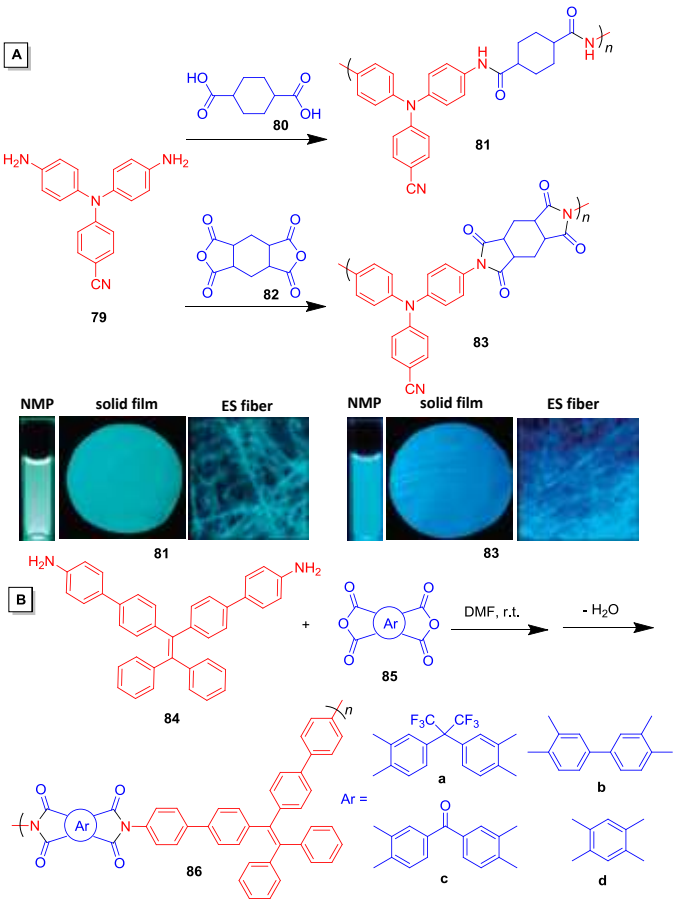

Scheme 14 Synthetic routes of high-performance polyimides (A) **81**, **83** and (B) **86a–d** through polycondensations. Insets: photographs of **81** and **83** in solution, solid film, and ES fiber states taken under illumination of a 365 nm UV light. Adapted with permission from Ref. 46. Copyright 2013 The Royal Society of Chemistry.

2.5 Polycondensation

As one of the fundamental polymerization reactions, polycondensation of amine and acid/anhydrides was used to prepare the rarely reported high performance aromatic polyimides with fluorescent characteristic. Polyamide **81** and polyimide **83** were prepared from cyanoarylamine-containing diamine monomer **79** by phosphorylation polycondensation with **80** and a one-pot high temperature solution polycondensation method with **82**, respectively (Scheme 14A).[46] In *N*-methyl-2-pyrrolidinone (NMP) solutions, they absorb at 310 nm (**81**) and 313 nm (**83**); emit at 497 nm (**81**) and 443 nm (**83**) with Φ_F of 14% (**81**) and 34% (**83**). In solid film, the Φ_F value increases to 46% (**81**) and 65% (**83**). They could both be utilized to prepare nanofibers by an electronspinning (ES) method and the Φ_F value was further enhanced in the form of ES nanofibers (57% for **81** and 70% for **83**), which show typical AIE characteristics (Scheme 14A, inset photos).

Generally, high performance aromatic polyimides show poor solubility in organic solvents. By introducing the twisted nonplanar AIEgens into the backbone of polyimide, enhanced solubility might be expected. As such, a rigid nonplanar TPE-containing diamine **84** was reacted with four aromatic tetracarboxylic dianhydrides **85a–d** through a conventional two-step procedure in DMF to form precursor, followed by thermal cyclodehydration to afford four polyimides **86a–d** (Scheme 14B).[47] The resulting polymers were soluble in polar solvents such as NMP, dimethylacetamide, DMSO, DMF and *m*-cresol. They also exhibited good thermal stability with 5% weight-loss temperature in nitrogen in the range of 571–592 °C. Furthermore, the rigid nonplanar conjugated structure bestows the polyimide films with light color and good transparency with more than 85% transmittance in the visible region, in comparison with other reported functional polyimides containing triphenylamine moieties which appeared as dark red brown to deep brown.[48] Monomer **84** shows typical AIE effect with its maximum PL emission at 463 nm in solid state, while the polyimides **86a–d** possess maximum PL emission at 470–494 nm in film state.

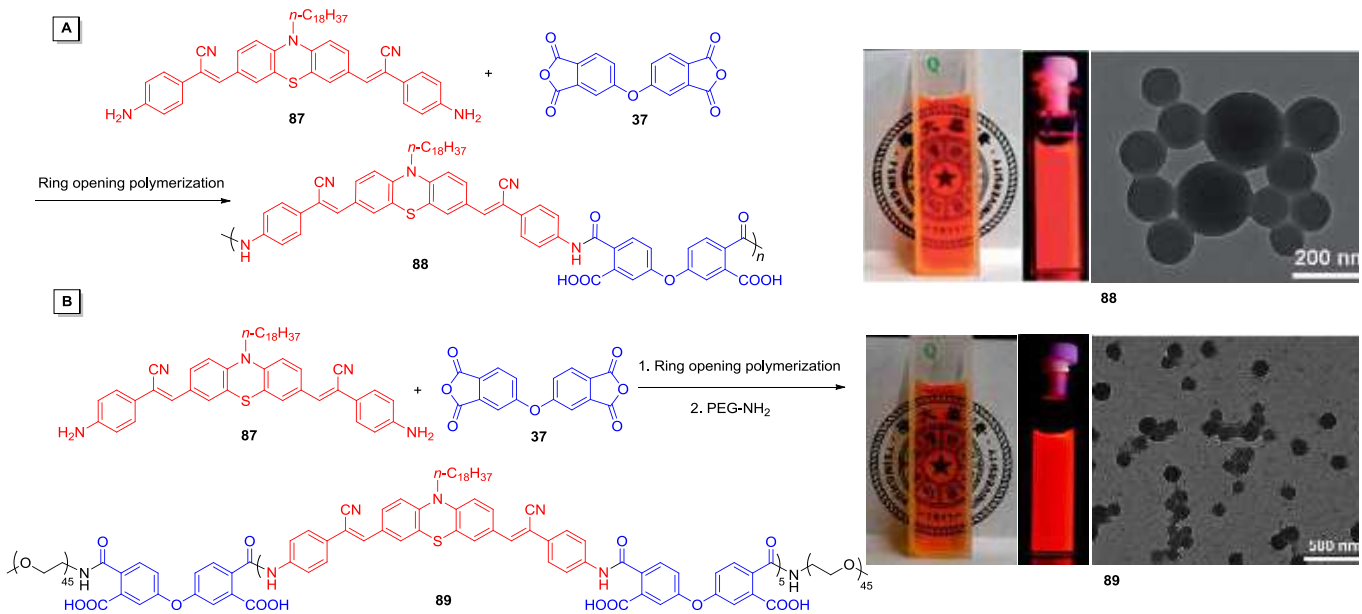

Scheme 15 Synthetic routes of polymer **88** through anhydride ring-opening polymerization with amino-end AIE dye and its further reaction with amino-terminated PEG to prepare **89**. Insets are the visible images taken under daylight, fluorescent images taken under 365 nm UV excitation, and TEM images of the nanoparticles of **88** and **89** dispersed in water. Adapted with permission from Ref. 49 and 51. Copyright 2014 The Royal Society of Chemistry.

2.6 Ring-opening polymerization

Recently, ring-opening polymerization was used to build AIE-active polymers. AIE dye **87** with two amino groups can facilely react with 4,4'-oxydiphthalic anhydride **37** in air through one-step room temperature anhydride ring-opening polymerization to generate fluorescent polymer **88** (Scheme 15A).[49] With newly formed carboxyl groups, the obtained polymer derived from the inherent hydrophobic AIEgen was transformed into an amphiphilic polymer. When **88** was dispersed in aqueous solution, the molecules tended to self-assemble into nanoparticles with diameters of 100–200 nm. The cores of the nanoparticles consisted of hydrophobic AIEgens and other aromatic groups with hydrophilic carboxyl groups covered on the surfaces (Scheme 15A, inset photo). The obtained nanoparticles hence exhibit high dispersibility in aqueous media and strong fluorescence. With a broad excitation wavelength from 320 nm to 530 nm, the maximum emission of **88** in water was at 607 nm. The red emission color, high efficiency, broad excitation, along with good water dispersibility, is highly beneficial for potential cell imaging applications.

Polyethylene glycol (PEG), a hydrophilic polymer with good biocompatibility, low immunogenicity and high water solubility, has been widely utilized for surface modification of various polymers and nanoparticles.[50] As such, it was chosen to further modify polymer **88** through one-pot PEGylation under room temperature in air without catalysts and initiators. In this work, AIE dye **87** was first reacted with 4,4'-oxydiphthalic anhydride **37** through ring-opening polymerization to afford polymer **88** with the polymerization degree of 5 based on the feed molar ratio (Scheme 15B).[51] Amino-terminated PEG was then added to react with the anhydride end functional groups of the polymer via a ring-opening condensation reaction. The resulting PEGylated polymer **89** tended to self-assemble into spherical nanoparticles with uniform diameter of about 100 nm and excellent water dispersibility in pure aqueous solution (Scheme 15B, inset photo). The nanoparticles of **89** showed strong red fluorescence in water with the emission peak located at 600 nm and they can also be excited with broad wavelength region from 325 to 590 nm. Moreover, the obtained fluorescent nanoparticles were expected to be more stable compared with the previously reported fluorescent organic nanoparticles[52] as the AIE chromophores were covalently incorporated into the polymer nanoparticles.

2.7 Hydrosilylation polymerization

There are also a few AIE polymers with heteroatoms in the main chain reported which are prepared from a series of newly developed addition polymerization approaches. For example, hydrosilylation reactions between alkynes and silylhydrides catalyzed by various transition metal catalysts are well established approaches to construct vinyl silane derivatives. Through the polymerization based on such hydrosilylation reactions, poly(silylenevinylene)s bearing silicon atoms can be easily obtained, which may exhibit unique σ*–π* delocalization along the polymer backbone due to the interaction of the σ* orbitals of the silicon atoms and the π orbitals of the carbon-vinylene bonds.[53]

The alkyne polyhydrosilylations of 1,2-bis(4-dimethylsilanylphenyl)-1,2-diphenylethene **91** with terminal dialkynes 4,4'-diethynylbiphenyl **90a**, bis(4-ethynyl-2-methylphenyl)dimethylsilane **90b**, 3,6-diethynyl-9-heptylcarbazole **90c**, and 1,1-dimethyl-2,5-bis(4-ethynylphenyl)-3,4-diphenylsilole **90d** were reported (Scheme 16A).[54] The polymerizations were mediated by $Rh(PPh_3)_3Cl$ in THF in a regioselective fashion, furnishing poly(silylenevinylene)s **92a–d** with high molecular weights (M_w up to 36 500) and stereoregularities (*E* content up to 100%) in satisfactory yields. This polymerization is also suitable for internal alkyne monomers. For example, 2,5-bis-(2-trimethylsilylethynyl)thiophene **93** was reacted with **91** in the presence of $Rh(PPh_3)_3Cl$ in refluxed THF to give polymer **94** with a high M_w in good yield (Scheme 16B). All the poly(silylenevinylene)s were weakly emissive when molecularly dissolved in solutions but became strong emitters when aggregated in poor solvents or fabricated as thin films in the solid state. The Φ_F values of **92a–d** and **94** in the solution state were as low as 0.24–3.17%, while their nanoaggregates emitted at wavelengths similar to those of the solutions with higher Φ_F values (13–31%), duly verifying their AIE features.

Similar polymerization can also be realized with various silanes. Hydrosilylation polymerizations of 1,1-dimethyl-2,5-bis(4-ethynylphenyl)-3,4-diphenylsilole **95** with aromatic silylhydrides including 1,4-bis(dimethylsilyl)benzene **96a**, 4,4'-bis(dimethylsilyl)biphenyl **96b**, 2,5-bis(dimethylsilyl)thiophene **96c**, and 2,7-bis(dimethylsilyl)-9,9-dioctylfluorene **96d** was carried out in the presence of $Rh(PPh_3)_3Cl$ catalyst in refluxed THF to afford a series of silole-containing poly(silylenevinylene)s **97a–d** (Scheme 16C).[55] The polyhydrosilylation reactions proceed efficiently and regioselectively, yielding polymers with high molecular weights (M_w up to 95 300) and good stereoregularity (*E* content close to 99%) in high yields (up to 92%). The emission of polymers **97a–d** is quite weak at ~506 nm when molecularly dissolved in dilute THF solutions with Φ_F of 0.99–1.44%. Their thin films, on the other hand, shown green emission with bathochromically shifted emission maximum of 519–533 nm. The Φ_F values of the thin film were boosted to 7.7–22.0%, suggesting that they are all AIE-active.

Different reaction conditions were reported and could be applied to various monomer structures. For example, 5*H*-dibenzo[b,d]silole **98** and 2,7-diethynyl-9,9'-spirobifluorene **99** was reacted with a catalytic amount of H_2PtCl_6 under an argon atmosphere in toluene at 60 °C for 36 h to afford poly(tetrasilolediethynylspirobifluorene) (Scheme 16D).[56] An excess amount of trimethoxylsilane was then added for end-capping to generate polymer **100**, which provides a reactive end group for covalent attachment to a silica surface. The polymer exhibits AIE effect and its solid thin film has a blue emission as shown in Scheme 16D, inset photo. The facile modification of silica with the fluorescent polymer using trimethoxylsilyl end groups to covalently link **100** to a silica gel thin layer chromatography support allows for more convenient and efficient detection in fluorescent sensing processes.

In step polymerizations, when one of the monomer possesses more than two reactive functional groups, polymers with nonlinear architecture, especially hyperbranched polymers will be easily obtained. The rhodium-catalyzed alkyne polyhydrosilylation of A_2-type monomer 1,2-bis(4-ethynylphenyl)-1,2-diphenylethene **101** and B_3-type monomer tris(4-dimethylsilylphenyl)amine **102** can afford a silicon-containing hyperbranched polymer **103** with σ*–π* conjugation (Scheme 17A).[57] Monomer **101** was prepared from McMurry coupling reaction and generally contains both *E*/*Z* isomers with very similar physical and chemical properties. Under the catalysis of the commonly used catalyst $Rh(PPh_3)_3Cl$ for alkyne hydrosilylation in refluxed THF, hyperbranched polymer **103** with M_w of 75 100 was obtained in 71% yield after stirring for 24 h. Upon photoexcitation, the THF solution of **103** is weakly luminescent at 500 nm with a Φ_F value of 0.01%. In the THF/water mixture with 90% water content, the PL intensity of **103** is ~23-fold higher than that of its THF solution. The λ_{em} in thin film is similar to the solution and the Φ_F value is raised to 34.7%, 3470-fold higher than that of the THF solution.

When the number of the reactive functional groups in the monomer increases, there is great possibility to form crosslinked

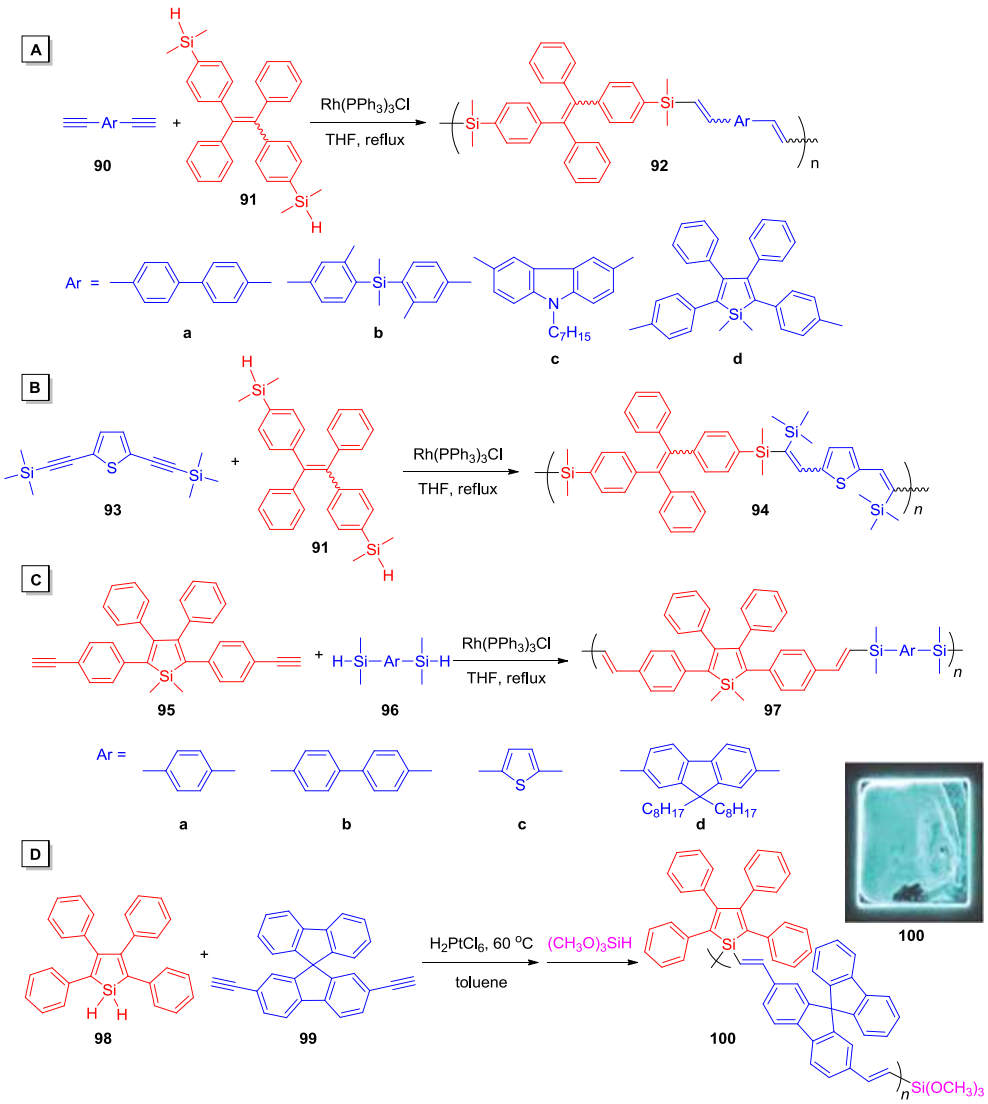

Scheme 16 Synthetic routes of TPE/silole-containing linear poly(silylenevinylene)s through polyhydrosilylation. Inset is the fluorescent image of drop-casting polymer film of **100** on quartz slides. Adapted with permission from Ref. 56. Copyright 2012 The Royal Society of Chemistry.

systems which results in polymer products with poor solubility and processability. With the unique structure of AIEgen-containing monomers which are typically twisted and bulky, even $A_2 + B_4$ type monomer strategy can be successfully adopted in the polyhydrosilylations to prepare hyperbranched polymers. A B_4-type 3-silolene monomer, 2,2,5,5-tetrakis(dimethylsilyl)-1,1-dimethyl-3,4-diphenyl-3-silolene (TDMSHS) **104** was polymerized with 1,1-dimethyl-2,5-bis(4-ethynylphenyl)-3,4-diphenylsilole **95** in the presence of Karstedt's catalyst in refluxed THF to generate a soluble stereoregular silole-containing hyperbranched poly(silylenevinylene) **105** with high molecular weight (M_w of 146 000) and high yield (95%) after stirring for 10 h (Scheme 17B).[58] The dilute solution of **105** emits green light at 510 nm with Φ_F of 2.66%. Unlike other poly(silylenevinylene)s, the emission only increases slightly even when a large amount of water was added to the THF solution, suggesting that the aggregation formation has little effect on the luminescent process of **105**. The geometric constraint arising from the three-dimensional structure of TDMSHS should lead to loose and random alignment of **105** when they aggregate in poor solvent. Such chaotic stacks may generate large free volume in the aggregate in which the phenyl rings of the silole units may still be able to rotate, consuming energy nonradiatively and partially quenching the light emission, thus resulting in the observed weak AIE effect.

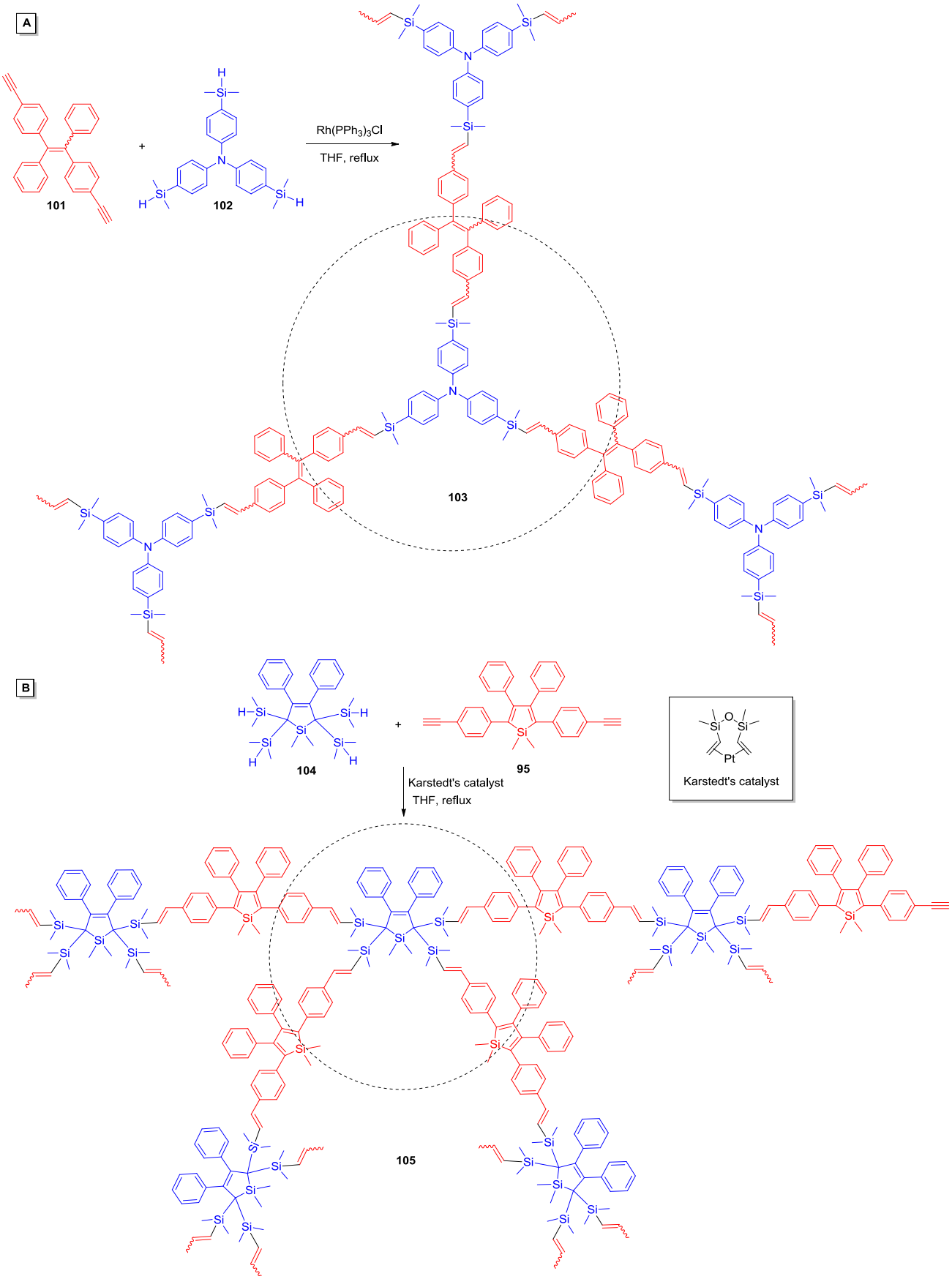

Scheme 17 Synthetic routes of hyperbranched poly(silylenevinylene)s **103** and **105** through polyhydrosilylations.

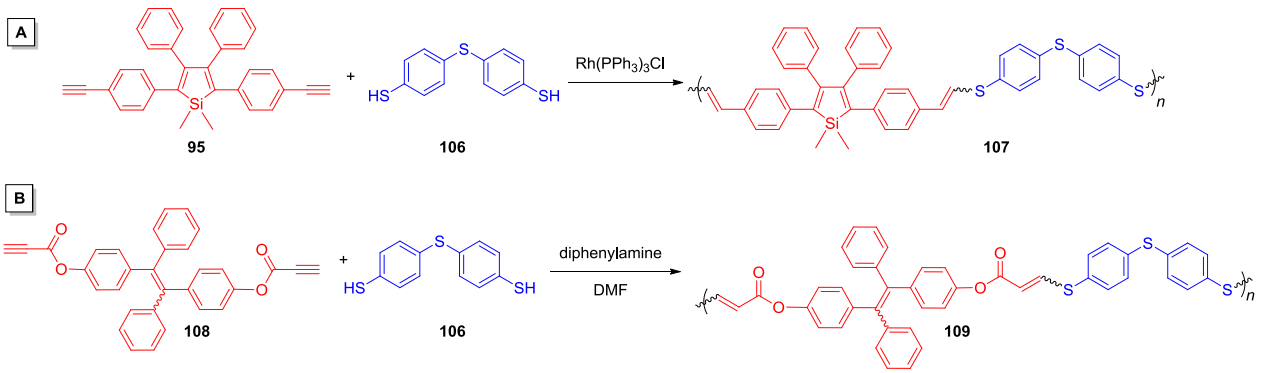

Scheme 18 Synthetic routes of poly(vinylenesulfide)s **107** and **109** through Rh-catalyzed or metal-free alkyne polyhydrothiolations, respectively.

2.8 Hydrothiolation polymerization

Besides silicon, sulfur is another element with rich electro/optical properties and the thiol-yne click polymerization towards regio- and stereoselective synthesis of sulfur-rich acetylenic polymers has thus been researched with particular interest. The atom-economical alkyne polyhydrothiolation of aromatic diyne **95** and dithiol **106** was catalyzed by rhodium complexes, which proceeded smoothly under mild condition at room temperature in a regioselective manner, producing sole anti-Markovnikov product of poly(vinylene sulfide) (PVS) **107** with high molecular weight (M_w up to 31500) and stereoregularity (*E* content up to 100%) in high yield (95.2%) (Scheme 18A).[59] Unlike the limited monomer scope and low structural selectivity of the radical- and nucleophile-initiated alkyne hydrothiolations, the rhodium-catalyzed system is expected to work efficiently for a large variety of functional monomers and possess high regio- and stereoselectivities. The catalytic efficiencies of $Rh(PPh_3)_3Cl$, $[Rh(nbd)Cl]_2$, and $[Rh(nbd)(PPh_3)_2]^+PF_6^-$ were tested for the polymerization and $Rh(PPh_3)_3Cl$ is of particular interest, which provides 100% *E*-vinylene structure in the polymer product. The stereostructures of **107** can be readily tuned by either engineering control on the sequential addition of monomers during the polymerization process or postmanipulation by light irradiation. In pure THF solution, **107** is weakly emissive at 520 nm. Addition of water into the THF solution induces its chains to aggregate, which red-shifts and enhances its light emission by 2.6-fold in 80 vol % aqueous mixtures compared with that in pure THF solution. Slight PL intensity decrease was observed when the water fraction is changed from 80 vol % to 90 vol %, which may be attributed to the reduction of the effective polymer concentration induced by the precipitation of the large aggregates.

The development of metal-free polymerization reactions has attracted much interest among polymer chemists in recent years because of their remarkable advantages, such as environmental benignity, economic benefit, and ease in polymer purification.[60] The products do not suffer from the detrimental effects of metallic ions in the catalyst residues, maintaining the light emitting and non-linear optical properties of the polymers. In addition, functional groups that are toxic to transition metals can be incorporated in the monomers, which helps widen the scope of polymer structures derived from the reactions. The polyhydrothiolation between diyne and dithiols towards sulfur-rich functional poly(vinylenesulfide)s was then explored under metal-free conditions. The alkyne polyhydrothiolation of 4,4'-thiodibenzenethiol **106** and arylene dipropiolate **108** was mediated by amines (Scheme 18B).[61] In the presence of such organobase, the nucleophilicity of the thiol group increases, which improve the efficiency of its addition reaction. Various amines were tested and diphenylamine works most efficiently for the reaction. The metal-free alkyne polyhydrothiolation of **106** and **108** proceeded at room temperature in DMF in the presence of 1.2 M diphenylamine under nitrogen in a regioselective fashion, furnishing sole anti-Markovnikov products of poly(vinylenesulfide) **109** with high M_w of 21000 and high stereoregularities (*Z* content of 78.1%) in 73.5% yield. Polymer **109** is AIE-active and it can be fabricated into a luminescent thin film.

2.9 Three-component polymerization

Multicomponent reactions have garnered much attention because of their atom-economy, high efficiency, environmental friendliness, high throughput, etc. A series of three-component alkyne polymerization reactions were developed recently and further utilized to prepare AIE polymers. For example, diyne monomer **101** and aldehyde monomer **110** can react with BCl_3 **111** without any metal-catalyst and afford linear polymers with well-ordered polymer structures **112**. Polymer **112** is AIE-active (Scheme 19A).[62] Through a series of optimization of reaction conditions, precise control of the molar ratio of monomers was identified to be crucial to afford polymers in decent yield with high M_w. After stirring the dichloromethane solution of the three monomers at 0 °C for 2 h and 25 °C for 20 h, polymer **112** was obtained in 93% yield with M_w of 17 800. Upon photoexcitation, a green light with 502 nm emission maximum was observed for **112**. By increasing the volume fraction of water, a nonsolvent for **112**, an enhancement in emission intensity was observed while keeping the spectral profile unchanged.

Another programmable polymerization route for the synthesis of AIE polymers via one-pot reaction has been reported (Scheme 19B).[63] The three-component polycoupling reactions of terephthalaldehyde **114**, dibenzylamine **115** and 1,2-bis(4-ethynylphenyl)-1,2-diphenylethene **113a** or 2,5-bis(4-ethynylphenyl)-1,1-dimethyl-3,4-diphenylsilole **113b** are catalyzed by indium(III) chloride in *o*-xylene at 140 °C. The reaction carried out under nitrogen for 20 h afforded soluble polymers **116a–b** with well-defined structures and high molecular weights (M_w up to 51 200) in high yields (up to 94%). The Φ_F values of the solid thin films of **116a** and **116b** are 14.3% and 11.6%, respectively, which is much higher than the Φ_F value of their solution states, 1.5% (**116a**) and 2.9% (**116b**).

2.10 Suzuki polycoupling

While condensation polymerization generally offer nonconjugated AIE polymers with AIEgens embedded in the polymer backbone, transition-metal catalyzed modern organic coupling reactions as well as cyclizations can generate conjugated AIE polymers with AIEgens in the main chains. Transition metal-catalyzed carbon-carbon coupling reactions, including but not limited to Suzuki, Wittig, Heck, McMurry, Sonogashira, Hay-Glaser coupling reactions, are the most

widely used reactions to construct semiconducting conjugated compounds with unique photoelectronic properties. Consequently, they play an important role in building AIE polymers with the simple design of connecting AIEgens through C–C, C=C, C≡C, and C≡C–C≡C bonds.

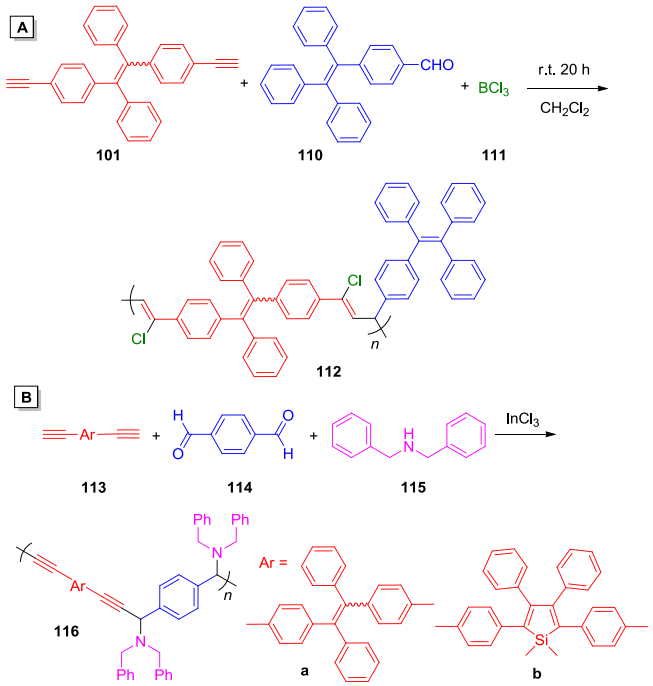

Scheme 19 Synthetic routes of polymers **112** and **116a–b** through three-component polymerizations.

The polymerization of TPE-containing dibromide **117** and diboronic acid **118** under the reaction condition of Suzuki coupling reactions facilely generates linear polymer **119** with TPE building blocks linked with C–C single bonds (Scheme 20A).[64] With the twisted TPE moieties, polymer **119** has good solubility despite its fully conjugated structure without flexible alkyl chains to enhance the solubility. Such rigid structure also endows high thermal stability with a decomposition temperature of 528 °C. The Φ_F values for THF solution and aggregate state of **119** are 1.2% and 28%, respectively, suggesting it is AIE-active.

Polyfluorene is a promising blue-light emitter due to its large band gap, efficient PL and electroluminescence (EL), good solubility, thermal and oxidative stability. However, it is well-known to have diminished fluorescence in the aggregated states, in other words, it is aggregation-caused quenching. ACQ-active fluorene and AIE-active TPE can be combined in a single polymer by standard Suzuki cross-coupling polymerization. Under the standard palladium-mediated Suzuki coupling reaction, the polymerizations between TPE-containing bromide **120**, dibromofluorene **123**, and diboronic ester fluorene **124** at different feed ratios afford conjugated copolymers **125a–d** with different TPE-to-fluorene ratios in the polymer backbone (Scheme 20B).[65] As a comparison, the polymerization of **120** and TPE-containing boronic ester **121** give pure TPE-containing linear polymer **122** with potential modifiable side chains, while the polymerization of **123** and **124** afford pure polyfluorene **126**. Fig. 3 shows the fluorescent images of the solutions, aggregates and films of **122**, **125a–d** and **126** under UV irradiation. Polymer **122** is a typical AIE polymer with non-emissive solution and highly emissive aggregates and film. On the contrary, polyfluorene **126** is a representative ACQ polymer with emissive solution and faintly emissive aggregates and films. When the TPE content is larger than 10% in the polymer backbone, in the cases of **125a–c**, the solution emission is turned off, while the aggregate and film emission

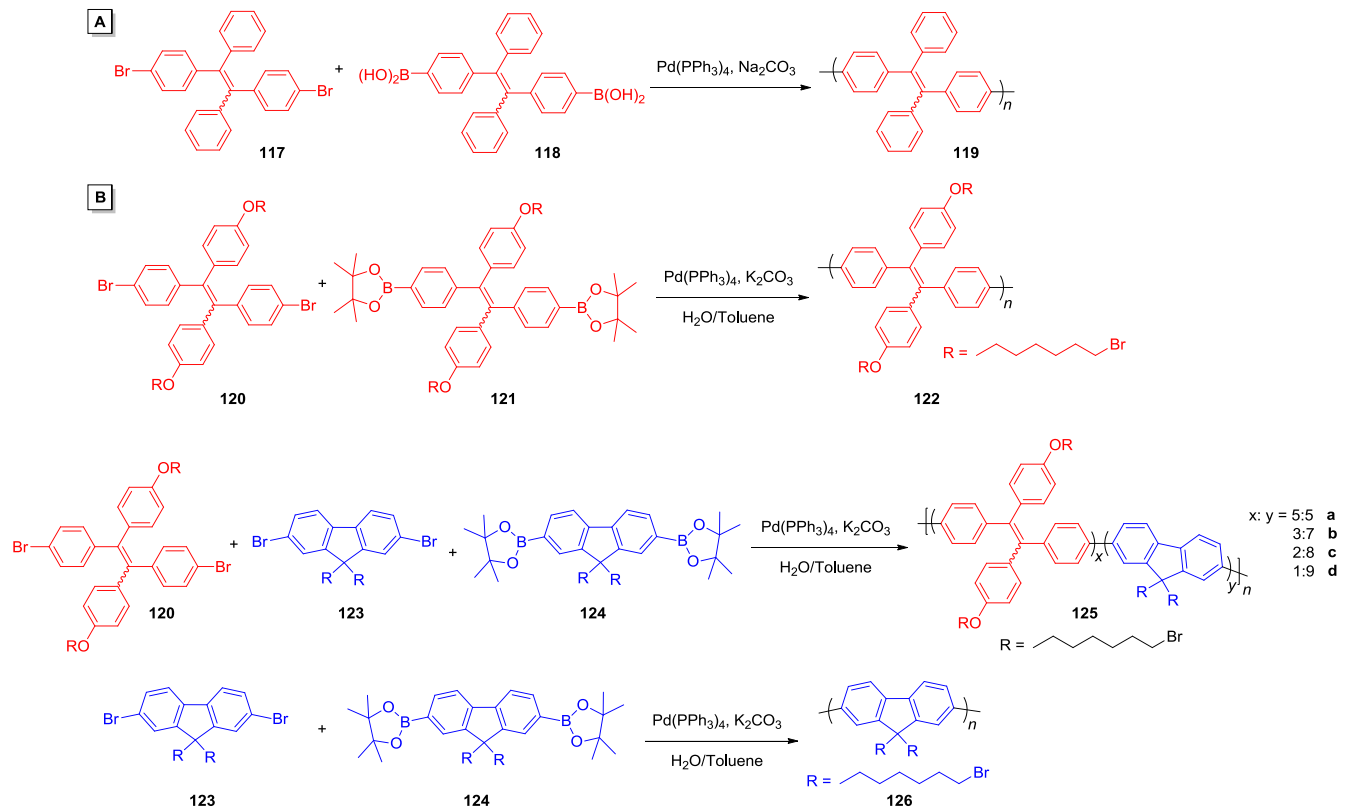

Scheme 20 Synthetic routes of TPE and/or fluorene-containing conjugated polymers through Suzuki polycouplings.

dramatically increase. PL spectra suggest that the copolymers **125a–d** all possess dual-channel fluorescence with their AIE peaks at ~510 nm and ACQ peaks at ~415 nm. A clear trend is suggested that with increasing ratio of TPE, the polyfluorene with ACQ characteristic was gradually converted into AIE polymers.

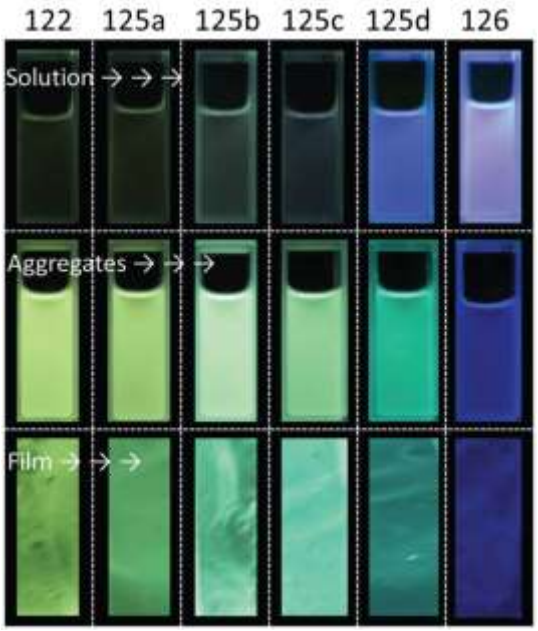

Fig. 3 Fluorescence photographs of THF solutions, aggregates in THF/water mixtures with 99% water, and films of **122**, **125a–d**, and **126** under UV illumination at 365 nm. Adapted with permission from Ref. 65. Copyright 2013 Wiley-VCH.

Electron donors/acceptors can also be incorporated into AIE polymers to achieve various emission colors based on the rational design of the HOMO and LUMO distribution. Three TPE-containing dibromides **127**, **130** and **132** with different electron-donor and acceptor units were reacted with fluorene-containing diboronic ester **128** under the reaction conditions of Suzuki coupling polymerization (Scheme 21A) to generate polymers **129**, **131** and **133**.[66] All the three polymers have poor emission in their THF solutions with Φ_F <1%, while their emissions in films are much stronger at 550 nm (**129**), 501 nm (**131**) and 665 nm (**133**), respectively. In particular, the strong D-A structure of **133** leads to a substantial intra-chain charge transfer from the diethylamino donor groups to the benzothiadiazole acceptor groups, forming a dipole moment and resulting in a red emission. The fluorescent films of the polymers have high Φ_F values which can be developed as fluorescent sensors. For example, the thin film of **129** has a bright green emission with a Φ_F of 43.9%.

Alternatively, different building blocks such as fluorene, spirobifluorene, carbazole and 1,3,4-oxadiazole moieties were introduced into the conjugated polymers to bring unique properties such as twisted topological structure and hole/electron transporting activity. The polymerizations of bromo-substituted TPE **117** and boronic esters **134**, **138** or **140** proceed smoothly through the Suzuki coupling reaction using $Pd(PPh_3)_4$ as catalyst, Na_2CO_3 as base, and THF as solvent (Scheme 21B).[67] After three days, the end-capping groups phenylboronic acid **135** and bromobenzene **136** were added to react with the bromo- and boronic ester terminal groups to afford polymers **137**, **139** and **141**, respectively. It was reported that this capping prevents the fluorescence quenching of the active terminal groups. On the other hand, polymer **144** was prepared from the Suzuki reaction of 1,3,4-oxadiazole derivative **142** and TPE-containing boronic ester **143**. As mentioned before, the TPE structure can turn such ACQ polymers to AIE polymers. Indeed, all the four polymers emit in the range of 504–515 nm with aggregated state fluorescent Φ_F up to 33.4%. They all show fluorescent enhancement from solution to aggregated states with $\alpha_{AIE,\Phi}$ values of 21 (**137**), 39 (**139**), 35 (**141**) and 31 (**144**).

Siloles possess high electron acceptability and fast electron mobility and silole–based polymers normally possess low-lying LUMOs which can serve as efficient electron-transporting materials in OLEDs.[68] As such, they were incorporated into the conjugated AIE polymers through Suzuki coupling polymerizations. Silole monomer **145** with two 4-(*N*, *N*-dimethylamino)phenyl substitutions on the silicon atom was synthesized and copolymerized with 2,7-fluorene derivatives **146** and **147** at feeding ratios of 1% (**a**), 10% (**b**) and 20% (**c**) to afford copolymers **148a–c** (Scheme 22A).[69] In THF solution, **148a** with low silole content only exhibits two blue emission peaks at 418 and 440 nm, attributed to polyfluorene. With increasing silole content, the silole emission peak appears at ~506 nm in the solutions of **148b** and **148c**. The relative intensity of the silole peak to the fluorene emission of **148b** and **148c** is 30% and 60%, respectively. In the solid film, although **148a** still has strong blue emission from the fluorene segments, the green emission originating from the silole units already reaches a relative intensity of 75% of the blue peak, demonstrating the AIE nature of the silole units. In the film of **148b** and **148c**, the silole emission becomes the major PL peak and the fluorene emission almost disappears. This work demonstrates a clear example of turning ACQ polymers to AIE polymers through incorporating AIEgens into the polymer, showing that the amount of the AIEgens correlate with the PL behavior.

Carbazole-based derivatives normally possess high emission Φ_F in the solid state, high hole affinity and good hole-transporting ability for OLED applications.[70] A series of green-emissive soluble conjugated polyfluorene-carbazole-silole-containing random copolymers **151a–d** were successfully synthesized by Pd(0)-catalyzed Suzuki coupling reaction, where the sum of the molar ratios of **149** and **150** was kept constant, while their ratio was tuned (Scheme 22B).[71] In dichloromethane solutions, **151a–b** with less silole content exhibit the combined contribution from carbazole and fluorene and emit at ~420 nm, while the PL peaks of **151c–d** show a bathochromic shift to 520 nm, which is attributed to the silole emission. In the thin film state, the blue emissions of **151a–b** from the carbazole and fluorene blocks are weakened and the PL spectra display a greenish-blue emission at 470 and 481 nm, respectively. Compared to the solution PL spectra, the largely enhanced greenish-blue emission of the films is caused by the intra-chain energy transfer and AIE of silole moieties.

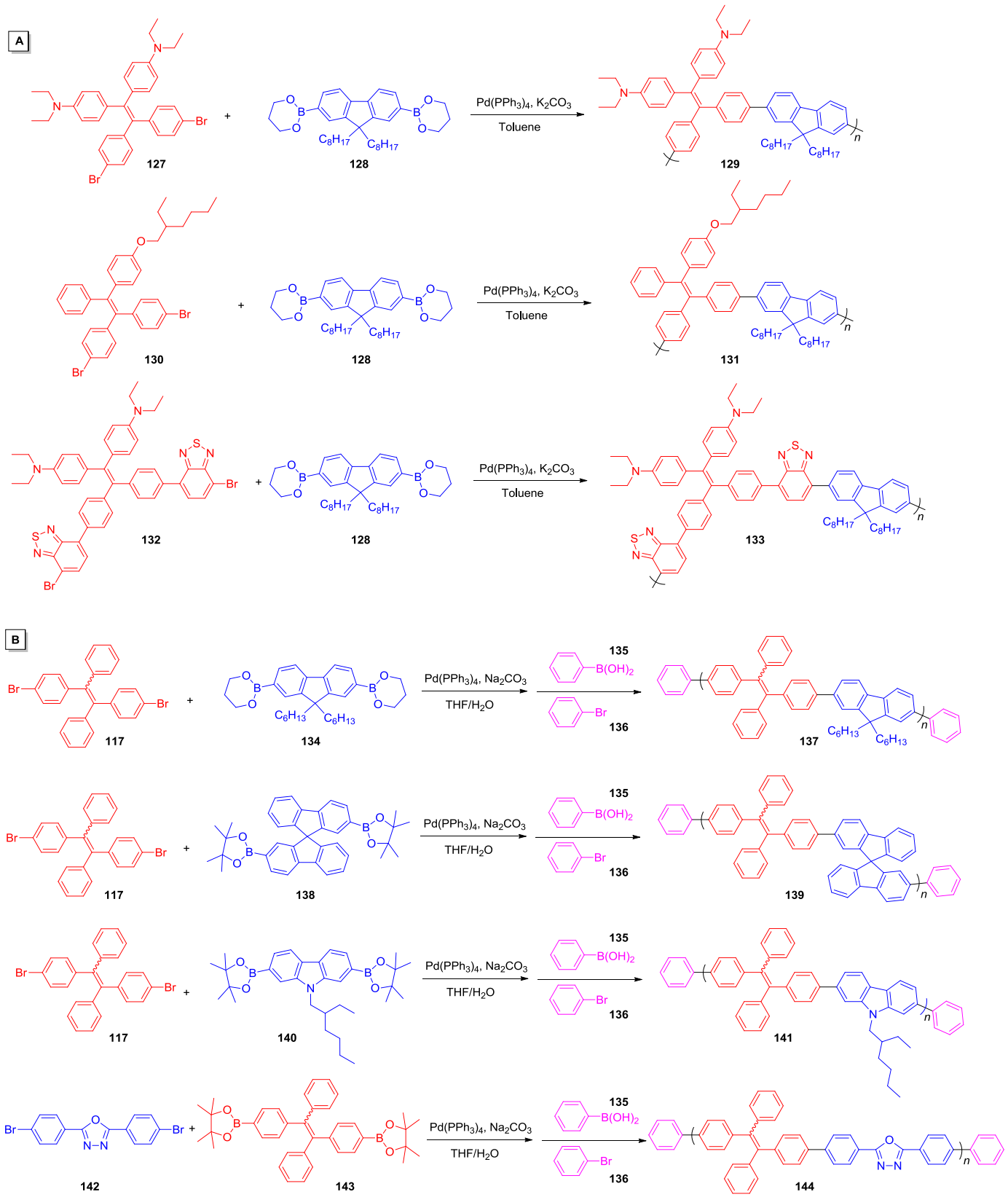

Scheme 21 Synthetic routes of TPE-containing conjugated polymers through Suzuki polycouplings.

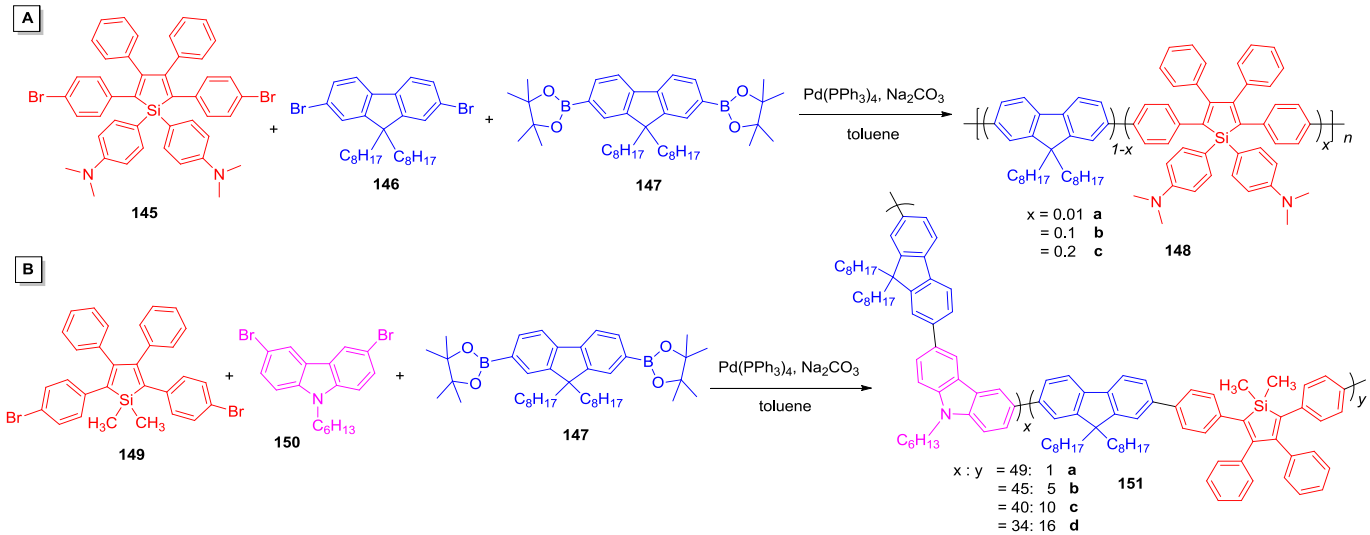

Scheme 22 Synthetic routes of silole-containing conjugated polymers through Suzuki polycouplings.

2.11 Wittig/Heck/McMurry polycoupling

C=C bond linkage represents the best conjugation among carbon-carbon single/double/triple bonds. Wittig, Heck and McMurry coupling reactions are widely used reactions to generate new C=C linkages for the construction of AIE polymers with good conjugation among the building blocks.

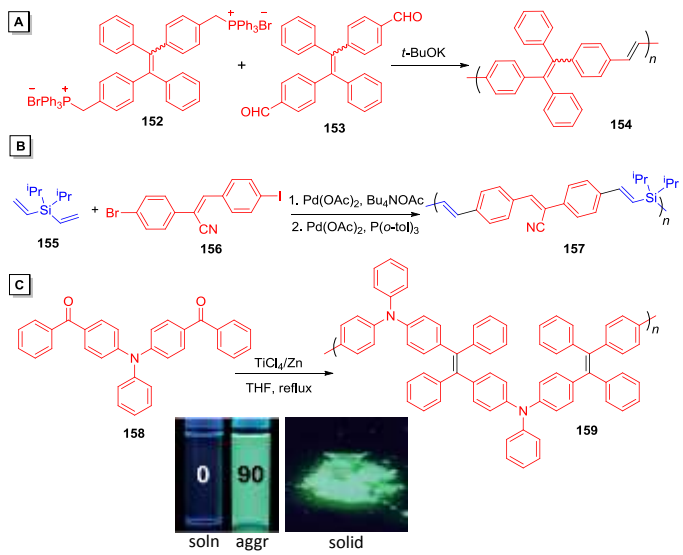

Scheme 23 Synthetic routes of polymers **154**, **157** and **159** prepared from Witting, Heck, and McMurry polycouplings, respectively. Insets are the fluorescence images of solution, nanoaggregates in THF/water mixture with 90% water content and solid powder of **159** taken under 365 nm UV irradiation. Adapted with permission from Ref. 74. Copyright 2012 Wiley-VCH.

For example, the Wittig reaction between TPE-containing phosphorus ylide **152** and TPE-containing dialdehyde **153** undergoes polymerization under the basic condition to form linear polymer **154** with TPE units connected with C=C bonds (Scheme 23A).[64] The THF solution of polymer **154** emits weakly at 520 nm with Φ_F of 3.4%. When it aggregates in the aqueous media, the Φ_F value increased to 64%. Compounds with good conjugation are reported to exhibit large two-photon absorption (TPA) cross sections.[72] Polymer **154** associated with good conjugation and AIE feature thus shows aggregation-induced two-photon excited fluorescence (TPEF) as will be discussed in section 4.6.

The Heck reaction of vinylsilane **155** and AIEgen-containing aryl halide **156** facilely afford an alternating dialkylsilylene[divinyl(cyanostilbene)] copolymer **157** with unidirectional orientation of the cyano substituents (Scheme 23B).[73] The emission profile of **157** was studied in THF and mixed solvents of THF and *n*-hexane because it is highly soluble in THF but sparingly soluble in *n*-hexane. In dilute THF solution, it emits at 493 nm. It is worth noting that the Φ_F of **157** was significantly enhanced from 10% to 50% as the ratio of *n*-hexane increased. The presence of the bulky isopropyl group significantly enhances the quantum yield upon aggregation.

The McMurry coupling reaction, on the other hand, can directly generate AIEgens in situ during polymerization. The *bis*-ketone intermediate **158** can undergo such polymerization to produce the TPE-triphenylamine polymer **159** (Scheme 23C).[74] The fluorescent photos of solution, nanoaggregates and solid powder are shown in the inset photo of Scheme 23C. In THF solution, moderate emission at approximately 410 nm can be detected, attributed to the triphenylamine moieties. Upon addition of water, the emission at 410 nm decreases and a peak at 510 nm emerges, which increases along with the amount of water. In the solid film, the emission Φ_F reaches 57%.

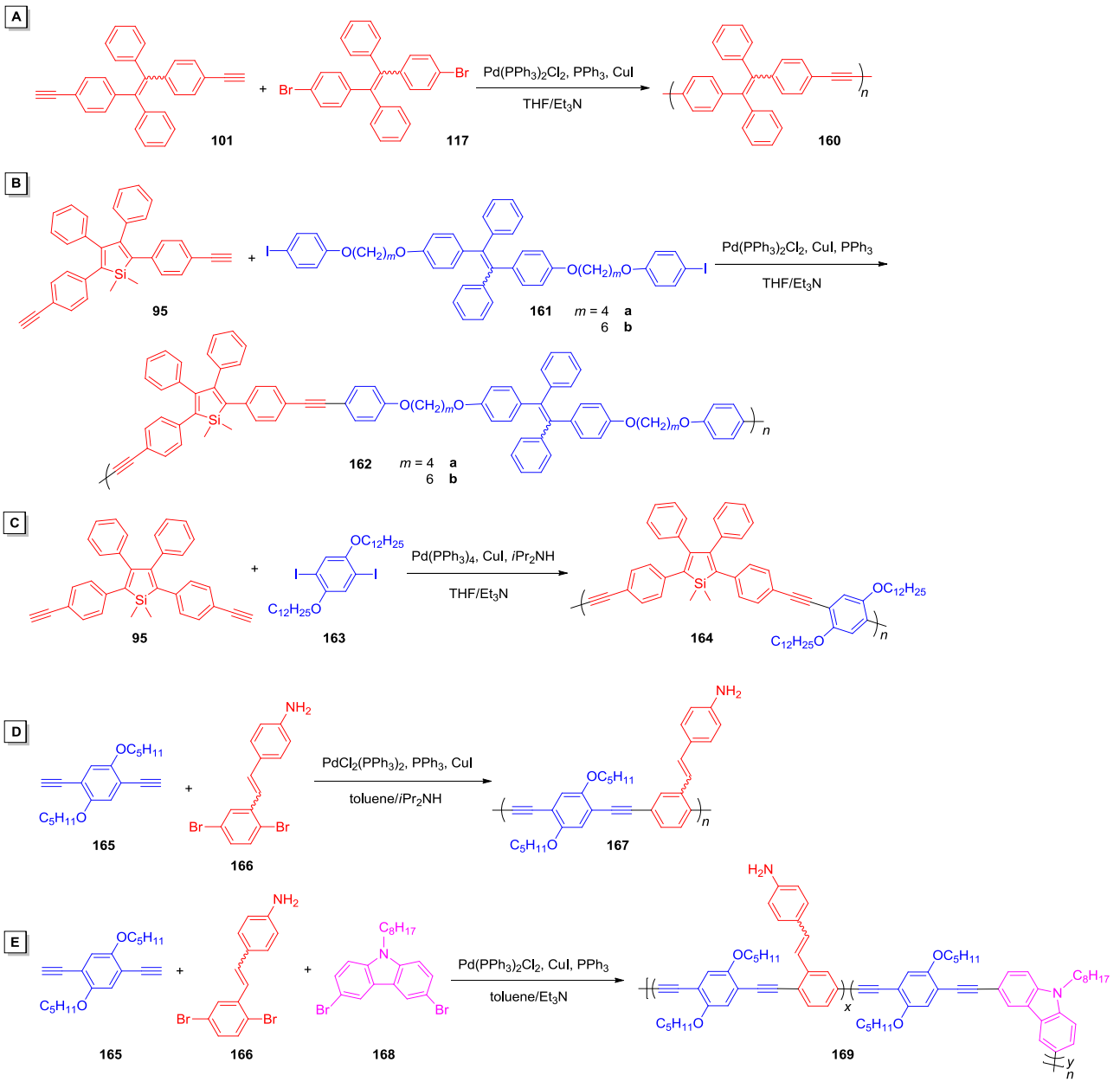

Scheme 24 Synthetic routes of poly(arylene ethynylene)s through Sonogashira cross-coupling reactions.

2.12 Sonogashira polycoupling

The Sonogashira coupling reaction is an extensively used reaction that connects aromatic building blocks in the AIE polymers with C≡C bonds. For example, TPE-containing diyne **101** and dibromo-substituted TPE **117** was reacted under the conditions of the Sonogashira coupling reaction to obtain linear polymer **160** with TPE units linked with C≡C bonds (Scheme 24A).[64] The THF solution of **160** emits at 502 nm and the addition of water increase the emission efficiency with a $\alpha_{AIE,\Phi}$ value of 16.

Silole-containing diyne monomer was also used to prepare AIE polymers through Sonogashira polycouplings. Silole-containing diyne **95** and TPE-containing di-iodides **161a–b** were reacted in the presence of $Pd(PPh_3)_2Cl_2$, CuI and PPh_3 in a THF/Et_3N mixture under nitrogen for 24 h to give luminescent polymeric products **162a–b** (Scheme 24B).[75] Polymer **162a** emitted weakly at 505 nm in solution. Addition of poor solvent, water, aggregated its chains, which positively restricts the intramolecular motions of the fluorophores and blocks the channels for the excitons to decay non-radiatively. When water fraction increases, its PL was enhanced and peak intensity was obtained in 70 vol % aqueous media. Due to the structural similarity, the PL behavior of **162b** resembles that of **162a**. Similarly, silole-containing polymer **164** was prepared from **95** and **163** in THF and diisopropylamine at 80 °C for 48 h in the presence of a catalytic amount of $[Pd(PPh_3)_4]$ and CuI (Scheme 24C).[76] The polymer showed moderate fluorescence as solutions in THF with Φ_F of 8.0%. The addition of water into solutions of **164** in THF resulted in a notable enhancement of the emission intensity. The Φ_F values in the aqueous mixtures with 90% water fractions were 12.3%, suggesting its AIE characteristics.

AIE polymers without typical AIEgens were also prepared through Sonogashira coupling reaction. Poly(phenylene ethynylene)s **167** with 4-vinylaniline pendant groups were prepared by the palladium-catalyzed Sonogashira coupling polymerization between

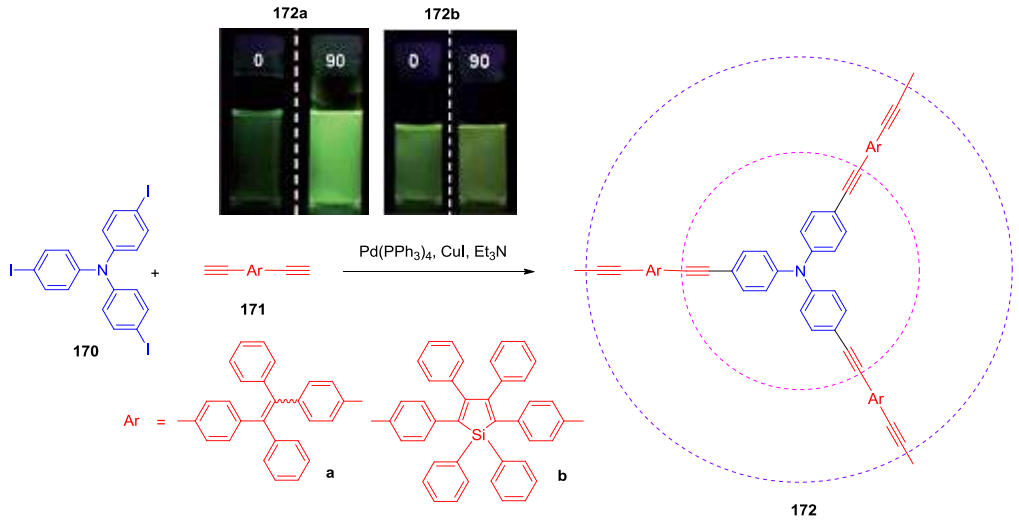

Scheme 25 Synthetic routes of hyperbranched poly(arylene ethynylene)s **172a–b** through Sonogashira polycouplings. Insets: fluorescence photographs of **172a–b** in THF and THF/water mixtures with 90 vol % water taken under UV illumination. Adapted with permission from Ref. 80. Copyright 2012 Wiley-VCH.

1,4-diethynyl-2,5-bis(pentyloxy)benzene **165** and 4-[2-(2,5-dibromophenyl)vinyl]-aniline **166** in a mixture of toluene and diisopropylamine (Scheme 24D).[77] When molecularly dissolved, the dilute THF solution of **167** is virtually luminescent and emits at 470 nm with a shoulder peak at 500 nm. When large amount of hexane was added into the solution, the magnitude of the PL was increased by 3-fold. Φ_F of **167** in the mixtures of THF/hexane increased with increasing fractions of hexane. Interestingly, if the amino groups in **167** were changed to hydrogen atoms, the luminescence of the resulting polymer is quenched in the aggregated states. It is reported that the intensity of emission of alkyl-substituted poly(*p*-phenylene ethynylene)s was strongly associated with the size and geometry of the side chain, which affected the torsion angle and the relative movement of the phenyl rings.[78] Because of the existing pendant amino groups, the inter-chain and intra-chain hydrogen bonding interactions in **167** strengthen and widen the distance between the polymer backbones, thus avoiding nonradiative decay processes caused by π–π stacking. Furthermore, a third component was added to this polymerization. Under similar Pd-catalyzed Sonogashira coupling polymerization conditions, monomers **165**, **166**, and 3,6-dibromo-9-octylcarbazole **168** was polymerized to afford poly(phenylene-ethynylene-carbazole) **169** with the ratio of aniline units to ethynyl-benzene units to carbazole units at 0.54: 1: 0.46 (Scheme 24E).[79] The THF solution of polymer **169** emits at 491 nm with a Φ_F of 7.05%. Nonsolvents such as water, methanol and hexane were added into the solution of **169** to study the aggregation emission. When adding water, the fluorescent intensity first gradually decreased, but the intensity then increased when more than 60% water was added. When methanol was added into the THF solution, emission enhancement was not observed; when *n*-hexane was added, there was emission enhancement. For both **167** and **169**, the amino groups can strengthen the intermolecular and intramolecular interactions of the polymers and restrict the non-radiative energy transitions, which provide a new model for designing highly emissive conjugated polymers by adjusting side-group interactions.

If the monomers in the Sonogashira polycoupling were designed to have more than two functional groups, hyperbranched polymers can be obtained. Tris(4-iodophenyl)amine **170** with three functional groups was thus coupled with 1,2-bis(4-ethynylphenyl)-1,2-bis(phenyl)ethene **171a** and 2,5-bis(4-ethynylphenyl)-1,1,3,4-tetraphenylsilole **171b** in THF/Et_3N at room temperature using $[Pd(PPh_3)_4]$ and CuI catalysts (Scheme 25).[80] To prepare soluble polymers with high M_w, long flexible alkyl chains are commonly used to decorate the polymers. In this work, with decreased monomer concentration of ~10.5 mM, conjugated hyperbranched polymers **172a–b** were obtained in good yield and high M_w up to 86 100. They are fully soluble hyperbranched polymers without any alkyl chain decorations, which should be attributed to the propeller-like twisted configurations of the TPE and triphenylamine moieties as well as the hyperbranched architecture which efficiently impeded the strong intermolecular π–π stacking interactions. **172a** is emissive in solution with a Φ_F of 1.89%. In its 90% aqueous mixture, the PL intensity at 526 nm increased about 8-fold. On the other hand, **172b** showed no significant change upon aggregation in aqueous media, most likely due to the bulky and crowded structure.

Not only can the Sonogashira coupling reaction be conducted between alkynes and aromatic halides, but it can also be used between alkynes and carbonyl chlorides.[81] The polymerization of TPE-containing diyne **101** and commercially available dicarbonyl chloride **173** was studied under the Sonogashira reaction condition (Scheme 26A).[82] After studying the effect of the catalyst concentration, reaction time, sequence of monomer addition, and organic base concentration, the optimized reaction was conducted at a catalyst concentration of 5 mM with one equivalent triethylamine, which proceeded smoothly, affording **174** with good solubility and high M_w. **174** emits a yellow light at 550 nm in THF solution. The addition of water enhanced the emission intensity by more than 10-fold in a 90% aqueous media and slightly hypsochromically shifted the spectrum. Polymer **174** can further react with N_2H_4 **175** rapidly and efficiently to afford **176**, causing significant fluorescent enhancement, therefore it can be potentially used as a fluorescent "turn-on" sensor as will be discussed in section 4.1.

Changing the catalysts and the reaction conditions can generate polymer products with totally different chemical structures from the exact same monomers. A new polymerization route for the regio- and stereoselective synthesis of linear poly(arylene chlorovinylene) **177** was reported by decarbonylative polyaddition of the same alkyne **101** and aroyl chloride **173**, which proceeds smoothly, producing linear poly(arylene chloro *Z*-vinylene)s in a regio- and stereoselective manner in high yield (Scheme 26B).[83] **177** emits green light at 520 nm in THF solution. Addition of 90% of water into its solution slightly enhanced its light emission, while keeping the spectral profile unchanged.

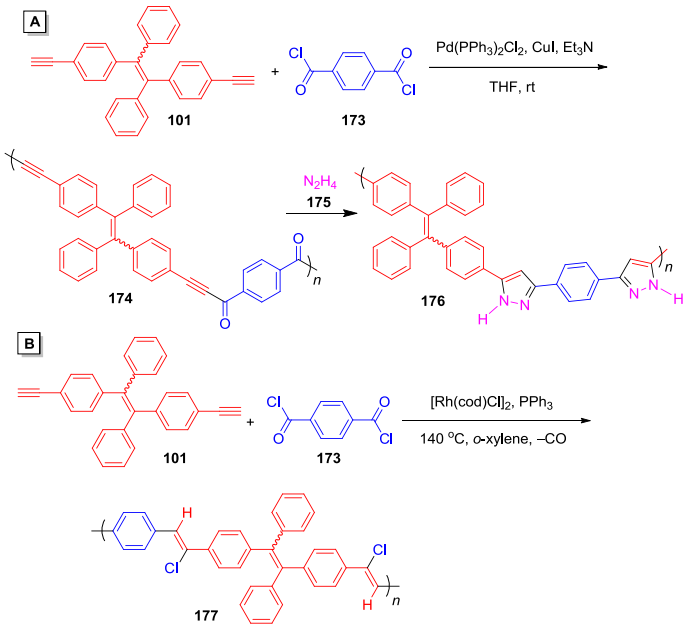

Scheme 26 Synthetic routes of polymers **174** and **177** through transition metal-catalyzed polycouplings between dialkyne **101** and dicarbonyl chloride **173**.

2.13 Hay-Glaser polycoupling

Terminal carbon-carbon triple bonds can be self-coupled to form C≡C–C≡C group through the Hay-Glaser coupling reaction. For such polymerizations, only a single component of monomer with one type of functional group is involved. This is a great advantage considering that no strict stoichiometric balance of two/multi-monomers is required to obtain high molecular weight polymer products. Take TPE-containing diyne monomer **101** for example, it can be self-coupled under the catalysis of CuCl and tetramethylethylenediamine (TMEDA) in *o*-dichlorobenzene to form linear polymer **178** with TPE units linked together with diyne units (Scheme 27A).[37] Similarly, silole-containing diyne monomer **179a–b** can also be polymerized under the same condition, forming soluble linear polyynes **180a–b** in quantitative yields with high M_w up to 54 200. The aggregates of the polymers **178** and **180a–b** emit in the range of 503–523 nm with $\alpha_{AIE,\Phi}$ values of 39 (**178**), 5 (**180a**), and 4 (**180b**). Cross coupling between *N*,*N*-bis(4-ethynylphenyl)aniline **181** and TPE-containing monomer **101** can furnish AIE-active random copolymer **182** quantitatively with M_w of 72 800.

Potentially modifiable sites can be introduced to AIE polymers through such polycouplings. For example, TPE-containing diyne monomers **183** and **186** with one or two reactive bromoethoxy groups can be polymerized through Hay-Glaser coupling reaction at 50 °C in the presence of CuCl and TMEDA in *o*-dichlorobenzene. After 5 h, TPE-containing polyynes **184** and **187** were facilely obtained with high yield (up to 99%) and high M_w (up to 38 900),

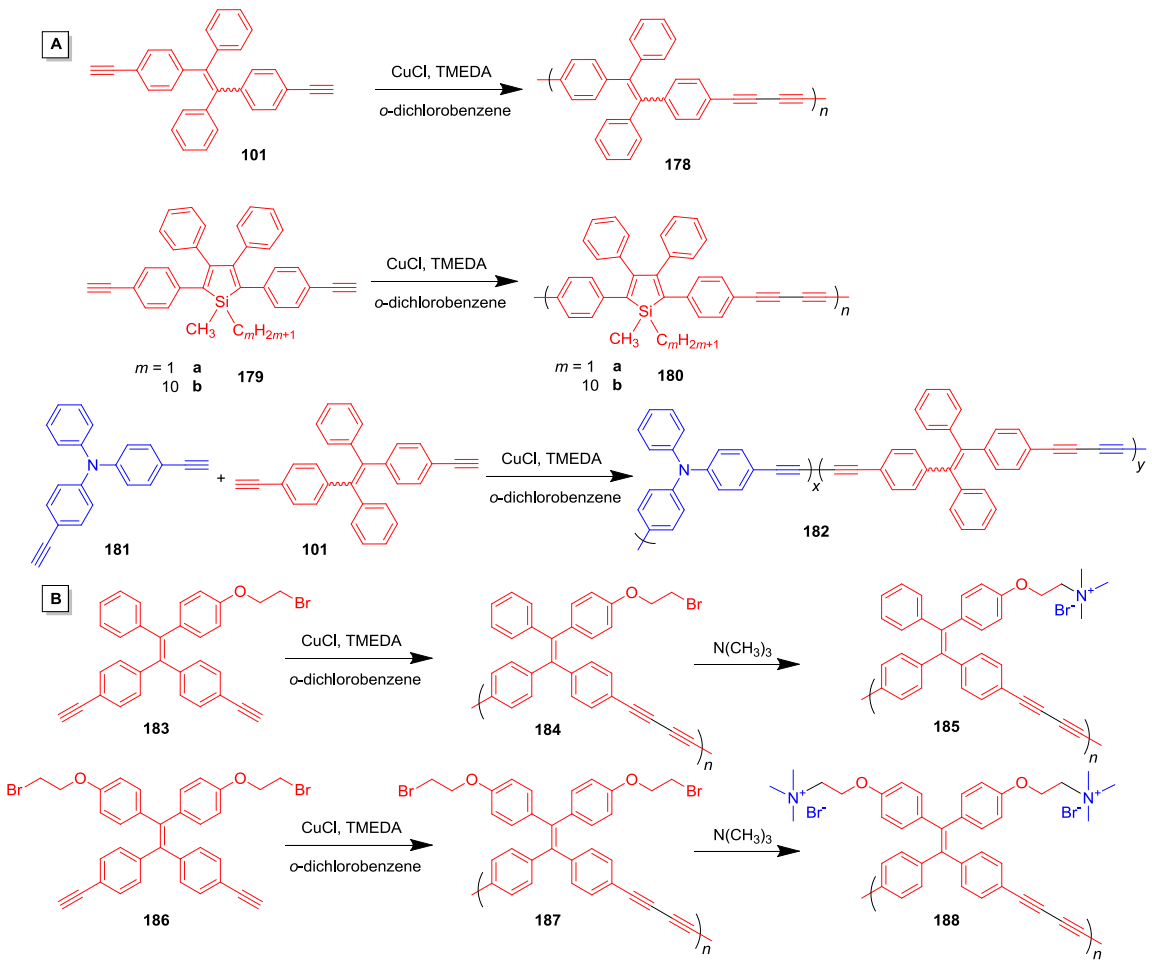

Scheme 27 Synthetic routes of AIEgen-containing polyynes through Hay-Glaser polycouplings.

respectively (Scheme 27B).[84] As shown in Fig. 4, **184** is nonemissive in solution, when its chains aggregate in the presence of water, an emission peak emerges at 536 nm. Unlike **184**, **187** emits faintly even in THF solution. They both show enhanced fluorescent intensity with the $\alpha_{AIE,\,I}$ values of 65 (**184**) and 15 (**187**). The steric effect of the two bromoethoxy groups in **187** might inhibit the free rotation of the TPE units to some extent, thus rendering the polymer emissive in solution. It also makes the polymer adopt a more twisted structure, and hence a bluer emission is detected in the aggregated state than in that of **184**. Both polymers can be further modified by positive charges to form polyelectrolytes **185** and **188**, which may be potentially utilized in biosensor applications.

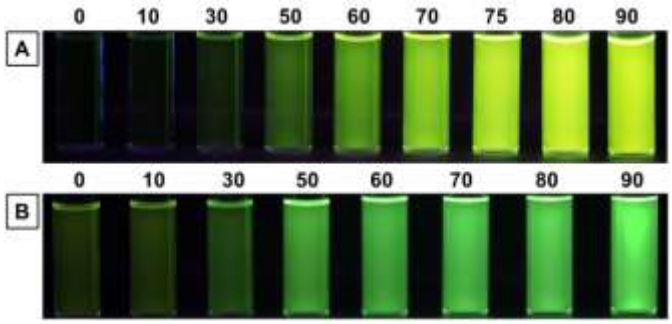

Fig. 4 Fluorescence photos of (A) **184** and (B) **187** in THF/water mixtures with different water fractions taken under 365 nm UV irradiation. Adapted with permission from Ref. 84. Copyright 2013 Wiley-VCH.

2.14 Cyclotrimerization Polymerization

Cyclization polymerization represents another efficient approach for constructing conjugated polymers. Different from polycouplings in which the monomers were connected through C–C, C=C, C≡C, or C≡C–C≡C linkages in the polymer product, cyclization polymerization generate new aromatic rings in situ which directly serve as linkages to connect each repeating unit of the polymers. In particular, cyclotrimerization is an appealing reaction where three C≡C bonds are reacted together to form a new benzene ring. Like the Hay-Glaser polymerization, only a single monomer component with one type of reactive group is involved in the polymerization which simplifies the monomer synthesis and polymerization condition control to a great extent. With this in mind, this idea was applied to prepare AIE-active hyperbranched polymers with large M_w. The remaining challenge would be the solubility of such a conjugated aromatic polymer system with hyperbranched architecture.

A series of A_2-type silylenediyne monomers **189a–c** were polycyclotrimerized under the catalysis of $TaBr_5$ to afford soluble hyperbranched poly(silylenephenylenes) **190a–c** with M_w of up to 19 700 (Scheme 28A).[85] $TaBr_5$ was used instead of $TaCl_5$, owing to its comparatively lower catalytic activity, reducing the likelihood of uncontrollable propagation to give insoluble gels. From the cyclotrimerization of C≡C bonds, 1,2,4-trisubstituted and 1,3,5-trisubstituted benzenes may form, so both isomeric structures exist in the polymer product. Although the monomers are neither AIEgens, nor efficient luminogens, polymer **190a–c** emit at 380 nm after the new benzene ring is formed which extend the conjugation.[86] When water is added into a THF solution of **190a**, nanoaggregates of the polymer are formed and its photoluminescence is enhanced. Fluorescent Φ_F of a solid film of the polymer (23%) is much higher than that of its THF solution (7%), verifying its AIE nature. The fluorescent photo of the solid powder of **190a** under UV irradiation is inset in Scheme 28A.

After successful exploration of this polymerization approach, AIEgen-containing 1,1-dialkyl-2,5-bis(4-ethynylphenyl)-3,4-diphenylsiloles **191a–b** were used as monomers to be polymerized under similar reaction conditions. The polymerization was catalyzed by $TaBr_5$ in toluene at a catalyst concentration of 2.5 mM. After stirring at room temperature for 1 h, soluble hyperbranched poly(2,5-silole)s **192a–b** were obtained with high molecular weights (up to 250 000) and high yields (up to 98%) (Scheme 28B).[87] The polymers are somewhat luminescent at 508–510 nm in their THF solutions because the silole units are located within the stiff polymer backbone, which limit their intramolecular rotations to some extent. Addition of water into THF solutions induces their aggregate and enhances their PL. The Φ_F of the THF solutions of **192a** and **192b** is 3.0% and 5.2%, respectively, and the values in the THF/water mixtures with 90 vol % water is 15.4% and 18.4%, respectively. Additionally, the Φ_Fs in the solid state is 25.6% (**192a**) and 23.3% (**192b**).

The polycyclotrimerization of TPE-functionalized diyne is also explored (Scheme 28C).[88] The polymerization of TPE-containing diyne monomer **101** was catalyzed by $TaBr_5$, affording the hyperbranched polymer **193**. With the twisted structure of TPE units inside the polymer backbone, even without any solubility-enhancing alkyl chains, the product retains good solubility while possessing high M_w. The THF solution of **193** emits faintly at 501 nm; when 95% water was added to the solution, the PL intensity increases by 11-fold (Fig. 5A). The Φ_Fs for its solution, aggregates and solid is 3%, 45% and 47%, respectively.

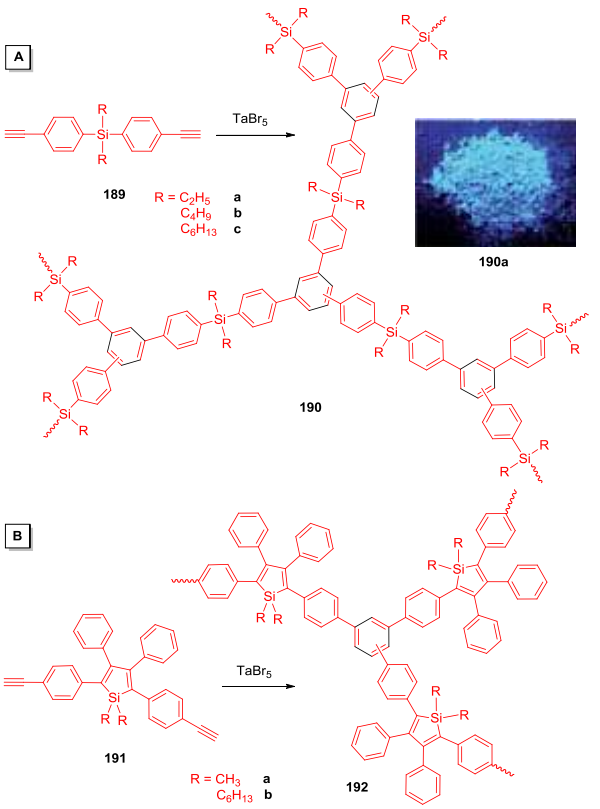

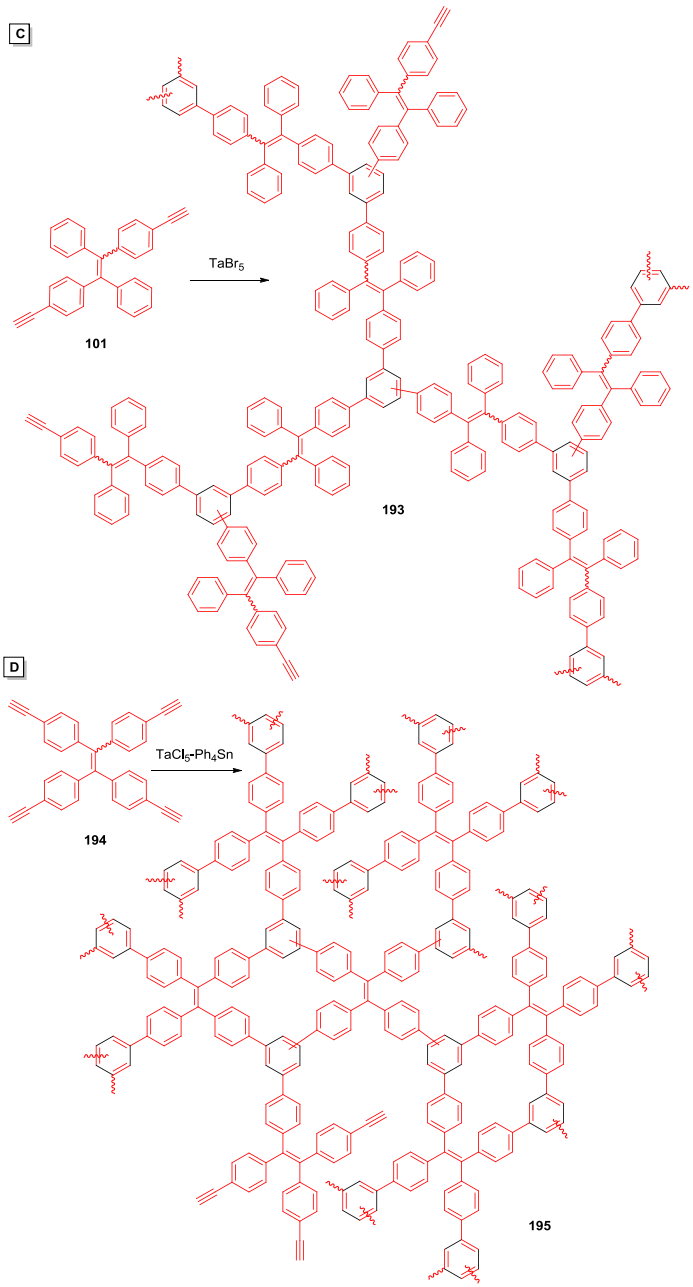

Scheme 28 Synthetic routes of hyperbranched poly(arylene)s through alkyne polycyclotrimerizations. Inset: fluorescent image of solid powder of **190a** under UV irradiation. Adapted with permission from Ref. 86. Copyright 2010 The Royal Society of Chemistry.

With the successful preparation of soluble hyperbranched AIE polymer from polycyclotrimerization, the homocyclotrimerization of monomers with multiple functional groups were further explored. A TPE-containing A_4-type tetrayne, named 1,1,2,2-tetrakis(4-ethynylphenyl)ethene **194** was synthesized for the homopolycyclotrimerization (Scheme 28D).[89] The $TaCl_5$–Ph_4Sn catalytic system with high catalytic activity was chosen considering that the severe steric hindrance of the polymerization might result in low monomer activity. To obtain soluble hyperbranched polymer with high M_w, the reaction condition was optimized with low monomer concentration of 0.05 M and 5% catalyst loading ratio to afford soluble hyperbranched poly(tetraphenylethene) **195** with high M_w of 280 000 in high yield of 97%. Despite weakly, **195** emits at 523 nm in THF solution. The emission intensity starts to increase in the presence of a small amount of water and reaches its maximum value at 95 vol % aqueous media. As shown in Fig. 5B–E, the polymer powder appears yellow under daylight, which gives green, yellow and red emission when exposed to UV, blue and green illumination, respectively.

Besides C≡C, C≡N triple bond can also undergo cyclotrimerization to form 1,3,5-triazine.[90] Moreover, the reaction is straightforward in the sense that no regioisomers are involved in the structure of the product. Cyclotrimerization of nitriles was thus developed as new metal-free polymerization method to construct an AIE-active hyperbranched polymer. TPE-containing monomer **196** with two aromatic cyano functional groups was synthesized and polymerized under the catalysis of strong organic acid CF_3SO_3H to afford hyperbranched polytriazine **197** with a M_w of 16 600 (Scheme 29).[91] **197** is AIE-active and the $\alpha_{AIE,\Phi}$ value is 9.

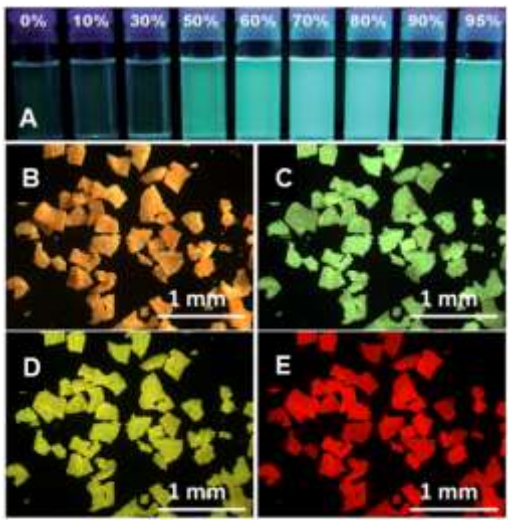

Fig. 5 Fluorescence images of (A) **193** in THF/water mixtures with different water fractions taken under 365 nm UV irradiation. (B–E) Fluorescence images of solid powder of **195** taken under different light illuminations. Excitation wavelength: (B) daylight, (C) 330–380 nm, (D) 450–490 nm and (E) 510–550 nm. Adapted with permission from (A) Ref. 88. Copyright 2012 The Royal Society of Chemistry; (B–E) Ref. 89. Copyright 2013 Wiley-VCH .

2.15 Click Polymerization

Alkyne-azide click reaction is a popular reaction in polymer chemistry and biological modification. Its recent developments in polymerization are summarized in several review papers.[92] It is an efficient and convenient approach to prepare AIE polymers with unique functionalities.

For example, 1,3-dipolar polycycloaddition was conducted between diyne monomer **198** and TPE-containing diazide monomers **199a–b** (Scheme 30A).[93] The polymerization was first carried out using $CuSO_4$/sodium ascorbate in a THF/water mixture under "standard" click reaction condition. The resultant polymers **200a–b** were insoluble due to the low solvating power of the aqueous mixture to the polytriazoles. The click polymerization in organic media using an organosoluble catalyst $Cu(PPh_3)_3Br$ was then adopted in THF at 60 °C for 12 h to produce **200a** with a M_w of 12 100, which is partially soluble in THF. Its cousin **200b** with longer methylene spacers, on the other hand, possessed enhanced solubility

and can be completely dissolved in THF even when the M_w reached 36 600. The click polymerization under the catalysis of Cu(I) regioselectively generates 1,4-substituted triazole structures. Both polymers are virtually nonluminescent when molecularly dissolved in their good solvents. When large amounts of water (> 60 vol %) are added into the solutions, strong PL peaks are observed at 481 nm under identical measuring conditions. The changes in the Φ_F values of **200a–b** in aqueous mixtures with different water fractions further confirm the AIE characteristics of the polymers. In pure solvent, THF, **200a** and **200b** give small Φ_F values (0.16% and 0.18%, respectively). In 90 vol % aqueous mixtures, the Φ_F of **200a** and **200b** reach ~17.8% and 16.9%, which are 111- and 94-fold higher than those in the pure solutions, respectively.

The click reaction between aromatic azides and aromatic alkynes can also afford processable polytriazoles with AIE characteristics. Monomer **201** with two azide groups directly linked to the 2,7-positions of fluorene was reacted with diyne monomers **202a–b** under the catalysis of $Cu(PPh_3)_3Br$ to afford linear polymers **203a–b** (Scheme 30B).[94] Similarly, fluorene-containing diyne **204** and aromatic diazides **205a–b** can react to produce polymers **206a–b** through click polymerization. As shown in the inset of Scheme 30B, polymers **203a** and **206a** are AIE-active, while **203b** and **206b** with phenyl groups replaced by hydrogen atoms are not, suggesting that subtle structural variation from TPE to stilbene units can lead to different PL behavior upon aggregation.

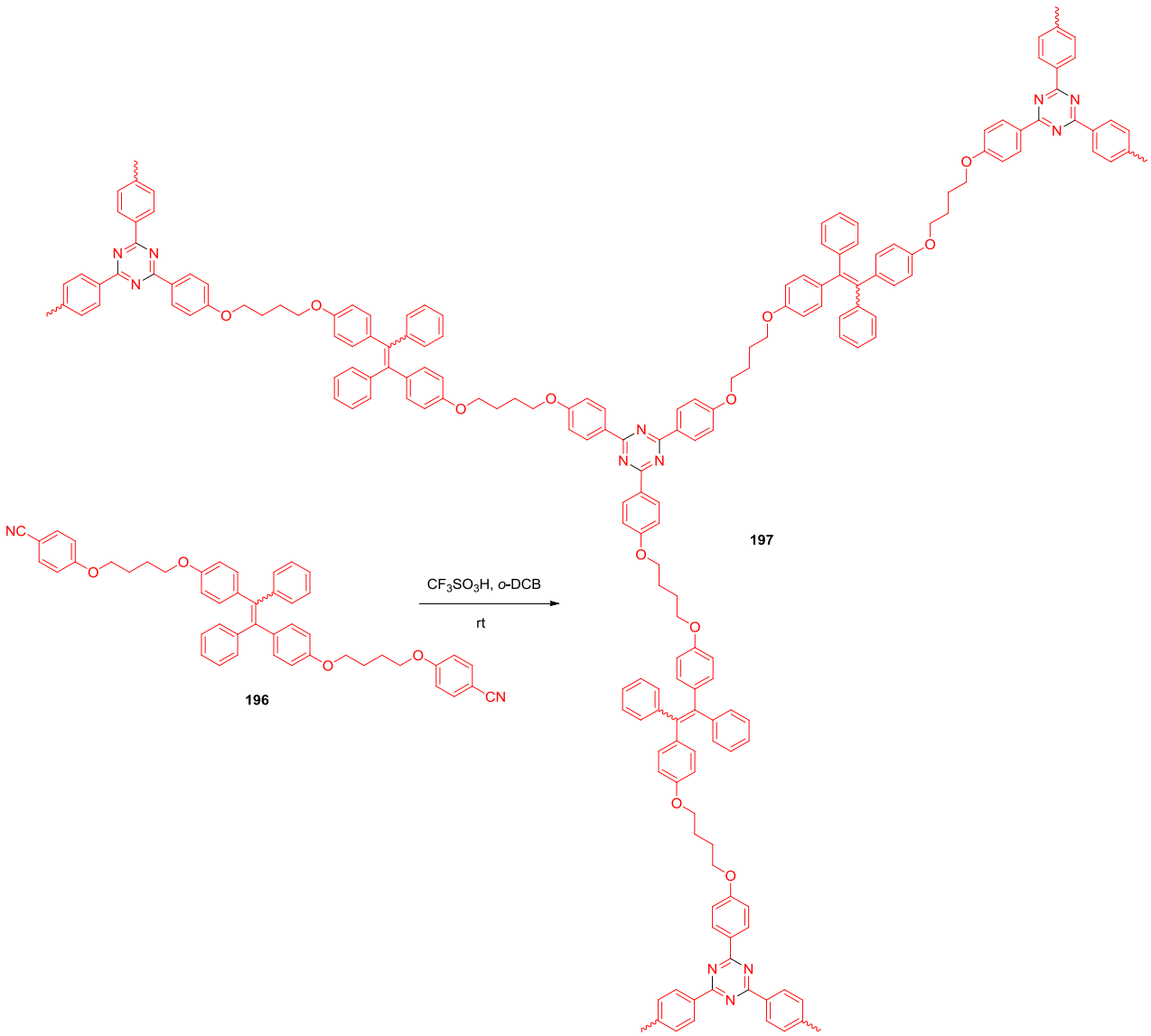

Scheme 29 Synthetic route of hyperbranched poly(1,3,5-triazine) **197** through polycyclotrimerization of nitrile **196**.

As introduced before, metal-free polymerization is of great importance and enjoys a range of benefits. In the Cu(I)-catalyzed azide-alkyne click polymerizations, the removal of metallic residues after reaction is always a great challenge. The metal-free click polymerization of activated alkynes and azides are thus of great interest to avoid such problem. The general design principle for such metal-free click polymerization is to attach electron-withdrawing groups on the alkyne/azide monomers to enhance the monomer activity, thus enabling the thermal polymerization to react smoothly without metal catalysis. As such, bis(aroylacetylene) monomer **207**

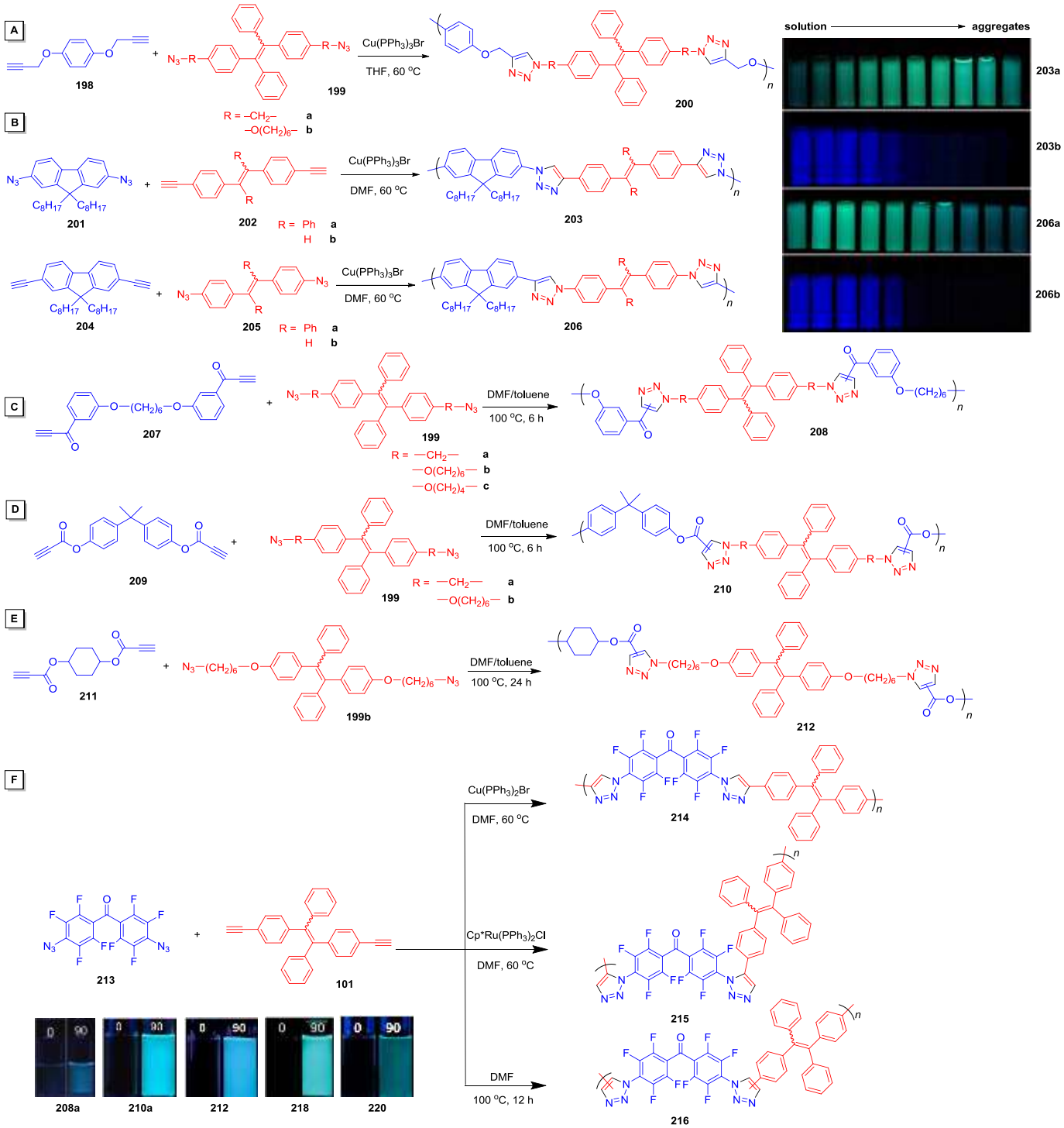

Scheme 30 Synthetic routes of TPE-containing linear poly(aroyltriazole)s through click polymerizations. Insets: fluorescence photos of (B) **203a–b** and **206a–b** in THF/water mixtures with different water fraction and (F) the poly(aroyltriazole)s in pure THF and a THF/water mixture with 90 vol % water content taken under illumination of a handheld UV lamp. Adapted with permission from (B) Ref. 94. Copyright 2014 The Royal Society of Chemistry; (F) Ref. 95. Copyright 2009 Wiley-VCH; Ref. 96. Copyright 2011 Springer; Ref 97. Copyright 2012 The Royal Society of Chemistry; Ref. 99. Copyright 2011 The Royal Society of Chemistry; Ref. 100. Copyright 2013 American Chemical Society.

with carbonyl groups directly linked on the terminal C≡C bonds were designed and synthesized, from which higher activity could be expected. Indeed, the thermal click polycycloaddition reactions of a series of TPE-containing diazides **199a–c** and **207** proceeded well in a solvent mixture of DMF/toluene (1:1 v/v) at a moderate temperature of 100 °C. The metal-free click polymerizations initiated by simple heating propagated smoothly in an open atmosphere without protection from oxygen and moisture and furnished poly(aroyltriazole)s **208a–c** with high molecular weights (up to 25 200) and high regioregularities ($F_{1,4}$ up to 95%) in high yields (up to 85%) (Scheme 30C).[95] In pure THF, **208a–c** all exhibit negligibly small Φ_F values (~0.1%), and in THF/water mixtures with 90 vol % water content, the Φ_F values of **208a–c** are increased to 7.1%, 1.9%, and 1.5%, respectively.

The same monomer design strategy was used in the click polymerizations of aromatic and aliphatic dipropiolates. For example, the 1,3-dipolar polycycloadditions of 4,4'-isopropylidenediphenyl dipropiolate **209** and TPE-containing diazides **199a–b** were carried out in polar solvents such as DMF/toluene at a moderate temperature of 100 °C for 6 h, producing poly(aroxylcarbonyltriazole)s **210a–b** with high M_w (23 900) and regioregularities ($F_{1,4}$ up to 90%) in high yields (up to 99%) (Scheme 30D).[96] The aliphatic dipropiolate **211** was also reacted with the TPE-containing diazide **199b** to prepare functional poly(aroyltriazole) under optimal reaction condition (Scheme 30E).[97] Polymer **212** with high M_w (23 500) and regioregularities ($F_{1,4}$ of 86.2%) was obtained in 99% yield. In THF solution, **210a**, **210b**, and **212** are nonemissive with the negligibly small Φ_F values of 0.62%, 0.38%, and 0.37%, respectively. The values increase gradually with the addition of water and reach 24.8% (**210a**), 21.5% (**210b**) and 30.1% (**212**) in the THF/water mixtures with 90 vol % of water content.

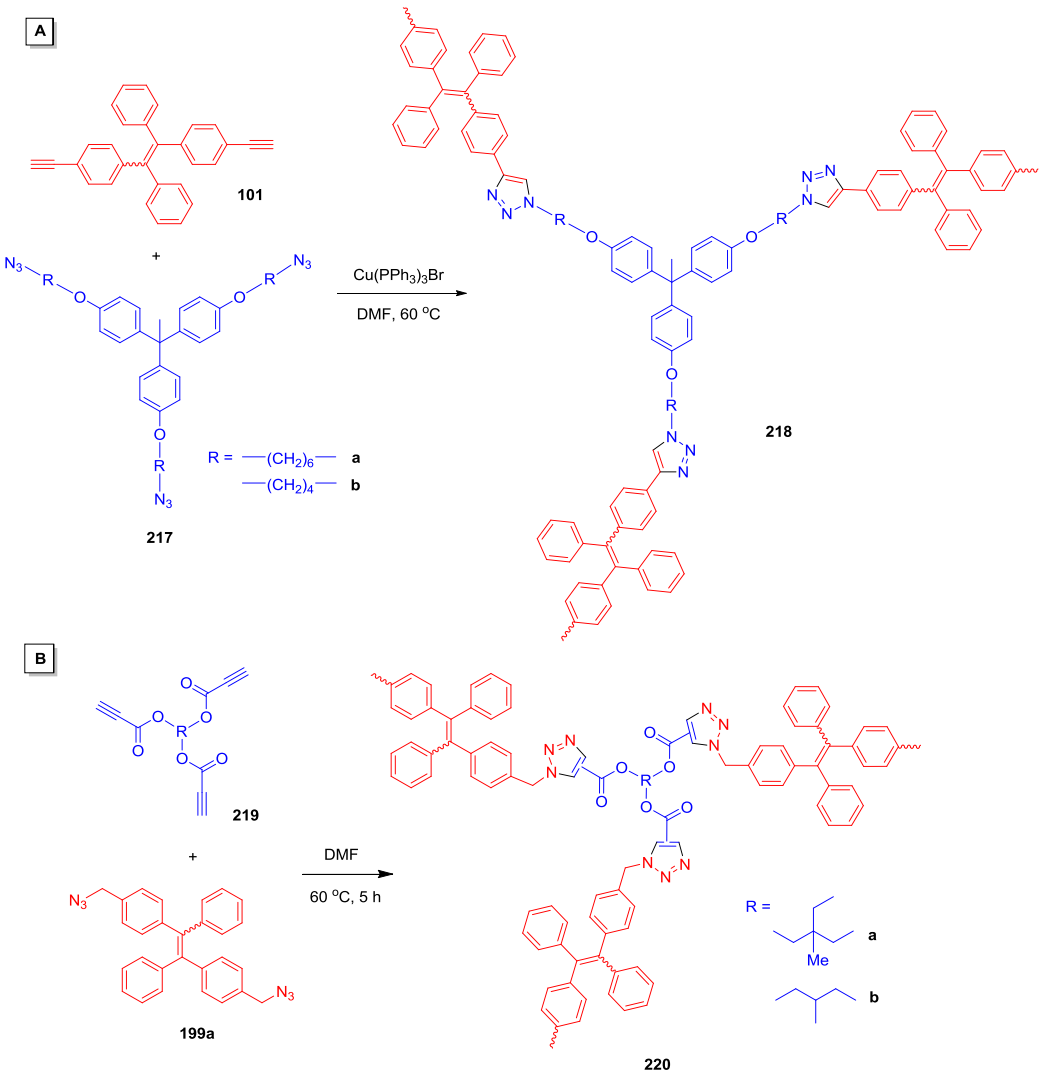

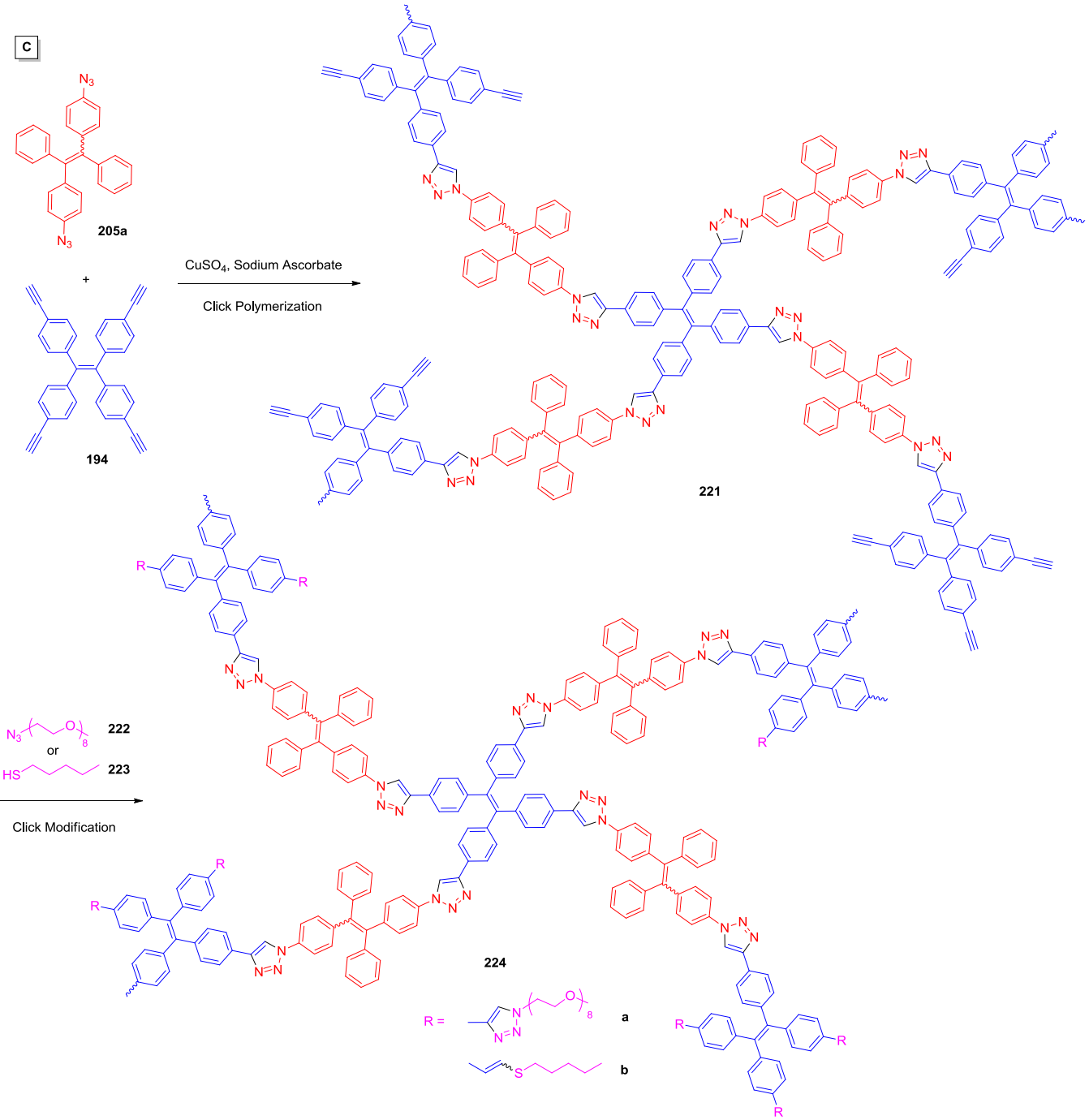

Scheme 31 Synthetic routes of TPE-containing hyperbranched poly(aroyltriazole)s through click polymerizations.

To gain a better understanding of the reaction pathway, various click polymerization conditions were compared. The activated aromatic azide of 4,4'-diazidoperfluorobenzophenone **213** was polymerized with diyne monomer **101** under three different catalytic conditions. When the polymerization was catalyzed by $Cu(PPh_3)_3Br$, 1,4-regioregular polytriazole **214** with a high M_w of 21 500 was obtained, while the catalysis of $Cp^*Ru(PPh_3)_2Cl$ affords 1,5-regioregular polytriazole **215** (Scheme 30F).[98] When the polymerization was conducted at 100 °C in DMF for 12 h, the polytriazole **216** with both 1,4- and 1,5-substituted triazole units was obtained. **214** and **216** are visually weak emitters in solution but intense PL peaks are recorded under the same condition when a large amount of water is added into their solutions, accompanied with gradual bathochromically-shifted emission. Intramolecular charge transfer between perfluorobenzophenone and TPE units might have taken place with the increase in solvent polarity. In 90% aqueous mixture, the highest emission intensities of **214** and **216** were recorded, which are 3.3 and 5.2-fold higher than those in their THF solutions, respectively. **215**, on the other hand, is non-emissive in THF and THF/water mixtures, which probably could be ascribed to the quenching effect of Ru catalyst residue.

Hyperbranched polytriazoles with AIE characteristics are also reported through $A_2 + B_3$ monomer strategy. $Cu(PPh_3)_3Br$-mediated click polymerizations of diyne **101** and triazides **217a–b** were conducted in DMF at 60 °C for 5–7 h, which readily furnished 1,4-regioregular hyperbranched polytriazoles **218a–b** with satisfactory

M_w (up to 12 400) in high yields (up to 88%) (Scheme 31A).[99] The Φ_F values of **218a** and **218b** are both negligible (0.11% and 0.14%, respectively) in pure solutions and remain almost unchanged until 40% of water is added. In the aggregated state, the $\alpha_{AIE,\Phi}$ value of **218a** and **218b** are calculated to be 348 and 230, which are two orders higher than some of the aforementioned polytriazoles. Furthermore, the Φ_F values of the spin-coated films of **218a** and **218b** are both measured to be 100% by integrating sphere.

Encouraged by the high efficiency of the metal-free click polymerization, the A_3-type tripropiolate monomers **219a–b** are polymerized with TPE-containing diazide **199a** to prepare hyperbranched poly(aroxylcarbonyltriazole)s (Scheme 31B).[100] After optimizing the polymerization conditions systematically, soluble hyperbranched polymers **220a–b** with satisfactory M_w and high regioregularities ($F_{1,4}$ up to 90.9%) were produced in high yields (up to 91.6%) in DMF at 60 °C without protection from oxygen and moisture. The $\alpha_{AIE,\Phi}$ values of **220a** and **220b** are 82 and 72, respectively.

A_2 + B_4 type monomer strategy is further adopted to construct soluble hyperbranched polytriazoles. The click polymerization of A_2-type diazide monomer **205a**, 1,2-bis(4-azidophenyl)-1,2-diphenylethene, and B_4-type tetrayne monomer **194**, 1,1,2,2-tetrakis(4-ethynylphenyl)ethene, was carried out in the presence of the classical $CuSO_4$/sodium ascorbate catalyst system in THF/triethylamine mixture with a minimal amount of water (Scheme 31C).[101] No gelation took place even when the polymerization was stirred at 60 °C for 12 h under nitrogen and hyperbranched polymer **221** with M_w of 47 100 was obtained in an excellent yield of 85.3%. With the ethynyl groups on the periphery, polymer **221** could be efficiently post-functionalized by azide-alkyne or thiol-yne click reactions. The functionalized PEG-N_3 **222** could be added after the click polymerization in one-pot and the PEG-functionalized polymer **224a** was produced after an additional 12 h. It is completely soluble in DMSO but partially soluble in THF because of the attached PEG segments. Alternatively, pentanethiol **223** was employed as a representative thiol compound to cap **221**. The alkyl sulfide-functionalized polymer **224b** was thus produced after they reacted in DMF at 80 °C for 24 h in the presence of AIBN, a radical initiator. The Φ_Fs of **221**, **224a** and **224b** in THF solutions are 4.31%, 5.04%, and 3.83%, respectively, while the values are increased to 23.83%, 33.48%, and 20.01% in 90 vol % aqueous mixtures. The thin film Φ_F values are 65.2% (**221**), 93.5% (**224a**), and 60.2% (**224b**). In general, **224a** has higher emission efficiency compared with the other two polymers in solution, aggregates and film. This might be attributed to the formation of compact nanoparticles of **224a** with a hydrophobic core consisting of TPE and triazole units and a hydrophilic shell composed of PEG chains.

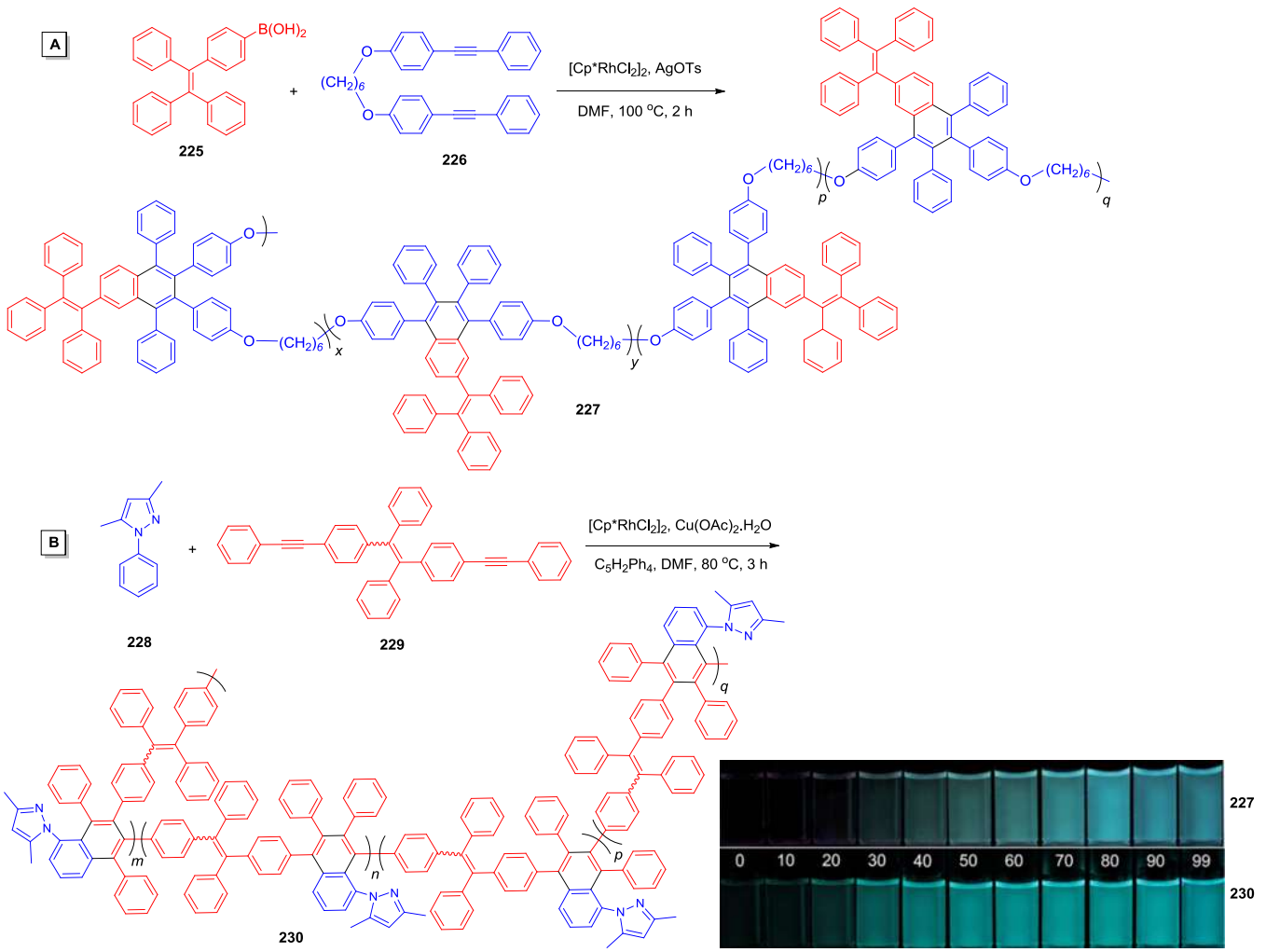

Scheme 32 Synthetic routes of multi-substituted naphthalene-containing polymers **227** and **230** through rhodium-catalyzed oxidative polycoupling of internal diynes. Insets: fluorescence photographs of **227** and **230** in THF/water mixtures with different water fractions taken under 365 nm UV irradiation. Adapted with permission from Ref. 102 and 103. Copyright 2013 The Royal Society of Chemistry.

2.16 Oxidative polycoupling

Last but not the least, development towards new polymerization methods shows great progress in recent years and the new approaches have been utilized to prepare AIE polymers.

The stoichiometric imbalance-promoted synthesis of polymer containing highly substituted naphthalenes was reported through rhodium-catalyzed oxidative polycoupling (Scheme 32A).[102] Oxidative polycoupling of AIEgen-containing (1,1,2-triphenylvinyl)phenylboronic acid **225** and 4,4'-(α, ω-alkylenedioxyl) bis(diphenylacetylene) **226** was carried out in DMF with $[Cp^*RhCl_2]_2$ as the catalyst and AgOTs as the oxidant, affording soluble polymer **227** with highly substituted naphthalene rings in 86% yield and a moderate M_w of 11 600. In the resultant polymer structure, regio-isomers were observed and four different structures coexisted in the product, including ortho-, para- and two types of meta-substituted naphthalene units. The Φ_F of **227** in THF solution was merely 0.18% and that in 90 vol % aqueous mixture was 4.15%, increasing by 23-fold. The Φ_F value can be further increased to 9.45% in the solid powder of **227**.

The atom-economical synthesis of poly(pyrazolylnaphthalene)s through another rhodium-catalyzed oxidative polycoupling between phenylpyrazoles and internal diynes was also reported (Scheme 32B).[103] The oxidative polycoupling of 3,5-dimethyl-phenylpyrazole **228** with 1,2-diphenyl-1,2-bis[4-(phenylethynyl)phenyl]ethene **229** was catalyzed by $[Cp^*RhCl_2]_2$ and 1,2,3,4-tetraphenylcyclopenta-1,3-diene and copper(II) acetate in DMF under stoichiometric imbalance conditions, affording soluble poly(pyrazolylnaphthalene) **230** with a molecular weight of 17 900. Similarly, four different regio-isomeric structures coexist in the polymer. Although **230** is constructed exclusively from rigid aromatic rings without any alkyl chain, it shows good solubility in common organic solvents, such as dichloromethane, chloroform, THF and toluene. It can be fabricated into tough, thin solid films by spin-coating or static-casting processes as well. From the THF solution to the aqueous mixture with 99 vol % water content, the relative PL intensity increased by 14-fold (Scheme 32, inset photo). The Φ_F of **230** in THF solution is 1.91% while it rose to 20.47% in 99 vol % aqueous media.

3. Structures and topologies

Through numerous polymerization methods discussed before, AIE polymers with various topological structures such as linear, zigzag, star-shaped, dendritic, hyperbranched, crosslinked, and three dimensionally ordered macromolecules can be easily accessed. As well, AIE polymers are normally based on typical AIEgens such as TPE, multiphenyl-substituted silole and DSA functional units. Recent years, new AIE-active compounds have been gradually developed such as tetraphenylthiophene derivatives, carborane derivatives, or even nonluminogen-containing compounds. In the following sections, polymers containing typical AIEgens or newly developed AIE-active moieties will be categorized based on their topological structures. In each section, examples of the corresponding structures will be discussed as well as how their structure affects their AIE nature.

3.1 Linear oligomers and polymers

Among various architectures of polymers, the linear shape is the simplest with repeating units linked together in a one-dimensional manner. Depending on the number of linearly linked repeating units, there are two types of linear shaped AIE macromolecules: linear oligomers and linear polymers.

Oligomers with identical structures and molecular weights are perfect models for the investigation of structure/property relationship. A series of amorphous fluorene-based oligomers **231–235** were end-capped with TPE groups to study the fluorescence change upon aggregation with different fluorene/TPE ratios, in comparison to random polymers **125a–d** as discussed in section 2.10. The two TPE units are installed on the terminal of fluorene oligomers with one to five fluorene units (Chart 2A).[104] As shown in Fig. 6A, when the number of fluorene unit increases, the THF solution gradually becomes emissive with the Φ_F increased from 0.3% to 2.1% from **231** to **235**. Energy transfer from the central fluorene units to terminal TPE units has taken place. When the number of fluorene units is small in **231**, energy transfer from fluorene to TPE occurs and the free rotation of TPE units then quenched the emission in the solution; when the fluorene number increases in **235**, the fluorescent quenching by the free rotation of two TPE units is not enough to quench the fluorescence from five fluorene units, thus the solution remains emissive and emit blue light from the fluorene units. Meanwhile, less water is needed to turn the non/weakly emissive solutions to emissive aggregates when there are more fluorene units. The Φ_Fs of the nanoparticles in THF/water mixtures with 90 vol % water content range from 25% to 41%, showing that the TPE end-capping groups have successfully transformed the linear oligofluorenes to AIE compound. The $\alpha_{AIE,\Phi}$ values for **231–235** are 125.3, 31.4, 28.2, 24.4, and 19.7, respectively. The highest solid state Φ_F of 68% was observed for **235**.

In another study regarding linear oligomers, a series of conjugated oligocarbazoles **236–238** with a 9,10-divinylanthracene (DVA) core has been synthesized (Chart 2B).[105] DVA segment as an AIEgen is installed in the centre of the linear oligomers and equal number of the carbazole units are linked with C=C bonds on both sides. With an increasing numbers of carbazole units and extending conjugation length, the solution emission is enhanced and the fluorescent enhancement after aggregation is gradually decreased (Fig. 6B, inset photo). The Φ_Fs of **236–238** in dilute THF solutions are 0.5%, 1.7% and 3.6%, respectively. Energy transfer from the carbazole units to the central DVA segment takes place. In the solution of **236**, the almost unrestricted intramolecular motions of the DVA segment can nonradiatively deactivate the excitons and quench the fluorescence. For **237** and **238** with large substitution groups and severe steric effect, however, the central DVA rotor is less free to rotate and results in slightly increased solution emission. In sharp contrast to their weak emission in the solution states, **236–238** emit strongly in the film state with Φ_Fs of 18.5%, 30.2% and 12.7%, respectively.

For linear polymers, there are various ways of integrating fluorophores into the polymer structures. As discussed in many previous cases, fluorophores can be embedded in the linear polymer main chain. Using thiophene-containing polymers as an example, a class of monodisperse nanoparticles of conjugated poly(bithiophene-*alt*-azulene)s **239a–f** were reported which have continuously tunable particle sizes over a wide range, up to 500 nm (Chart 3).[106] Nonemissive, molecularly dispersed polymer **239c** was aggregated into luminescent organic nanoparticles in mixed solvents as shown in the inset SEM image of Chart 3. The time-dependent fluorescence spectra of **239c** were investigated in the chloroform/methanol (1:1 v/v) mixed solvent for 4 h. Nanoparticles were gradually formed and grew in the mixed solvent and the fluorescence intensity at ~440 nm linearly increased with the particle size, demonstrating a unique size-dependent emission property. The significant enhanced emission of the nanoparticles upon aggregation is caused by the restricted intramolecualr rotation of the bulky alkyl groups and the restricted torsional motions.

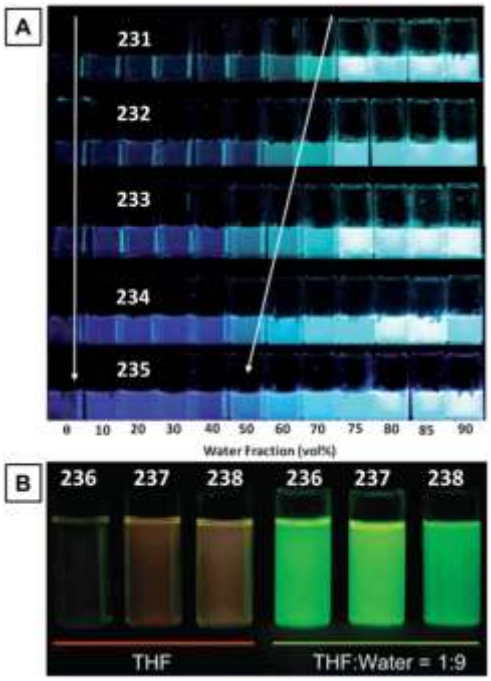

Fig. 6 Fluorescence photos of (A) **231–235** in THF/water mixtures with increasing water fractions from left to right and (B) **236–238** in THF solutions and THF/water mixtures with 90 vol % water fraction taken under the excitation of 365 nm illumination. Adapted with permission from (A) Ref. 104. Copyright 2012 The Royal Society of Chemistry; (B) Ref. 105. Copyright 2011 The Royal Society of Chemistry.

Besides incorporation into the main chains, the fluorophores can also be integrated as the side chains of linear polymers. For example, Hong's group reported the preparation of poly[2-(4'-vinylphenyl)-3,4,5-triphenylthiophene] **240** with pendant tetraphenylthiophene (TP) groups (Chart 3).[107] The molecules of **240** are dissolved in THF with no signal detected in the particle size measurement. However, in the THF/water mixtures with various water fractions, nanoaggregates with average diameters of 325–400 nm are detected and the suspended nanoparticles tended to shrink in size with increasing water content in the mixtures. As shown in the inset photo of Chart 3B, upon excitation at 330 nm, dilute THF solution of **240** emitted weakly and with the increasing water content, the corresponding solution mixtures exhibited a large enhancement in the emission intensity. More than 8-fold emission enhancement was observed for the 90 vol % aqueous solution compared to the THF solution. Φ_F of the THF solution of **240** is 4.42% and that of the 90% aqueous mixture is 37%. The Φ_F value measured from the solid is 55%, indicating an even higher extent of aggregation in the solid than in the solution aggregate suspensions.

In addition, there are also linear AIE polymers with fluorophores on the terminal or centre of the polymer backbones. Because of the versatile conformational possibilities of the polypeptide poly(γ-benzyl-L-glutamate) (PBLG), two PBLG-based polymers were prepared to probe the relationship between the secondary structure (α-helix) of polypeptides and the fluorescence (Chart 3).[108] Polymer **241** has a single PBLG chain tethered to TP, while polymer **242** has two. The mono-/di-amino functionalized TP initiators were used to polymerize the γ-benzyl-L-glutamate *N*-carboxyanhydride monomer through ring-opening polymerizations, to afford **241** and **242**, respectively. The THF solution of **241** is faintly emissive. From the 10 to 70 vol % water solutions, the emission intensities continuously grow until sudden emission reduction in the 90 vol % water solutions caused by precipitation. The two discernible, overlapped emission bands at 440 nm and 488 nm correspond to the monomer and the aggregate emissions, respectively. In contrast, the THF solution of **242** in THF emitted a large aggregate emission band located at 488 nm and inclusion of water resulted in little emission variation, which indicates that the steric restrictions from the two PBLG chains are large enough to prevent further aggregation of the TP fluorophores. The terminal TP units in **241** can easily approach each other to form aggregates with strong PL, while the intermolecular aggregation of the central TP unit in **242** is sterically blocked by the large α-helical PBLG chains. In addition, since the α-helical structure of PBLG can be disintegrated by adding trifluoroacetic acid (TFA), helix-coil transformation promoted by TFA alters the content of the secondary structures of PBLG chains. This helps the aggregation of the central TP fluorophores of **242** and lead to a large intensity jump of the aggregate emission compared to those observed in the neutral solutions. The emission of the solid films of **241** and **242** was also related to the relative fractions of the large α-helical secondary structure.

AIEgens can also be inserted into a linear polymer through polymer reactions. Three ethynyl-terminated poly(N-isopropylacrylamide)s (PNIPAMs) with different M_w were reacted with diazide-functionalized TP to furnish thermoresponsive polymers **243a–c** with two hydrophilic PNIPAM chains linked to the hydrophobic TP-centre (Chart 3).[109] Upon excitation at 320 nm, THF solution of **243a** emitted weakly. With the gradual hexane addition in the THF/hexane solvent mixtures, the resultant solutions significantly enhanced their emission intensities and an 83-fold intensity gain was achieved in the 90 vol % hexane solution when compared to THF solution (Inset photo, Chart 3C). Solutions of **243a** with low hexane content (< 60 vol %) have low Φ_F (~0.12%) but beyond that, Φ_F increase abruptly to reach 23% in the 90 vol % hexane solution, ~190 times of that in pure THF. The thermoresponsive PL emission will be discussed in section 4.2.

Another important group of linear polymers are conjugated polyelectrolytes (CPEs) with π-conjugated backbones and ionic side chains, which have unique properties such as good water solubility and dispersibility and can be used in various fields, especially in biological applications. CPE **244** with positive charges and ethylene glycol units was designed and synthesized (Chart 4).[110] The quaternized ammonium groups and hydrophilic oligo(ethylene glycol) linkages render **244** water soluble and in the water solution, **244** emits at 586 nm. Although graphene oxide (GO) is normally recognized as an efficient quencher for fluorescent materials, the fluorescence of **244** in 3 μM water solution increases up to 3.3-fold with the addition of GO from 0.2 to 2 μg/mL, accompanied with a slight blue shift of the emission maximum to 557 nm. GO can complex with amphiphilic **244** to create a hydrophobic environment for the polymer backbone which increases the PL. Further addition of GO into the same solution decreases the PL because **244** has been fully wrapped with GO and the quenching capability of GO plays a major role. In fact, such GO enhanced fluorescence is a general phenomenon for AIE-active fluorophores.[111]

Another water-soluble cationic conjugated polyelectrolyte **245** containing TPE and benzothiadiazole groups was reported (Chart 4).[112] Polymer **245** has great solubility in water and is insoluble in common organic solvents such as THF and acetone. The polymer is weakly emissive at 560 nm in water, but highly emissive when 99.9 vol % THF was added with a 7-fold fluorescence enhancement and a 30 nm red shifted emission color. The fluorescent images of water solution, water/THF (1:999 v/v) solution, and solid powder of **245** are shown in the inset photo of Chart 4.

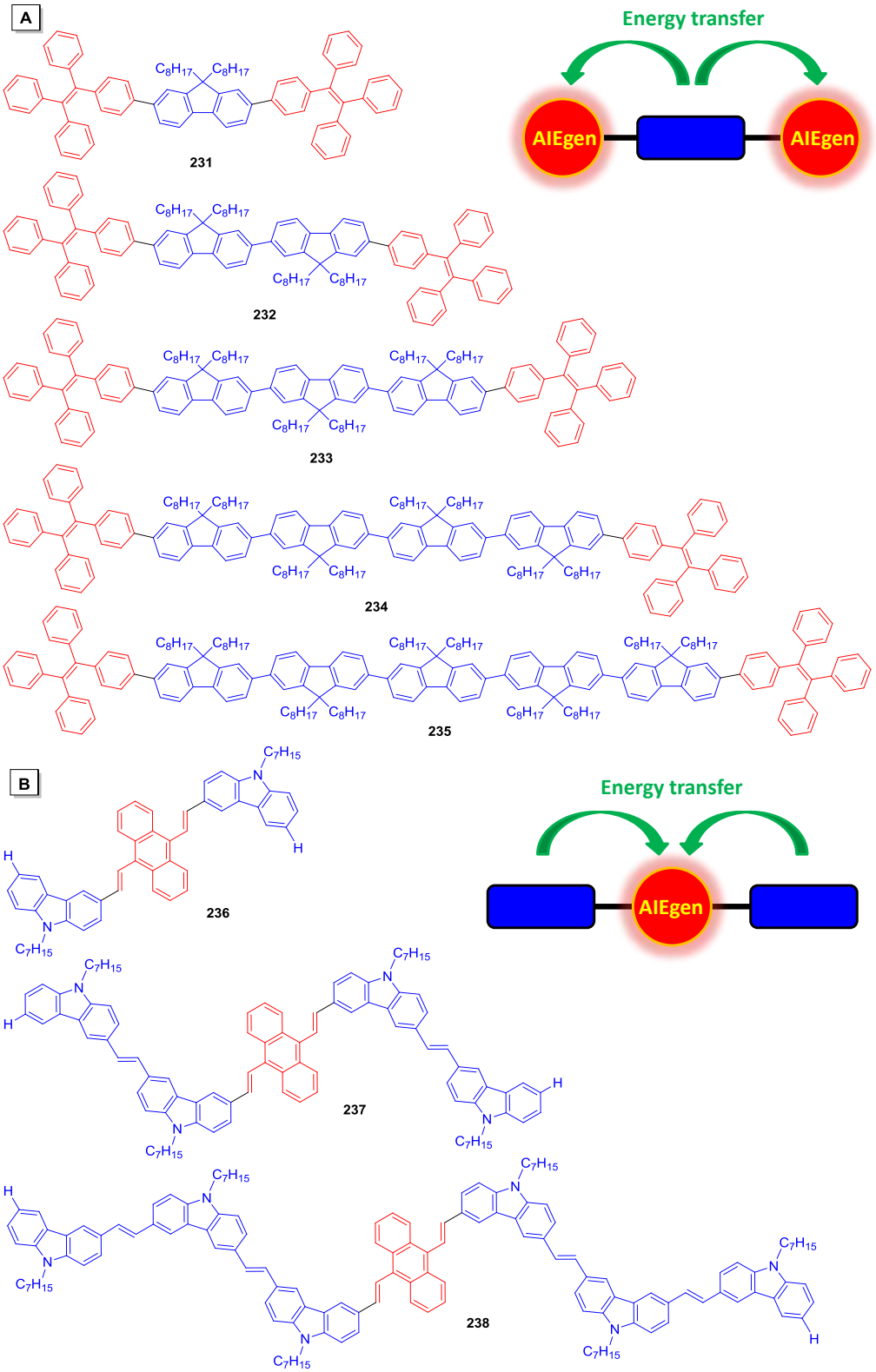

Chart 2 Chemical structures of conjugated oligofluorenes **231–235** end-capped with TPE and oligocarbazoles **236–238** with 9,10-divinylanthracene cores.

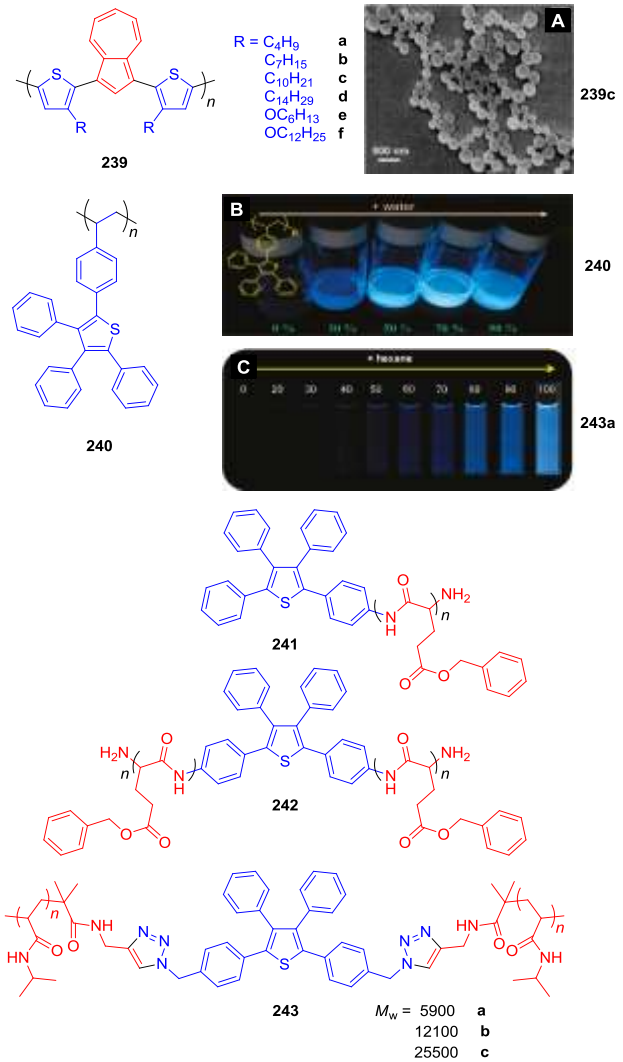

Chart 3 Chemical structures of AIE-active thiophene-containing linear polymers. Insets: (A) SEM image of nanoparticles of **239c**. Fluorescence photos of (B) **240** in THF/water mixtures with different water fractions and (C) **243a** in THF/hexane mixtures with different hexane fractions under UV illumination. Adapted with permission from (A) Ref. 106. Copyright 2005 American Chemical Society; (B–C) Ref 107 and 109. Copyright 2011 American Chemical Society.

A novel conjugated cationic polyfluorene **246** containing aminated tetraphenylethene (ATPE) units was designed based on the AIE property of the ATPE units and the fluorescent resonance energy transfer (FRET) from the blue-emissive fluorene segments to the yellow-emissive ATPE segments (Chart 4).[113] In the water solution, the emission of **246** was at 419 nm with a broad tail from 500 to 600 nm in THF solution. The strong blue emission could be attributed to the polyfluorene segments and no significant yellow emission from ATPE units was observed. With the obvious spectra overlap between the blue emission of the polyfluorene segments and the absorption of ATPE units, the energy transfer from the former to the latter should happen and the fluorescent Φ_F of **246** is determined to be 20% in aqueous solution. In the aggregated states, both the AIE effect of ATPE and the more efficient FRET from the blue-emitting polyfluorene segments to ATPE units amplify the yellow emission from the ATPE units dramatically. With these features, **246** can be used for fluorescent biosensor, as will be discussed in section 4.3.

The charges of the AIE-active CPEs can also be embedded in the polymer backbone. A conjugated poly(pyridinium salt) **247** with AIE features has been synthesized via the ring-transmutation polymerization reaction (Chart 4).[114] DMSO is a good solvent for **247** while water is not. The hydrophobic polymer chains of **247** tend to form aggregates in DMSO/water mixtures. Upon excitation at 400 nm, the DMSO solution of **247** emitted weakly at 615 nm. With increasing amounts of water, the corresponding solution mixtures exhibited up to 3-fold emission enhancement compared to pure DMSO solution of **247**. The AIE property is attributed to the restrictions of intramolecular rotations of conjugated backbone of **247** in the aggregate state.

There are also a few reports that by connecting two ends of the linear AIE polymers, the closed one dimensional topological structures such as cyclic AIE polymers were prepared.[115]

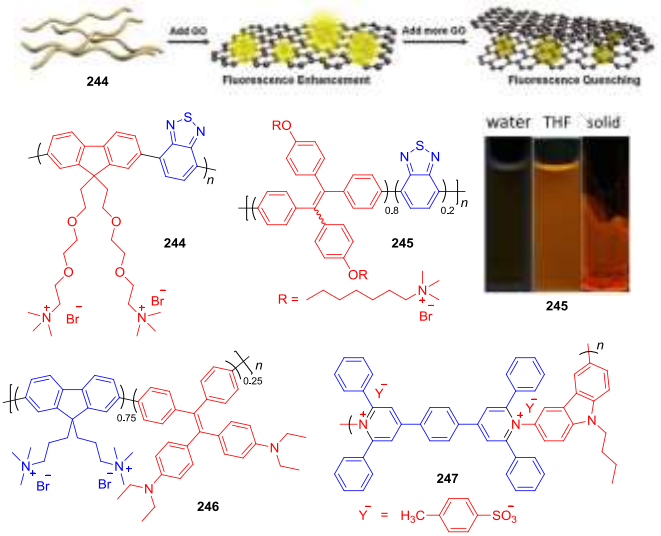

Chart 4 The schematic illustration of the graphene oxide concentration influence on the fluorescent intensity of **244** and the chemical structures of AIE-active linear polyelectrolytes **244–247**. Insets: fluorescence photographs of the water solution, THF solution and solid powder of **245** taken under UV illumination. Adapted with permission from Ref. 110. Copyright 2013 The Royal Society of Chemistry; Ref. 112. Copyright 2012 Acta Polymerica Sinica.

3.2 Zigzag polymers

Besides linear AIE polymers, there are also zigzag-shaped AIE polymers designed from bent building blocks. Carborane (1,2-dicarbadodecaborane) is such a candidate; it is an icosahedral boron cluster consisting of 10 boron atoms and 2 carbon atoms with three-centre two-electron bonds and three-dimensionally delocalized skeleton electrons (3D aromaticity). Carborane derivatives exhibit excellent thermal and chemical stabilities and possess a well-known highly polarizable σ-aromatic character. They are thus synthesized for the purpose of heat-stable materials, boron-neutron capture therapy, or coordination chemistry.[116] The introduction of luminescent π-conjugated segments onto the 1,2-position of the carborane would result in zigzag-shaped polymers.

Chujo's group reported a series of zigzag-shaped AIE-active alternating polymers **248a–d** with *o*-carborane and *p*-phenylene-ethynylene sequences prepared through Sonogashira-Hagihara palladium coupling polycondensation reactions (Chart 5).[117] **248a–c** with electro-donating π-conjugated linkers exhibited almost no emission in solution. In the mixed solvent of THF/water with 99 vol %

water content, they exhibited orange emission with emission maxima at 559, 550 and 583 nm, respectively, as well as large Stokes shifts which derived from charge transfer between the alternating donor and acceptor segments in the polymer backbone. The Φ_F of **248a** in THF solution is as low as <0.02%, while the value increased rapidly by 220-fold in the 99 vol % aqueous mixture. In the film state, **248a–c** displayed bright orange color as shown in the inset photo of Chart 5.

Polymer **248d** with axially chiral binaphthyl units in main chain was reported as the first example of introducing the *o*-carborane group into a chiral π-conjugated AIE polymer.[118] **248d** with electron-donating axially chiral linkers exhibited no emission in solution. Intramolecular charge transfer from electron-donating π-phenylene-ethynylene units to the antibonding orbital of C–C bond in *o*-carborane cluster resulted in nonradiative quenching process. In the mixed solvent of THF/water (1:99 v/v), **248d** emitted at 566 nm with Φ_F of 5% and in the film state, the Φ_F of **248d** is 23%, suggesting AIE phenomenon. This chiral polymer has two strong Cotton effects at 236 and 289 nm. Control experiments suggest that the employment of either meta-linked *m*-carborane or electron withdrawing groups to the polymer structures led to intense emission in solution state and no AIE feature.[117,118]

o-Carborane was also incorporated into polyfluorene to obtain zigzag-shaped polymer **249**.[119] In the chloroform solution, polymer **249** exhibits typical blue emission from the fluorene segments at ~ 420 nm and the *o*-carborane units in **249** give rise to small orange/red emissions, attributed to the energy transfer from the excited fluorene units to the electron deficient carborene cages. In the solid state, a green AIE peak appears, dominating at 520 nm, suppressing other emissions. The application of **249** as a vapochromatic photoluminescent sensor towards volatile organic molecules will be discussed in section 4.1.

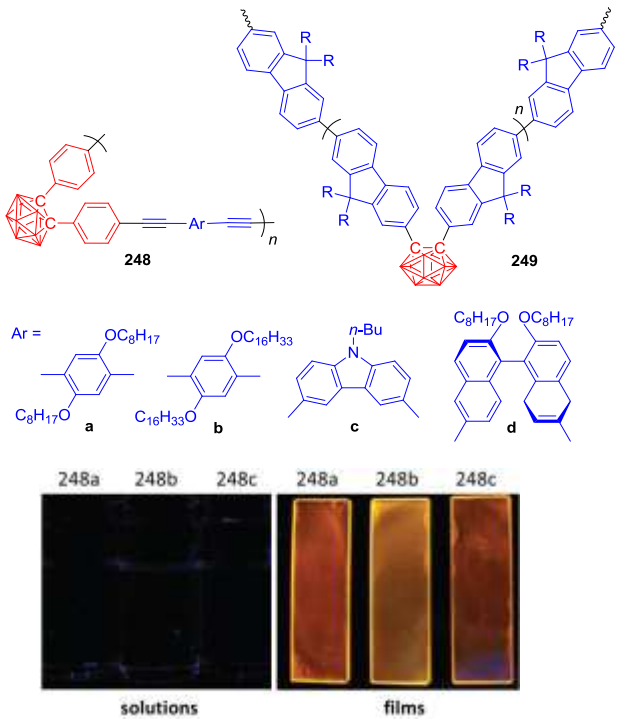

Chart 5 Chemical structures of *o*-carborane-containing zigzag-shaped polymers. Insets: fluorescence photographs of **248a–c** in solution and film states. Adapted with permission from Ref. 117. Copyright 2009 American Chemical Society.

3.3 Star-shaped macromolecules

The topological structures of the AIE macromolecules can be further extended to two/three dimensional architectures. A large number of star-shaped AIE oligomers have been reported. For example, a star-shaped luminogen **250** consisting of a triphenylamine core and three periphery 1,1,2,3,4,5-hexaphenylsiloles was reported (Chart 6).[120] Whereas **250** is practically nonemissive in the solution state with a Φ_F of 0.81%, it can be induced to emit intensely at 495 nm by aggregate formation (inset photo, Chart 6).

TPE derivatives have also been prepared as star-shaped oligomers. In compound **251**, TPE is designed as a core structure, while four triphenylethene moieties are attached on the periphery through Suzuki coupling reaction.[121] **251** emits at 502 nm in THF solution and the AIE effect is significant for **251** with fluorescent enhancement of about 20.1-fold in the aggregated states compared with the solution states. Similarly, compound **252** consisting of a TPE core and hydrophilic peripheral oligo(ethylene glycol) chains was synthesized.[122] This compound shows AIE nature which originates from the TPE core, and their peripheral oligo(ethylene glycol) chains impart water-solubility and thermosensitivity for the whole molecule. In another example, the TPE core is modified with four arms with discotic liquid crystalline units to obtain a star-shaped compound **253**.[123] This compound displayed both AIE behavior and liquid crystallinity. When mixed with 2,4,7-trinitrofluorenone, **253** exhibited a hexagonal columnar mesophase due to charge-transfer interactions in the binary mixture.

In addition to star-shaped siloles and TPEs, electron-donating diphenylamine, phenothiazine, or carbazole groups have been connected to the 1,4-positions of the benzene through bis(α-cyano-4-diphenylaminostyryl) conjugation bridges to form three triarylamine quadrupolar derivatives **254–256**.[124] The absorption maxima of these cyano-substituted diphenylamine styrylbenzene-based compounds **254–256** are located at 473, 443, and 435 nm, respectively, which is in agreement with the order of the increase of electron-donating ability of the donors: *N*, *N*-diphenylamine > phenothiazine > carbazole. They are very weakly fluorescent in THF, but their intensities increase by 230-, 70-, and 5-fold, respectively, in water/THF mixtures, in which they exhibit strongly enhanced red, orange, and deep yellow fluorescence (inset photo). With their large conjugation and strong electron donating/accepting groups, good two-photon absorption behaviour could be expected as will be discussed in section 4.6.

Another star-shaped gelator **257** was designed with carbazole as the building block and amide groups to serve as the linker to connect aromatic rings, providing hydrogen bonding sites and acting as anion receptors.[125] Only one emission peak at 358 nm was found in the dilute DMSO solution of **257** with a concentration of 1.0×10^{-7} M. When increasing the concentration to 1.0×10^{-5} M, a new emission band at 460 nm emerged and became dominant, which could be attributed to the aggregated species. **257** could form a supergel in DMSO and some DMSO-containing mixed solvents. SEM and AFM study revealed that a three-dimensional network composed of one-dimensional fibrous aggregates had formed and FT-IR and ^{1}H NMR spectra suggest that hydrogen bonding played a key role in the aggregation of **257**. Significant AIE effect was observed in the **257**-based gel, which was reported to be caused by the restricted molecular motion and the formation of *J*-aggregates in the gel state.

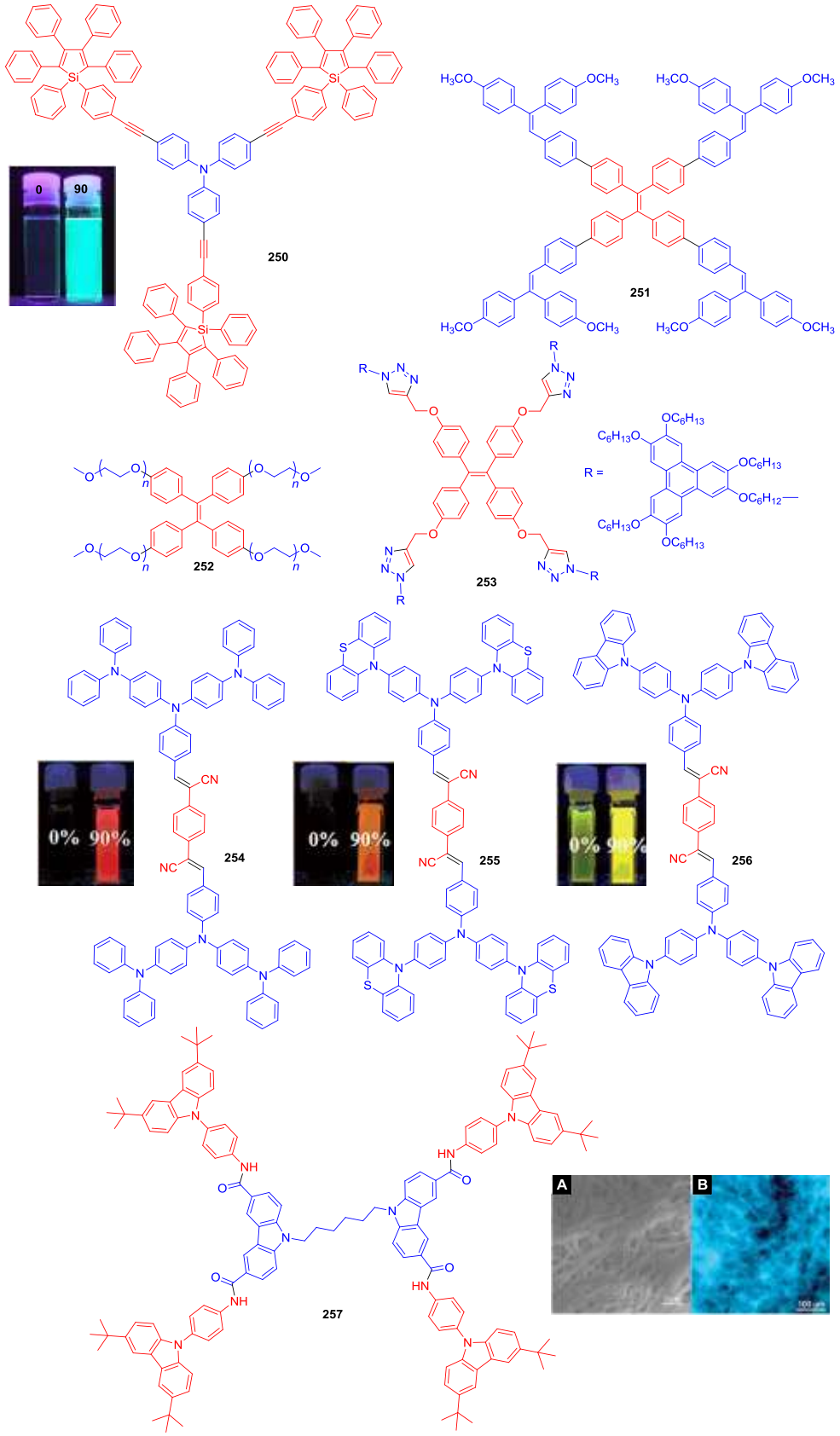

Chart 6 Chemical structures of star-shaped macromolecules **250–257**. Insets: fluorescence photos of **250**, **254–256** in THF solutions and the THF/water mixtures with 90 vol % water fraction taken under UV illumination; (A) SEM and (B) fluorescence microscopy images of xerogel **257** obtained from DMSO. Adapted with permission from Ref. 120. Copyright 2011 Elsevier Ltd; Ref. 124. Copyright 2011 Wiley-VCH; Ref. 125. Copyright 2011 The Royal Society of Chemistry.

3.4 Dendritic and hyperbranched polymers

Another type of AIE-active macromolecule with identical chemical structures and molecular weights is the dendrimers. Dendrimers are generally prepared from two methods: the convergent and the divergent or synthetic strategies. For AIE dendrimers, convergent strategy is favored to obtain perfect dendrimers with high generation. For example, benzenetricarboxamide-cored triphenylamine dendrimers **258-G0~G1** with electron-deficient aromatic core, electron-rich periphery shell and hydrogen bond array was reported (Chart 7).[126] The arylamine-tricarboxamide cores are expected to be the archetypal AIE luminogen, hence both of them show weak fluorescence in THF at room temperature with Φ_F of 0.11% (**G0**) and 0.27% (**G1**). By dropwise addition of the THF solutions into deionized water, the value increases to 2.6% and 4.8% in THF/water mixture with 90 vol % water fraction for **G0** and **G1**, respectively. Nanoparticles of **258-G1** with average diameters of 80 ± 20 nm were easily formed by dropwise addition of THF solution into water and the particles emit green light under excitation. The fluorescent enhancement of **258-G0~G1** was also observed at low temperature: the Φ_F were enhanced by approximately 100- and 50-fold to 11% and 14%, respectively at 77 K in THF glass.

Conjugated AIE dendrimers **259-G0~G2** are reported with a twisted DVA unit as the central core, which is symmetrically connected to multibranched amino-based dendrons through alkene linkers.[127] The DVA core possesses AIE behaviour and the amines are very efficient electron-donating groups as well as branching centers, providing strong interbranching coupling and two-photon absorption enhancement. The dendrimers show weak emission in dilute solution, because of twisted intramolecular charge transfer and the free intramolecular rotation. In contrast, the dendrimers emit in the range of 577–605 nm and high Φ_Fs (up to 85%) can be achieved in the nanoaggregates and solid states, owing to the restriction of intramolecular rotation and more planar conformations. The Φ_Fs value increases with the increasing generation. The fluorescence comparison of the solutions and the nanoaggregates of **259-G0~G2** are shown in the inset photo of Chart 7.

Besides conjugated AIE dendrimers, nonluminescent dendrons could be attached on AIEgens to afford AIE dendrimers (Chart 8). For example, dendritic phosphole oxides **260-G0~G3** display intense emission in the aggregate and solid states, but no emission in solution.[128] The fluorescent photos of **260-G1** is shown in the inset photo of Chart 8 as an example.

In another work, TPE core-containing dendrimers **261-G0~G4** were prepared through the convergent strategy from the corresponding dendritic benzyl bromides.[129] **261-G0** was almost nonemissive in THF solution, owing to the intramolecular motions; weak fluorescence emerges for **261-G1~G2**. On the contrary, **261-G3~G4** exhibited strong fluorescence at 487 nm even in solution (inset photo, Chart 8). The Φ_Fs also increase notably upon increment of the generation number. For instance, in THF solution, the Φ_F of **261-G4** was 23-fold higher than that of **261-G1**. The bulky dendrons may encapsulate the TPE core and shield the core from the solvent, meanwhile, they also enhance the barrier for intramolecular motion. Both factors inhibit non-radiative decay of the excitons and result in emission. Furthermore, the fluorescence of **261-G4** can be further enhanced through the addition of water into its THF solution.

Even when dendrons are attached on a non-AIEgen core, AIE dendrimers can still be obtained, as exemplified in AIE dendrimers **262-G0~G2**.[130] They are a class of dumbbell-shaped dendrimers with a *p*-terphenylene core. **262-G1** can form gel in xylene and the gel phase exhibited unusually enhanced fluorescence emission at 400 nm, demonstrating a supramolecular version of AIE. This was attributed to the steric effects of the dendritic branches and the solubility enhanced by periphery alkyl chains.

Hyperbranched polymers possess similar structure and property as dendrimers, but enjoy much simpler synthesis. Many hyperbranched AIE polymers have already been discussed in section 2. Here, a few examples of hyperbranched polymers with "irregular" architectures will be introduced. For example, TPE-based conjugated hyperbranched polymers **263a–c** can be facilely prepared through an "A_2+B_4" approach by a using one-pot Suzuki polycoupling reaction (Chart 9).[131] To avoid possible gelation, the monomer concentration was fixed at 0.04 mol/L and the end-capping reagents (phenylboronic acid/bromobenzene) were added to terminate the bromo and boronic ester end groups. Even after the TPE unit had been incorporated into the conjugated hyperbranched polymer, its phenyl rings could still rotate in solution despite the fact that there is less freedom than its small molecule. **263a** was thus a weak emitter when molecularly dissolved in pure THF with a negligible Φ_F value of 0.01%. When 90 vol % methanol was added into the solution, an intense PL peak centred at 510 nm was recorded under the same measuring conditions and the Φ_F value of the polymer increased to 24%, being 2310-fold higher than that in THF solution. **263b** and **263c** were also AIE-active, the $\alpha_{AIE,\Phi}$ values were 16 and 5.4, respectively. In addition, the PL peak intensity of the DMF/glycerol mixtures at higher than those in DMF/methanol mixtures as the same fraction of poor solvents. The increased solvent viscosity led to fluorescent enhancement.

Another conjugated hyperbranched polymer **264** constructed from carbazole and TPE moieties was reported through a similar "A_2+B_4" approach by using a one-pot Suzuki polycoupling.[132] The monomer concentrations were as low as 0.01 and 0.02 mol/L to minimize the possible formation of cross-linking insoluble polymer and the end-capping phenylboronic acid/bromobenzene were added to react with terminal groups. Upon excitation by 360 nm light, **264** was a weak emitter in THF solution and the PL spectrum gave an almost flat line. An intense PL peak centred at about 510 nm was recorded when a large amount of water was added to the solution. The Φ_F value of **264** is ~1% in pure THF, while at a water content of 90%, the Φ_F value of the polymer increased to 29.6%. Polymer **264** possesses relatively high-lying HOMO and LUMO energy levels, indicating good hole injection and transporting properties, which can be potentially utilized in PLED devices as will be discussed in section 4.5.

Furthermore, core-shell structure can be achieved within a single molecule with a hyperbranched conjugated polymer (HCP) core and poly(ethylene glycol) arms.[133] Hyperbranched conjugated polymer **265** was first prepared and then linear PEG arms **266a–b** were grafted on the surface of **265** through the acylhydrazone connection via Schiff-base chemistry to form polymer **267a–b** with core-shell structure and PEG segments of different lengths. In a nonselective solvent such as dichloromethane, **267a** exists in the stretched conformation, and its optical properties are similar to those of the HCP core. Acetonitrile, on the other hand, is a good solvent for PEG, but a poor solvent for HCP. With addition of such a selective solvent to the dichloromethane solution, the collapsed HCP core of **267a** is well wrapped in the interior of the unimolecular micelle by PEG arms. The emission of **267a** at 450 nm is increased dramatically with the increasing acetonitrile content. The emission intensity of the self-assembled unimolecular micelle is enhanced by more than 40-fold when compared with the solution.

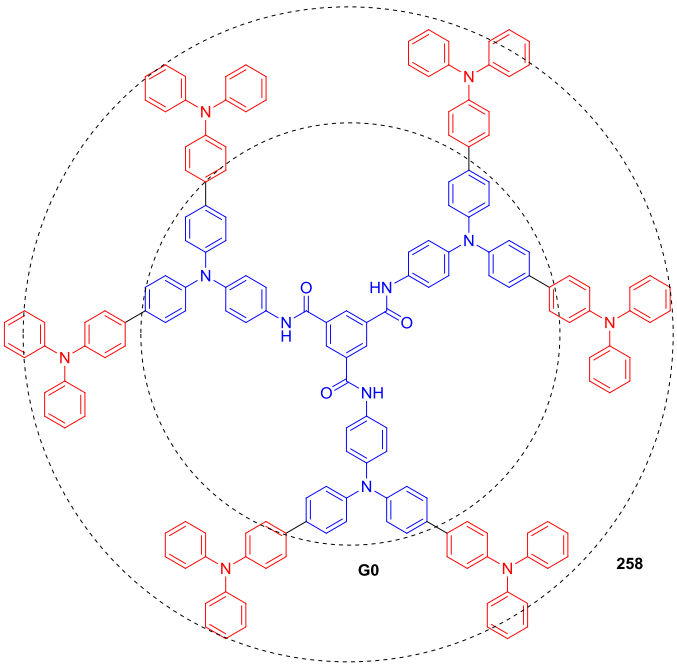

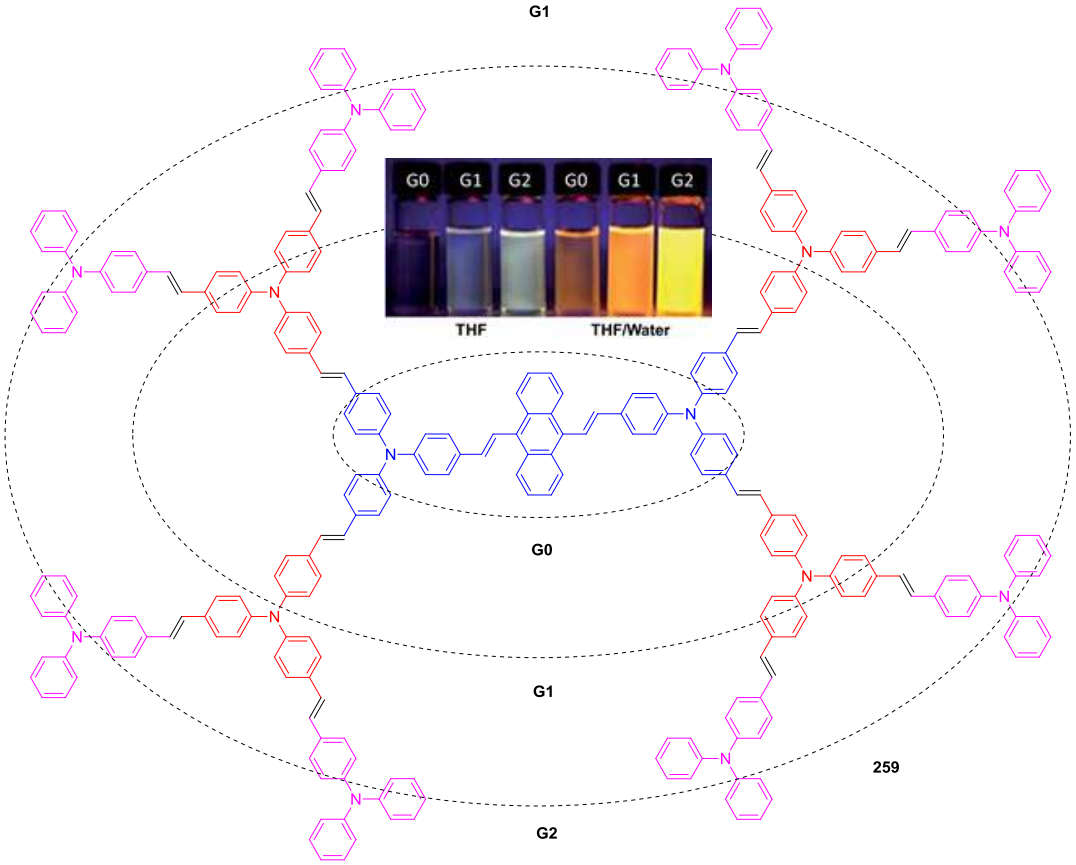

Chart 7 Chemical structures of the AIE-active dendrimers. Insets: fluorescence photographs of dendrimers **259-G0~G2** in THF and THF/water mixtures with 80 vol % water fraction taken under 365 nm UV irradiation. Adapted with permission from Ref. 127. Copyright 2014 The Royal Society of Chemistry.

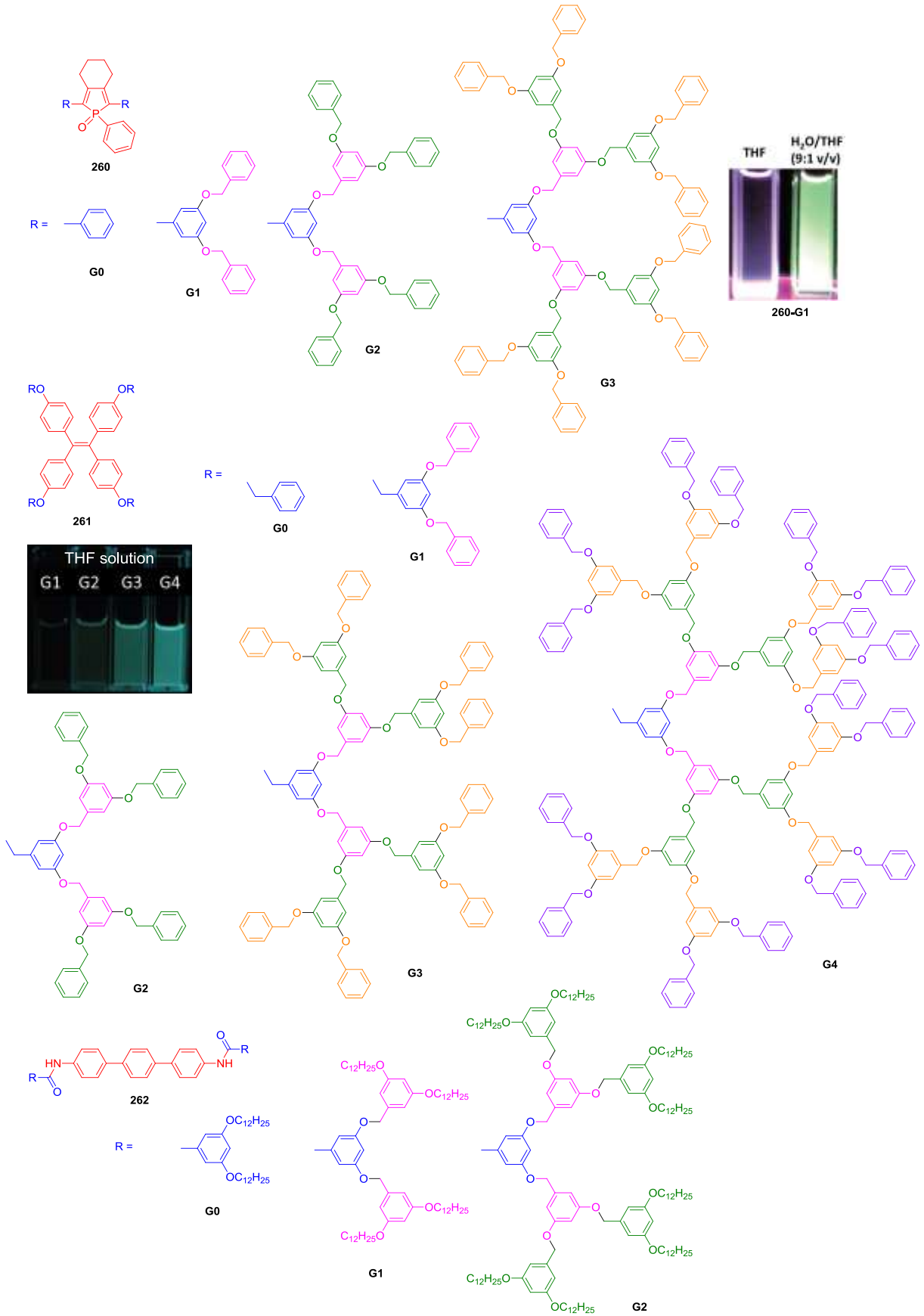

Chart 8 Chemical structures of dendritic compounds **260–262**. Insets: fluorescence photographs of **260-G1** in THF and THF/water mixture with 90 vol % water fraction and **261-G1~G4** in THF solutions taken under 365 nm UV irradiation. Adapted with permission from Ref. 128. Copyright 2009 The Royal Society of Chemistry; Ref. 129. Copyright 2012 Wiley-VCH.

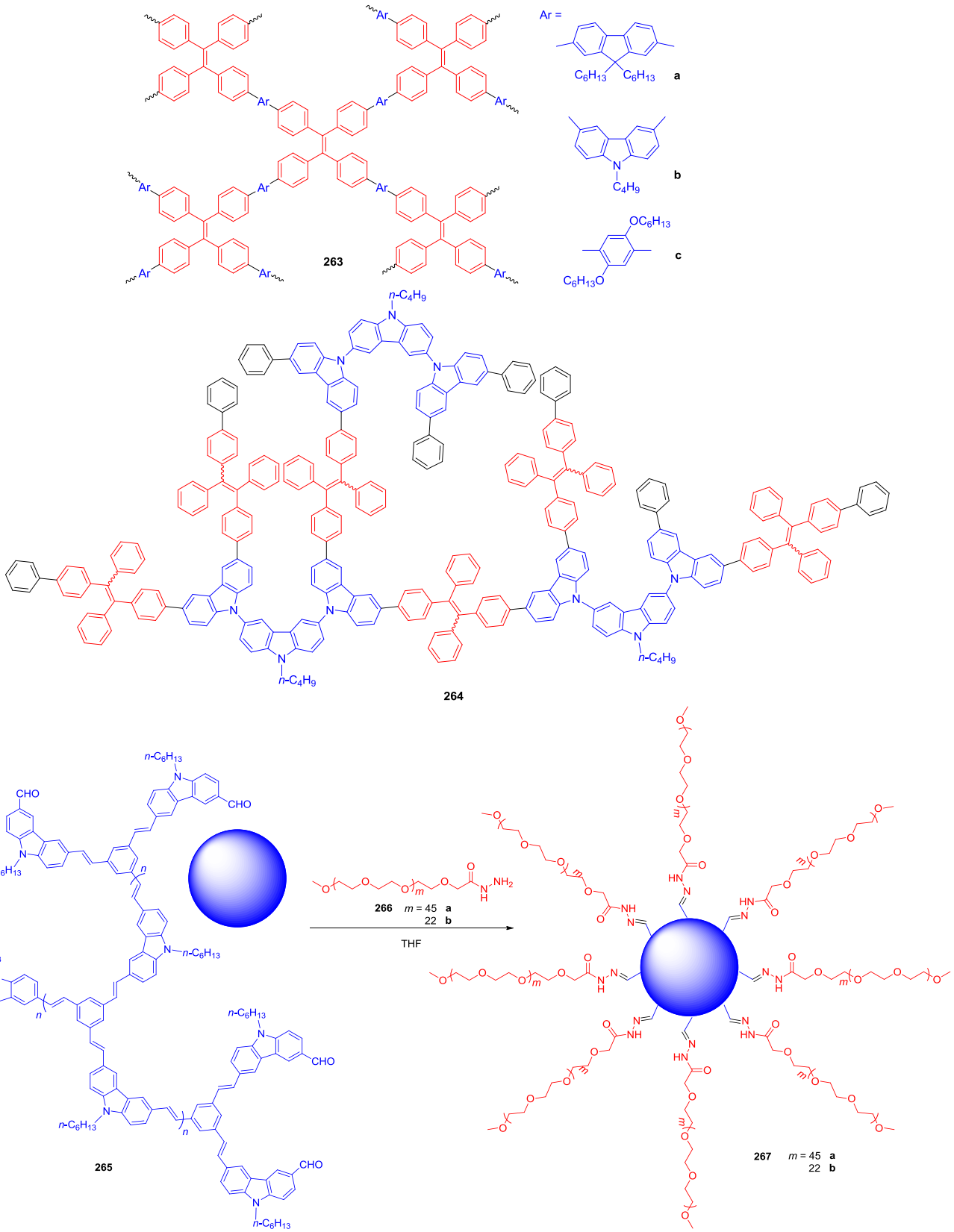

Chart 9 Chemical structures of hyperbranched polymers **263–265** and the synthesis of the star-shaped hyperbranched copolymers **267a–b**.

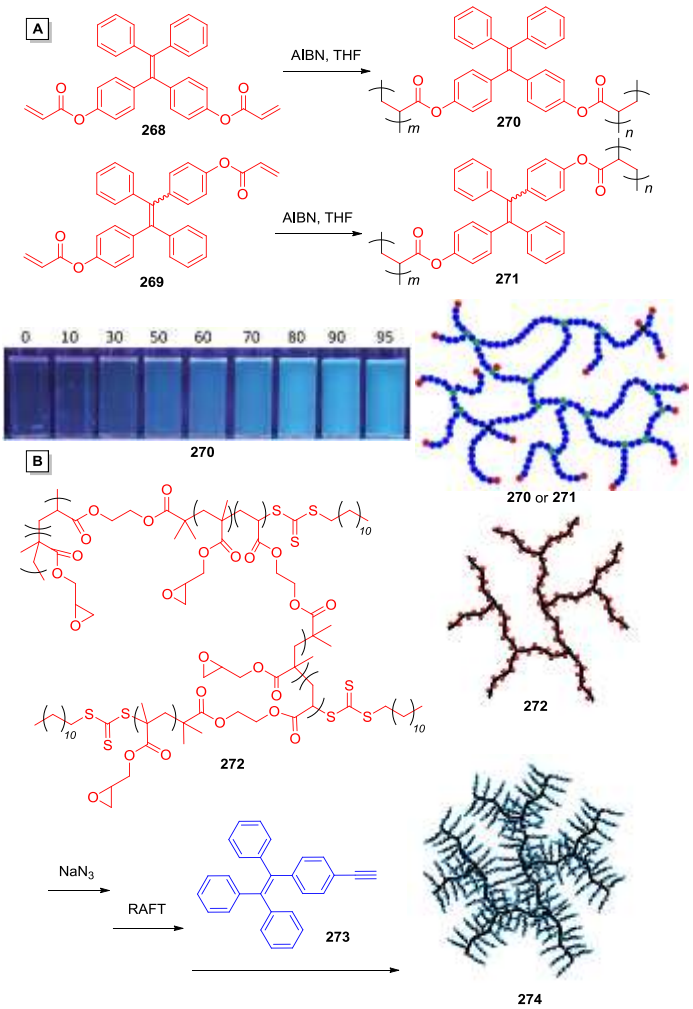

Scheme 33 Synthetic routes of (A) nonlinear polymers **270–271** with a glycogen-like topological structure and (B) dendritic molecular brush **274**. Insets: fluorescent photographs of **270** in THF/water mixtures with different water fractions taken under 365 nm UV illumination. Adapted with permission from (A) Ref. 134 and (B) Ref. 135. Copyright 2013 The Royal Society of Chemistry.

Nonconjugated AIE hyperbranched polymers with glycogen-like topological structures have also been reported with facile synthesis (Scheme 33A).[134] TPE-containing diacrylates **268** and **269** were polymerized using AIBN as an initiator in refluxing THF under mild reaction conditions in the absence of transition-metal catalyst and strong bases, furnishing polyacrylates **270** and **271** with glycogen-like structures and closed-loops in nearly quantitative yields. Despite their high M_ws with numerous chain interconnected points, **270** and **271** possess good solubility in common organic solvents. **270** is somewhat fluorescent in THF solution. Obvious fluorescence enhancement was observed when even a small amount of water was added to the THF solution, reaching a 33-fold enhancement in 95 vol % aqueous mixtures. **271** shows similar behaviour.

Multifunctional dendritic molecular brush (DMB) with pendant poly(glycidyl methacrylate) chains grafting on **272** were synthesized via a sequential reversible addition-fragmentation chain transfer polymerization approach (Scheme 33B).[135] TPE-containing alkyne **273** were then attached to the DMB intermediate with a conversion of 100% by click chemistry to afford TPE-functionalized dendritic molecular brush **274**. The skeleton of **274** exhibits flexibility and typical AIE effect. Upon gradual addition of water to the THF solution of **274**, the PL intensity increased. The fluorescent Φ_F of **274** in the aggregated state is two times higher than that of **273**, and reached 36.6% in 90 vol % aqueous media. The fluorescence of the compact and flexible scaffolds of the DMBs in different solvent system demonstrated topologically-induced emission.

3.5 Microporous polymers

Microporous polymers, with interweaving three dimensional scaffolds, exhibit potential applications in gas storage, gas separation, heterogeneous catalysis, etc.[136] Most porous organic polymers possess intrinsic properties of large surface areas, high chemical stabilities, and low skeletal density, which have drawn great interests of scientists in recent years.[137] Among them, TPE is a popular building block for construction of light-emitting conjugated microporous polymers (CMP), due to its propeller-like structure and AIE characteristics.

Tetrakis(4-bromophenyl)ethene **275** was used as a single component for the synthesis of the conjugated microporous polymer **276** through the Yamamoto coupling reaction, in which the TPE units are directly linked with each other by covalent bonds from four different directions to form an interlocked network (Scheme 34A).[138] The knitted network successfully restricts the rotation of the phenyl units, which are the major cause of fluorescence deactivation in TPE, thus providing intrinsic luminescence activity for the insoluble polymers. Time-dependent Yamamoto reactions were conducted to monitor the development of the porous network and the growth of π-conjugation. When the reaction time increases from 2 h to 72 h, the absorption band was red-shifted from 342 nm to 368 nm and the emission band also red-shifted from 538 nm to 551 nm, indicating extended π-electronic conjugation. The fluorescence images of **276** (product after 72h) in various solvents and solid state are inset in Scheme 34A, in contrast with the linear polymer analogue which only gives weak emission. The Φ_F value of **276** in THF suspension is 40%. The network structure promoted electronic conjugation, facilitated exciton migration, and enhanced luminescence activity.

TPE-based fluorescent microporous polymers were also prepared through Suzuki coupling polycondensations or oxidative coupling polymerizations (Scheme 34B–F).[139] The porous polymer **278** was synthesized efficiently by a Pd-catalyzed the Suzuki coupling polycondensation of **275** and **277**, while CMP **280** was obtained by an oxidative coupling polymerization of **279** promoted by anhydrous $FeCl_3$. Multi-component monomers can also be used to prepare CMPs through copolymerization. For example, Suzuki coupling polymerization of tetrabromide monomers **275** and **281**, reacted with diboronic acid **277** can generate CMP **282**. Similarly, a one-pot reaction of **275**, **283** and **277** can furnish CMP **284**. $FeCl_3$-promoted oxidative coupling between tetrathiophene **279** and **285** affords CMP **286**. Non-ordered, amorphous structures were observed for all these TPE-based microporous polymers due to the kinetic control of the polymerization, proven by the X-ray diffraction measurements. Incorporation of TPE moieties into such CMPs induced strong photoluminescence (530–610 nm) in the solid states. All the fluorescent microporous polymers possess large specific surface areas. Using the same linker monomer, the specific surface area of **282**, **284** and **286** prepared by two different core structural monomers is higher than those of the corresponding homopolymers **278** and **280**, as will be discussed in section 4.11.

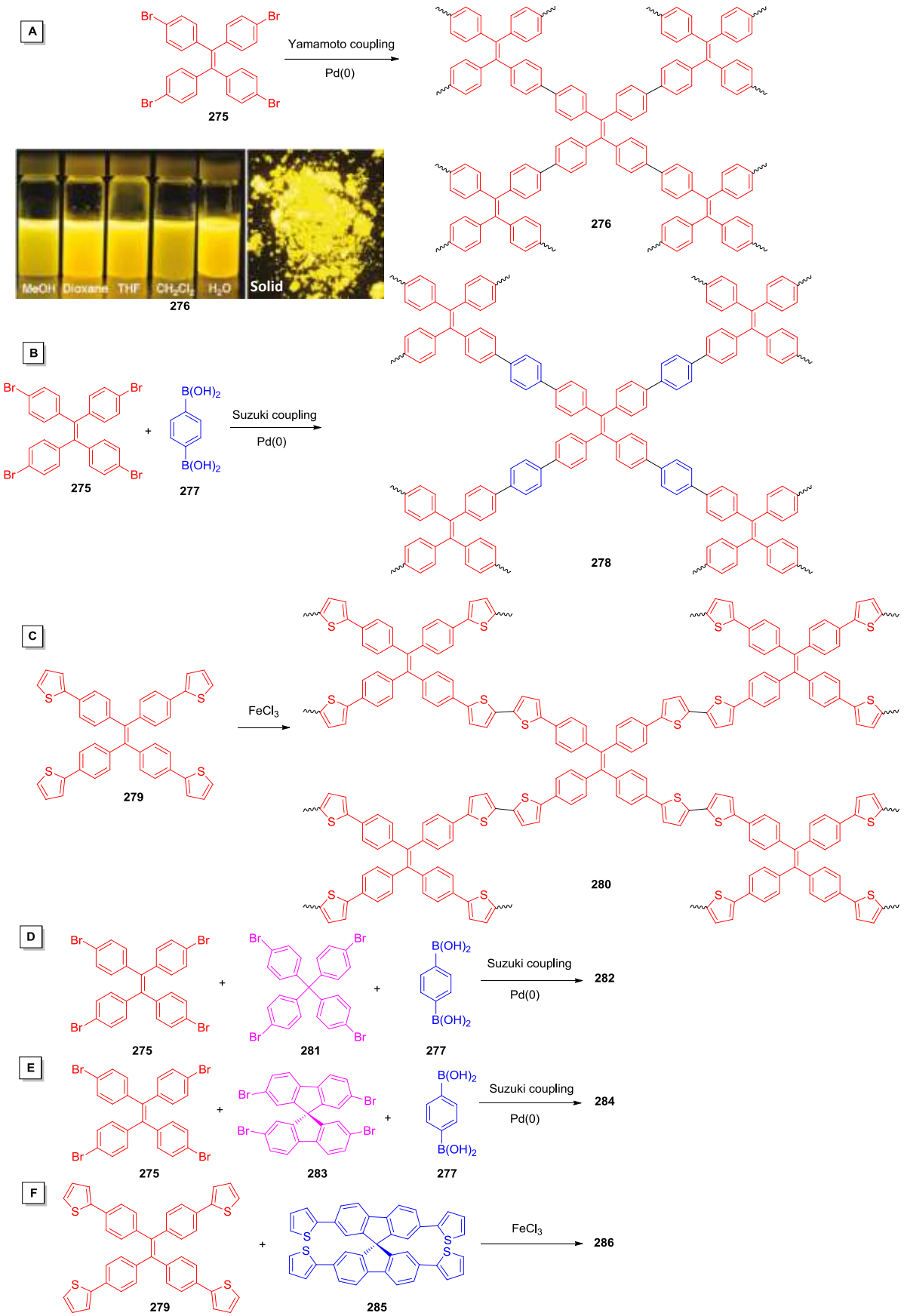

Scheme 34 Synthetic routes of conjugated microporous polymers through Yamamoto, Suzuki, and oxidative coupling polymerizations, respectively. Insets: fluorescence photos of **276** in MeOH, dioxane, THF, CH_2Cl_2, H_2O, and its solid powder taken under UV illumination. Adapted with permission from Ref. 138. Copyright 2011 American Chemical Society.

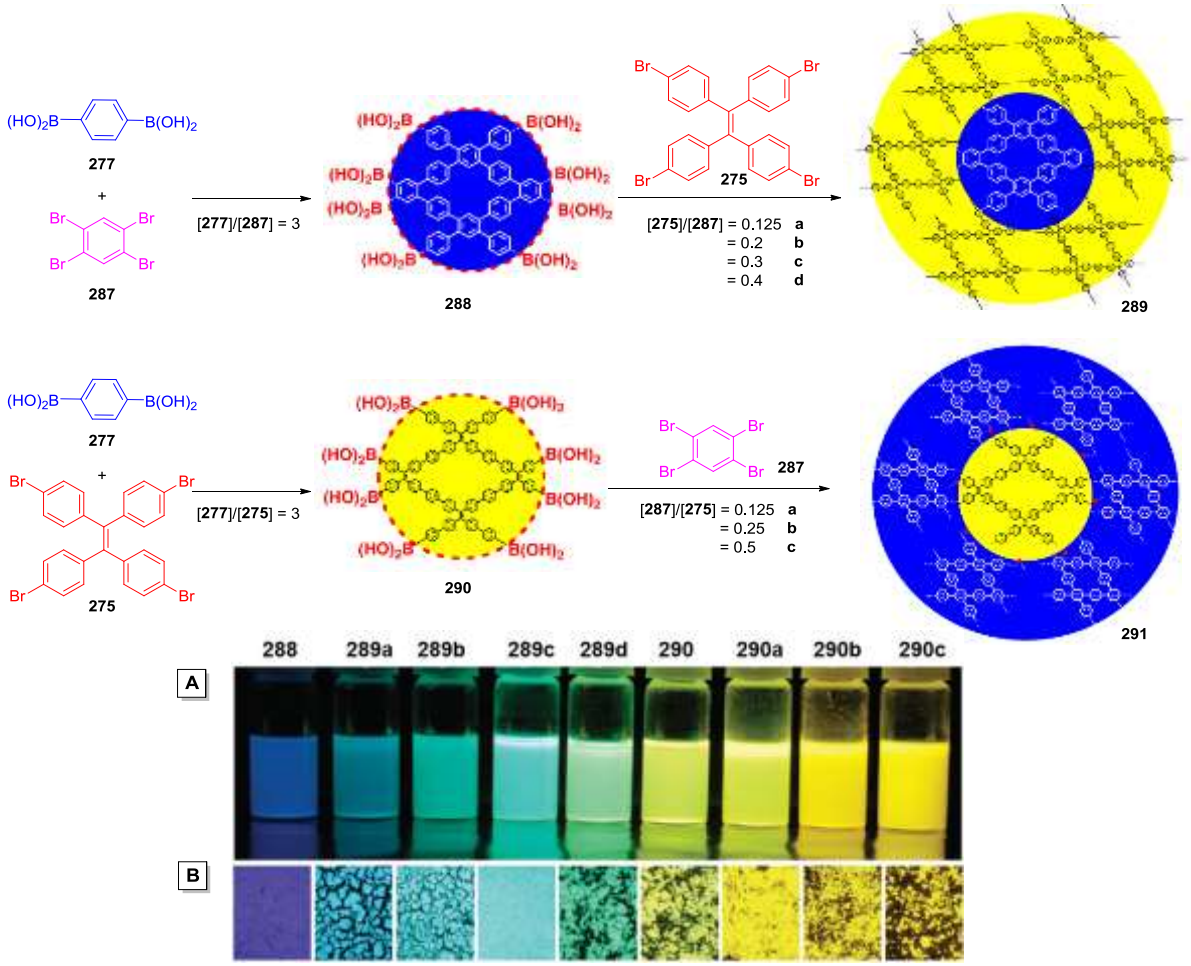

Scheme 35 Synthetic routes of the conjugated microporous polymers **289a–d** and **291a–c** with core-shell architectures. Insets: fluorescence photographs of (A) the conjugated microporous polymers dispersed in THF and (B) the solid powders of the polymers. Adapted with permission from Ref. 140. Copyright 2013 The Royal Society of Chemistry.

Recently, a core-shell strategy was adopted for the design of conjugated microporous polymers, and color-tunable light emissions were achieved while retaining high luminescence efficiency (Scheme 35).[140] Two types of CMPs with core-shell structures were prepared. In the first type, an excess amount of diboronic acid **277** was first reacted with tetrabromobenzene **287** at a molar ratio of 3:1 to from polybenzene core structure **288**, which could further be reacted with tetrabromo-TPE **275** to form core-shell structure **289a–d** with different **275**/**287** molar ratios and thus different shell thicknesses. Alternatively, it can be conducted in the opposite way: an excess amount of diboronic acid **277** was first reacted with tetrabromo-TPE **275** to form polyTPE core **290**, which was then modified with tetrabromobenzene **287** to afford the reversed core-shell structure **291a–c** with different **287**/**275** molar ratios. As can be seen from the inset photo in Scheme 35, both suspension and solid powder of **288** show blue emission, while thicken the TPE-containing shell layer in **289a–d** will gradually red-shift the emission color from 435 nm to 518 nm, attributed to the energy transfer from core to shell and the AIE nature of the shell. The absolute Φ_F of **288** is 15%, while that value increased to 23~24% in **289a–d**. On the other hand, the suspension and solid of **290** show yellow emission at 540 nm with the absolute Φ_F of 32%, thickening the shell layer did not significantly affect the fluorescence of **291a–c**. Energy transfer process from the shell to TPE-containing core took place. The porous core-shell networks extend π-conjugation, facilitate exciton migration, prolong the lifetime of excited states, and sustain light emissions irrespective of solvent and state.

By changing the building blocks as well as the reactions, the pore size of the CMPs can be tuned. The Hay-Glaser coupling reaction of terminal triple bonds was also used to build conjugated microporous polymer **292** through efficient polymerization of TPE-containing tetrayne **194** (Scheme 36A).[37] Unlike the other luminescent CMPs, **292** is soluble in common organic solvents and tough thin films can be easily prepared by spin-coating its solution. The PL study of **292** in THF/water mixed solvents shows that it emits at 540 nm and is AIE-active.

Fluorescent inorganic-organic hybrid microporous polymers have also been reported (Scheme 36B).[141] Cross-linked poly(tetraphenylethylene-*co*-cyclotriphosphazene) **295** was efficiently prepared through a one-step polycondensation between **293** and **294** under basic conditions and large scale product can be facilely obtained. **295** features remarkable fluorescent emission in both the suspension and solid-state as shown in the inset photo of Scheme 36B. The suspension of **295** in THF/water (1:9 v/v) displays a strong fluorescent emission at 462 nm and a Φ_F of 9.9%. The solid-state PL of **295** shows an emission peak at 485 nm, red-shifted 23 nm when compared with the suspension.

3.6 Supramolecular polymers

As crystals, polymers enjoy highly ordered structures and since solid state luminescence is an attractive topic in engineered crystalline

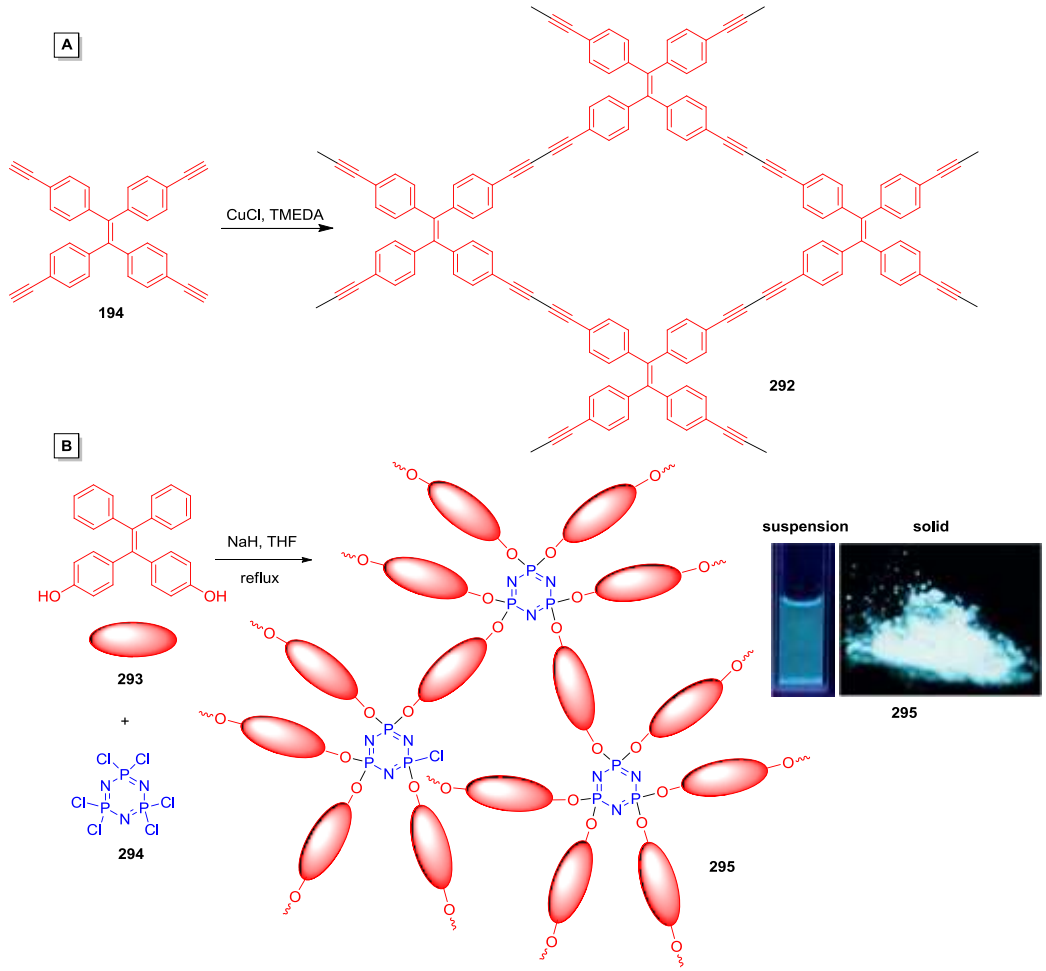

Scheme 36 Synthetic routes of the microporous polymers. Insets: fluorescence photographs of the suspension in THF/water (1:9 v/v) and solid powder of **295** taken under 365 nm UV illumination. Adapted with permission from Ref. 141. Copyright 2011 The Royal Society of Chemistry.

materials, AIEgen-based building blocks are particularly well-suited for such applications. There are a few examples of AIE polymer crystals with extended structures in three dimensional space and with repeating units linked through weak intermolecular interactions, such as hydrogen bonds, electrostatic charges, halogen bonds, etc.

For example, supramolecular assemblies **298a–c** between an AIE-active acid-functionalized TPE derivative **296** and three different bis(pyridine)s **297a–c** were constructed through crystal engineering (Scheme 37A).[142] In the crystal structures, each TPE unit is linked with two bis(pyridine) units in a one dimensional manner through the strong hydrogen bonding interaction between pyridine and acid groups. The crystals displayed charge-carrier capability, and the magnitude of semiconductivity varied systematically as a function of conjugation in the bis(pyridine) component. Crystals incorporating bis(pyridine)s displayed conductivities comparable to those of established organic semiconductors (μ_{eff} = 0.38 and 1.7 $\times 10^{-2}$ $cm^2/V \cdot s$, respectively).

Other supramolecular building blocks with AIE properties have been reported. For example, two TPE derivatives **299a–b** with either 4-pyridyl or 3-pyridyl groups substituted at the 4, 4', 4'', and 4''' positions were reported to be typical AIE-active.[143] The solid state fluorescence spectra of **299a–b** were found to be virtually identical with each other, displaying a broad emission centred at ~ 510 nm, while in the THF solution, **299a** was weakly emissive and **299b** is completely nonluminescent. They were both converted to their corresponding tetrapyridinium perchlorate salts upon exposure to $Fe(ClO_4)_3 \cdot xH_2O$ (Scheme 37B).[144] In the single crystal structures of the tetra-perchlorates **300a–b**, extensive hydrogen bonding networks were observed in 3D space involving pyridinium N-H groups, perchlorate anions and water molecules.

Moreover, halogen bonding interactions were reported to connect repeating units in the crystalline networks of TPE halobenzoyl esters **301a–b** (Scheme 37C).[145] In the crystal structure, halogen bonding interactions were observed linking **301a** to five neighboring molecules. Solid state luminescence was apparent in crystals of **301a** when illuminated with a hand-held UV light. Single crystals of **301a** were examined using confocal microscopy and a representative image was shown in Scheme 37, inset photo.

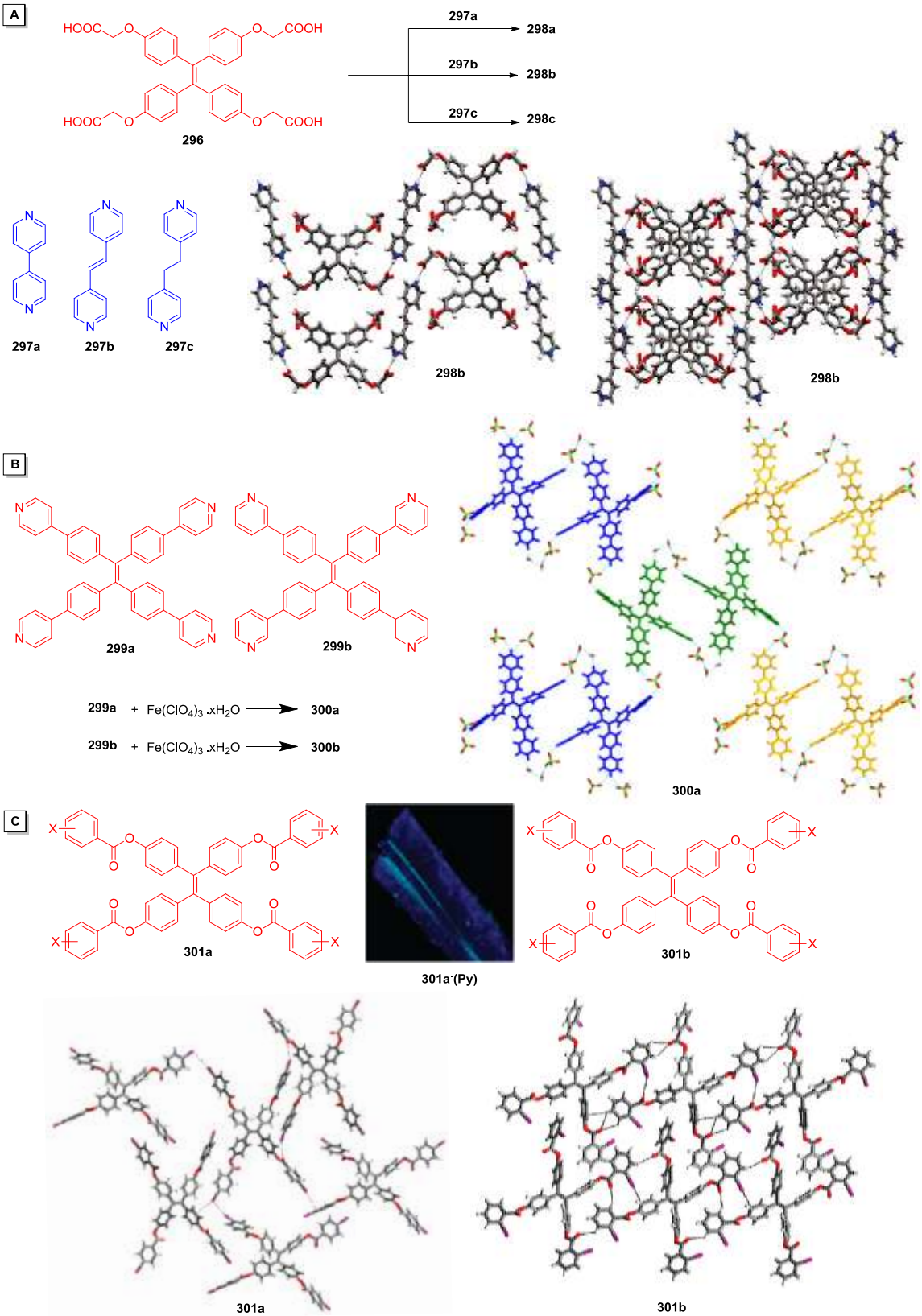

Scheme 37 Synthetic routes of crystallinic supermolecular polymers and 2D layer arrangement of single crystal structures of **298b**, **300a**, and **301a–b**. Inset: fluorescent confocal microscope image of **301a**·(Py) obtained from slow evaporation of pyridine solution of **301a**. Adapted with permission from (A) Ref. 142. Copyright 2011 American Chemical Society; (B) Ref. 144. Copyright 2011 Elsevier Ltd; (C) Ref. 145. Copyright 2012 American Chemical Society.

3.7 Metal-organic frameworks

Recently, AIEgens, especially TPE derivatives have been frequently incorporated into metal-organic frameworks (MOFs). For example, coordination of tetrakis(4-carboxyphenyl)ethene (TCPE) **302** to d_{10} ions produces luminescent MOFs exhibiting fluorescence lifetimes similar to those of molecular aggregates. Dilute solutions of **302** in methanol or DMSO are non-emissive and it is indeed AIE-active. The fluorophore was immobilized in a rigid MOF matrix by reacting **302** with $Zn(NO_3)_2{\cdot}6H_2O$ in a mixture of *N*, *N*-diethylformamide (DEF) and ethanol at 75 °C. The reaction produced yellow block crystals of $Zn_2(TCPE)(H_2O)_2{\cdot}4DEF$ **303** (Scheme 38A).[146] Similar reaction conditions involving $Cd(NO_3)_2{\cdot}4H_2O$ as the metal source produced yellow crystals of $Cd_2(TCPE)(DEF)(C_2H_5OH)_2{\cdot}DEF$ **304**. Spatial separation between the closest TPE cores in both **303** and **304** is much larger than in any reported TPE molecular derivatives. Despite the absence of close-packed TPE cores, both **303** and **304** are luminescent. They exhibit emission maxima of 480 and 455 nm, which is similar to the value observed for solid **302** (480 nm). The matrix coordination-induced emission effect is thus proposed that tight packing of the TPE chromophores is not necessary for turn-on fluorescence and anchoring AIE-type chromophores to metal ions within a rigid matrix serves as an alternative mechanism for restricting the rotation of the phenyl rings.

Similarly, a novel (4,8)-connected *scu* $[Co(tbe)_{0.5}(H_2O)_2]{\cdot}0.5H_2O$ **305** framework has been built by using the predesigned octahedral

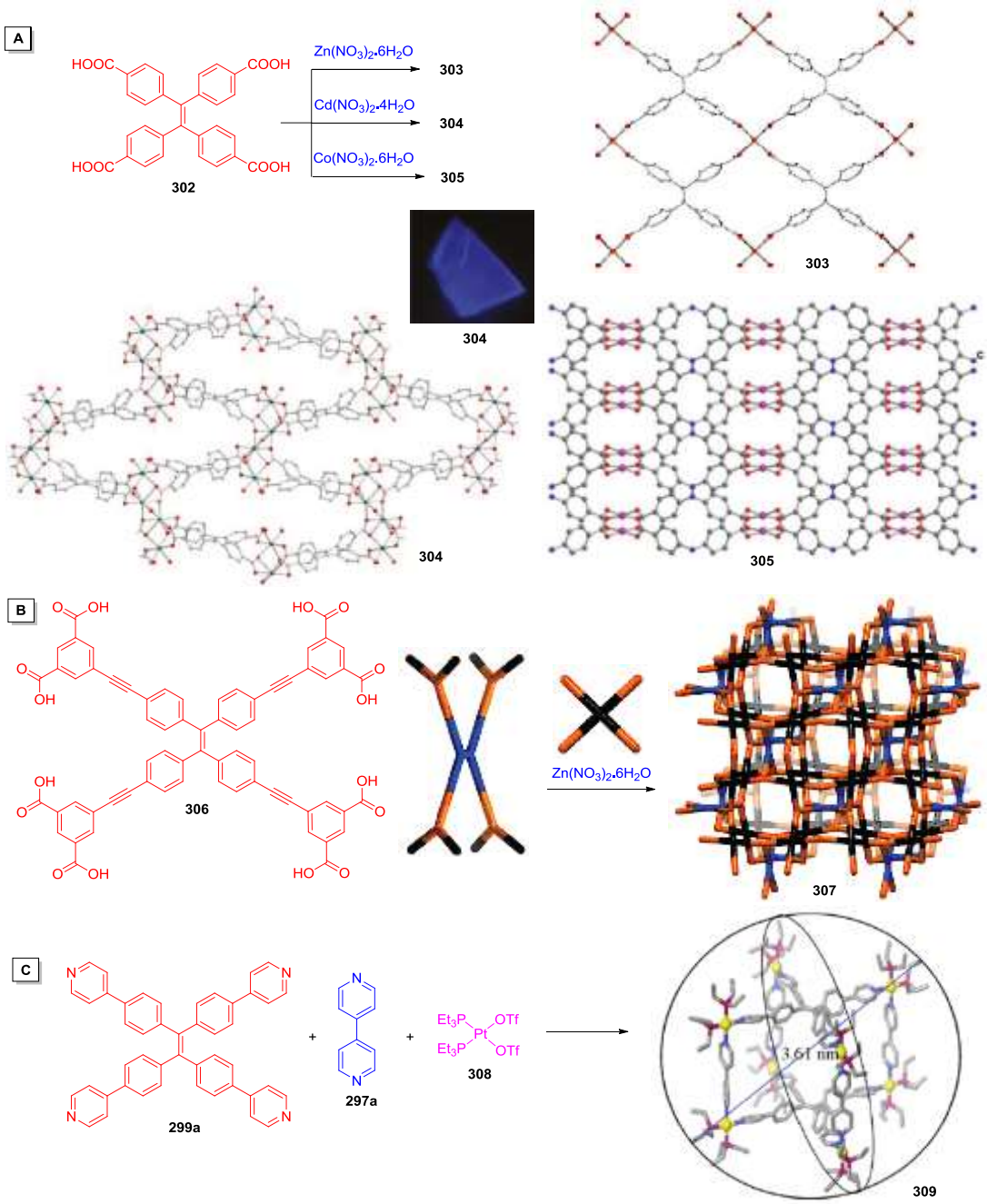

Scheme 38 Synthetic routes of metal-organic frameworks metallosupramolecular self-assembly. Adapted with permission from (A) Ref. 146. Copyright 2011 American Chemical Society; Ref. 147. Copyright 2013 The Royal Society of Chemistry; (B) Ref. 148. Copyright 2012 American Chemical Society; (C) Ref. 149. Copyright 2010 American Chemical Society.

node of **302** (Scheme 38A).[147] Red needle crystals of **305** were obtained by hydrothermal reaction of $Co(NO_3)_2 \cdot 6H_2O$ with **302**. In the single crystal, Co^{2+} ions are bridged by the ligands to form a 3D network and each Co^{2+} ion is octahedrally coordinated to four carboxylate oxygen atoms from four molecules of **302** and two H_2O molecules.

The design of a luminescent MOF with a near-dark off state represents a promising candidate towards high-surface-area turn-on fluorescent sensors. Elongated ligand bridges were designed to decrease the barrier of phenyl ring torsion, thus provide a fluorescent MOF with a default dark off state. A salient design feature in tetrakis[4-(3,5-dicarboxyphenylethynyl)phenyl]ethylene **306** are the *p*-ethynyl groups extending from the phenyl rings of the TPE core, which are known to promote almost barrierless torsional motion for neighboring phenyl rings. The ethynyl-extended octacarboxylate ligand **306** was hence designed and incorporated into a zinc-based MOF **307** (Scheme 38B).[148] **307** was composed of paddlewheel $Zn_2(O_2C)_4$ secondary building units bridged by the ligands into a 3D 3,3,4-connected net with *tbo* topology and Schläfli symbol. A Φ_F of 9% was observed for **307** which is significantly lower than that of $[Zn_2(TCPE)(DEF)_2] \cdot DEF$. The remarkable reduction of 26% in Φ_F and the presence of the nearly dark off state in **307** was attributed to the relaxed torsional motion of the phenyl rings in the TPE core. Despite the rigidity of the MOF lattice, the ligand **306** shows a dramatically reduced barrier to phenyl ring torsion and thereby a much lower fluorescence Φ_F compared with $[Zn_2(TCPE)(DEF)_2] \cdot DEF$ and an almost perfect off ground state.

In another example, AIE-active building block **299a** was also introduced into the multicomponent coordination-driven self-assembly of a tetragonal prism (Scheme 38C).[149] The four pyridine groups of **299a** acted as the faces of a tetragonal prism during the self-assembly, while the linear donor **297a–b** and 90° platinum triflate **308** are selected as pillars and corners of the tetragonal prism, respectively, under the combined interaction of edge- and face-directed self-assembly. When the three building blocks **299a**, **297a–b** and **308** are reacted in a stoichiometric ratio of 1:2:4, the formation of tetragonal prism **309** is formed via coordination-driven self-assembly without any template. Furthermore, the use of linear pillars with different lengths in the assembly leads to tetragonal prisms with different cavity size, which may result in applications in host-guest chemistry or as new micro-reactors.

3.8 Miscellaneous systems

Recently, new fluorescent polymers without traditional luminogens have been reported from various systems. Unlike the other AIE macromolecules with typical/atypical AIEgens, all the polymers discussed in this section possess no traditional fluorophores such as conjugated π-systems and some of them are even without any aromatic rings. These luminescent polymers challenge the current understanding on molecular fluorescence.[150] A new theory is urged to explain such unusual fluorescent systems.

A highly fluorescent melamine-based porous polymeric network **312** was reported by a microwave-assisted reaction of **310** and **311** (Chart10A).[151] **312** is stable and insoluble in water and common organic solvents. The benzene rings and triazine rings are scattered in a nonconjugated environment. However, the nanoparticles of **312** exhibit a remarkable fluorescent emission feature in both suspension and solid-state. Furthermore, nanoparticle suspensions of **312** in water exhibit significantly enhanced fluorescence emission at 467 nm with an increase in THF content, which may be due to the solvent-caused changes in aggregation state of **312** nanoparticles in water/THF mixtures. Another unusual strong fluorescence of a hyperbranched (3-hydroxyphenyl) phosphate **313** was also reported (Chart 10B).[152] **313** does not possess a rigid planar structure or obvious large π-system, yet it shows two emission peaks at 408 and 550 nm in different solvents. The terminal phenol groups and triphenyl phosphate structures were suggested to be responsible for each peak. After the terminal phenolic groups are converted to epoxide groups in **314**, the strong emission peak at 550 nm is barely seen in the solution, indicating that the terminal phenolic groups are responsible for the fluorescence peak at 550 nm. The inset photo shows the emission of **313** in THF/ethanol mixed solvents with different ethanol fraction under a UV lamp. When ethanol content increased, the green emission at 550 nm increased. The greatly enhanced fluorescence is explained by the extended π electron systems due to the unique phosphate structure, the somewhat stiff ether linkage due to the steric hindrance and hydrogen bonding, and the hyperbranched structures. The absorption and emission of solutions of **313** were dependent on the solvent polarity, pH value, concentration, and terminal groups.

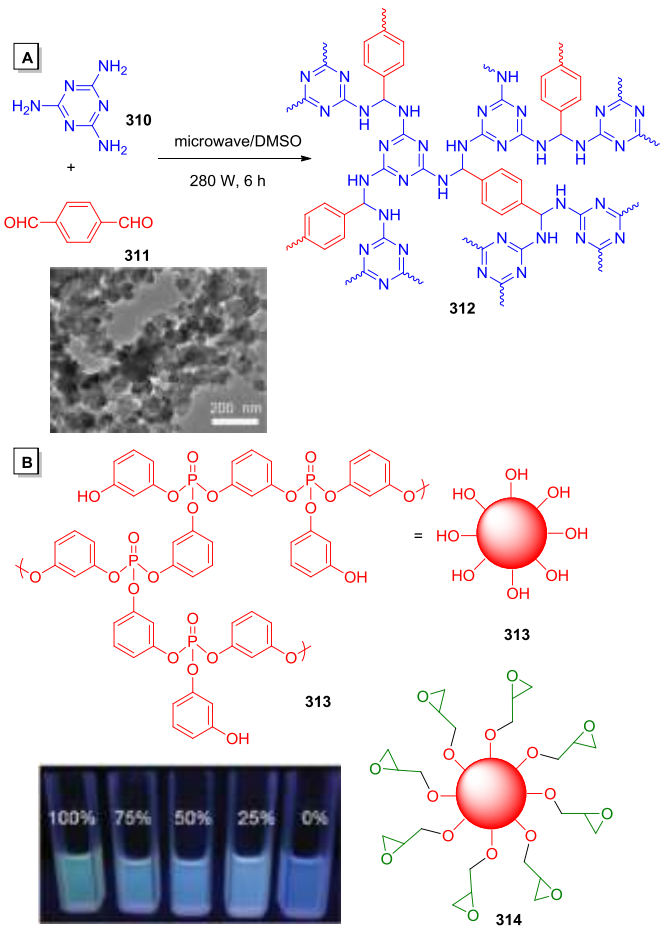

Chart 10 (A) Synthetic route of fluorescent nanoparticles of a melamine-based porous polymer **312** and (B) the chemical structure of a fluorescent hyperbranched phosphate **313**. Insets: TEM image of nanoparticles of **312** and fluorescence photos of **313** in THF/ethanol mixtures with different ethanol volume fractions taken under UV illumination. Adapted with permission from (A) Ref. 151. Copyright 2012 Elsevier Ltd; (B) Ref. 152. Copyright 2013 The Royal Society of Chemistry.

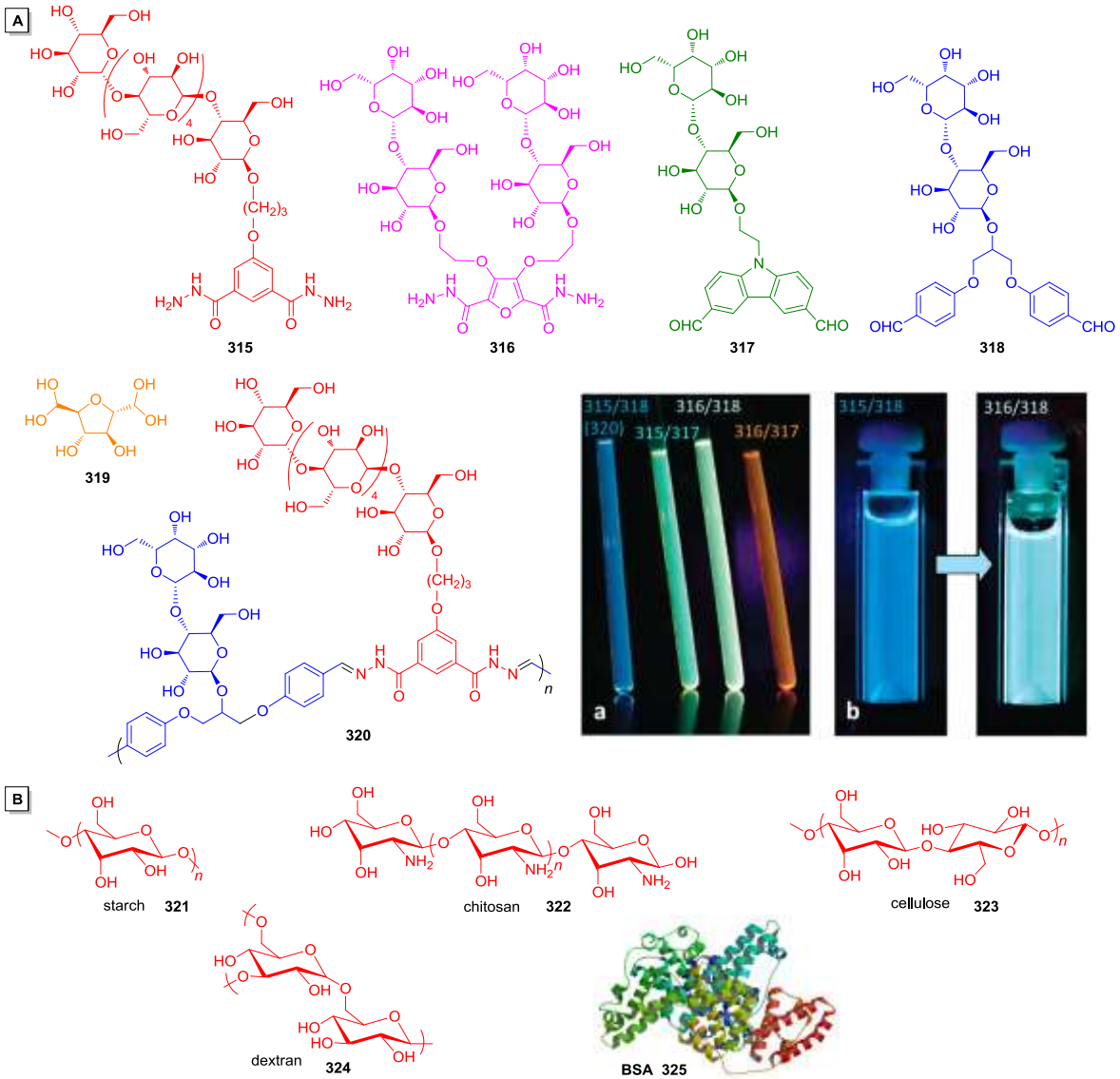

Chart 11 Chemical structures of (A) the bis-hydrazides **315–316**, the dialdehydes **317–319**, and a typical dynamic glycopolymer **320** prepared by polycondensation of bis-hydrazide **315** and dialdehyde **318** and (B) pure organic nonconventional luminescent compounds **321–325** with room temperature phosphorescence. Insets: fluorescence photos of (a) the polymers prepared from **315**/**318**, **315**/**317**, **316**/**318** and **316**/**317**, respectively, in D_2O at pD = 4 with an initial monomer concentration of 5 mM and (b) polymer **315**/**318** before (left) and after (right) chemical exchange with **316**. The photos were taken under UV irradiation. Adapted with permission from Ref. 153. Copyright 2008 Wiley-VCH.

A series of dynamic glycopolymers were generated by polycondensation through reversible acylhydrazone formation among components **315–319** bearing lateral bioactive oligosaccharide chains (Chart 11A).[153] For example, dynamer **320** was prepared through the reaction of **315** and **318**. They present remarkable fluorescence properties whose emission wavelengths are dependent on the constitution of the polymer and are tunable by constitutional modification through exchange/incorporation of components. The inset photo in Chart 11A shows the fluorescence of polymers prepared from **315**/**318**, **315**/**317**, **316**/**318** and **316**/**317**. The reversible character of these glycodynamers was demonstrated by covalent exchange reactions of a monomeric component by another, which resulted in modification of the fluorescence properties of the glycodynamer. The fluorescence of polymer **320** before and after the chemical exchange from **318** to **316** is shown in the inset photo. The emission color gradually red shifted. It was reported that the fluorescence is likely due to a tightly packed hydrophobic core isolating and rigidifying the chromophores.

More recently, efficient room temperature phosphorescence has been reported in natural compounds and polymers such as starch **321**, cellulose **323**, bovine serum albumin **325**, and some other carbohydrates which even do not possess small aromatic systems like benzene rings (Chart 11B).[154] Whereas being practically nonluminescent in solutions, they emit bright phosphorescence in the solid states with lifetime up to microseconds. The fluorescent photographs of rice, starch, cellulose and BSA are shown in Fig. 7.

As well, nonconjugated alternating copolymer poly[(maleic anhydride)-*alt*-(vinyl acetate)] **326** was prepared as colloidal particles (Chart 12A).[155] The unique photoluminescence from such a common, nonconjugated (both main and side chains), alternating copolymer was reported.[156] Its water and ethanol solutions are nonluminescent, while the colloidal suspension emits blue light at

419 nm under UV excitation. The residue of the initiator BPO used in the polymerization might play a role in the luminescence behaviour.

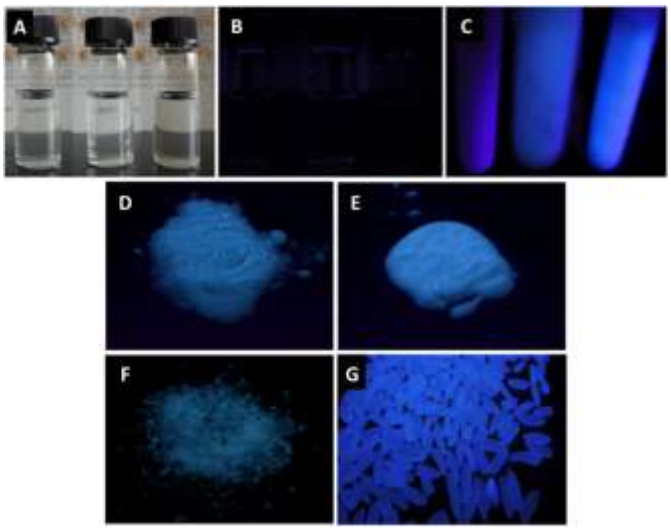

Fig. 7 Fluorescence photographs of (A–C) the solutions of starch **321** (left), cellulose **323** (middle), and BSA **325** (right) taken at (A–B) room temperature and (C) 77 K, and solid states of (D) starch **321**, (E) cellulose **323**, and (F) BSA **325**, and (G) rice. Photos were taken under (A) daylight and (B-G) UV illumination. Adapted with permission from Ref. 154. Copyright 2013 Springer.

Furthermore, Pucci reported aggregation-induced luminescence of polyisobutene succinic anhydrides (Chart 12B).[157] Four different polyisobutene succinic anhydrides **327–330** samples were collected after a reaction time of 4, 7, 10 and 14 h, respectively, between polyisobutene and maleic anhydride in large excess. They showed luminescence both in their neat form and in heptane solutions when the amount of functional groups per polymer chain was higher than a critical value. AIE phenomenon was strongly dependent on the number and the nature of interacting chromophores grafted on the polymer backbone and the associated quantum photoluminescent efficiency. Such fluorescence measurements might serve as an effective tool to determine the degree of functionalization of polyisobutene derivatives.

The aforementioned AIE luminescent polymers are by no means a complete collection of luminescent systems lacking conventional chromophores. The question, how do these systems luminesce, still remains. One common feature of all these polymers is that they are comprised of a large number of lone pair containing electron rich heteroatoms, cited as "heterodox clusters" in this review. The emission of the polymers discussed in this section are attributed to the aggregation of such non-emissive heterodox clusters. For example, aggregation of the heteroatoms as shown in Chart 12B may create new electronic communication pathways, rendering the polyisobutene succinic anhydride aggregates as a novel luminogen. The mechanistic investigation is still in progress to gain a deeper understanding and to draw more insight into these systems.

4. Functionalities and applications

AIE polymers enjoy both the advantages of AIE small molecules and polymer materials. Many of the practical properties and functionalities of AIE small molecules are applicable to AIE polymers, including fluorescent chemosensing, bioprobing, bioimaging, as well as fabricating light emitting devices. Because of the intrinsic properties of the polymer materials, especially conjugated polymers, AIE polymers display more advanced performance in such applications than their small molecular counterpart. For example, the conjugated polymer chains endow superior sensitivity compared with small molecule fluorescent dyes in the application of chemo- and bio-sensors; the facile processability is a predominant advantage in any kind of light emitting device fabrication; superior stability which enables long-term tracking of the cell for cell imaging applications.

Furthermore, integration of polymeric behaviours allows for applications beyond the scope of AIE small molecules. For instance, by combining AIE dyes and thermal sensitive polymers, constant reversible fluorescence signal response according to the environmental temperature change is achieved. Moreover, with their extended conjugation system, some luminescent polymers possess

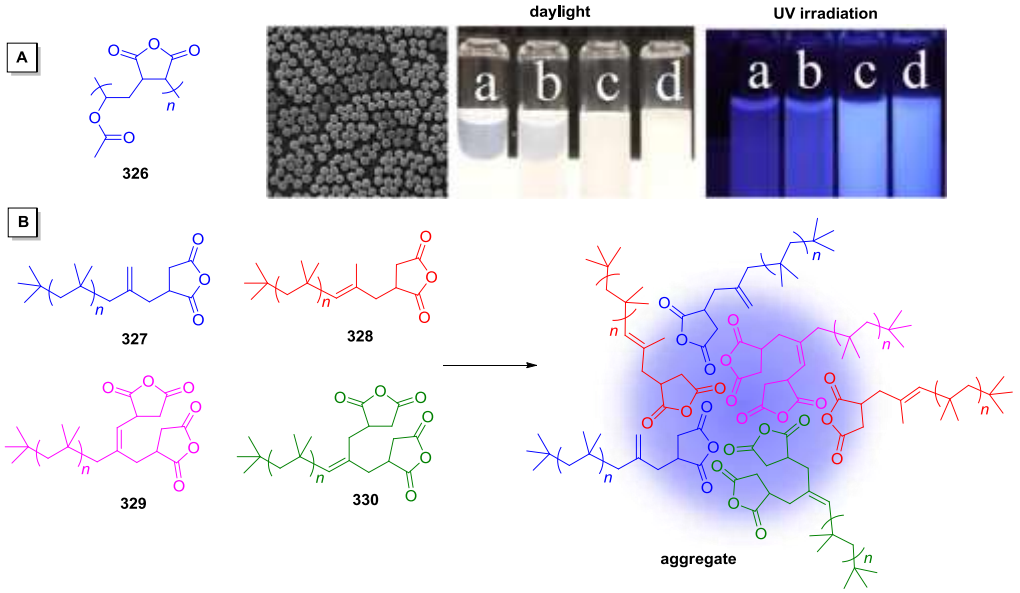

Chart 12 Chemical structures of (A) the alternating copolymer **326** and (B) compounds **327–330** prepared from the alder-ene reactions between polyisobutene and maleic anhydride. Insets: SEM image of the colloidal particles of **326** and images of the colloid suspensions with different concentrations taken under daylight and 365 nm UV irradiation, respectively. Colloid concentrations (wt%): (a) 0.05, (b) 0.1, (c) 1 and (d) 10. Adapted with permission from Ref. 156. Copyright 2007 American Chemical Society.

nonlinear optical properties, and with their rigid structure with repeating units, even polarized emission can be achieved. The films of the luminescent polymers also possess interesting functionalities such as high and tunable refractive indexes, photocrosslinkability, etc. The three dimensional structures bestow the materials with high porosity.

4.1 Fluorescent sensors

Fluorescent sensors based on conjugated AIE polymers have attracted much attention due to their fast, amplified response and superior sensitivity to analytes, in comparison to their low M_w congeners. The intrinsic autoaggregation of conjugated polymer chains is beneficial to the emission of AIE polymers, which avoid the problem of analyte-induced aggregation caused self-quenching. Among those, explosive detection is a commonly studied objective with its primary focus concerning safety since 2009.[42,93,95] Picric acid (PA) is chosen as a model for explosive analytes and the detection sensitivity was evaluated in the solution or aqueous suspensions. Quenching constants K_{sv} are calculated as a means of comparison and the quenching mechanism has been investigated to be static quenching.[86] By a simple comparison with AIE polymers consisting of similar building blocks but different topological structures, we can gain insight about the effect on sensitivity. The detection was also conducted in the solid state for convenient detection and potential devices.

Many different AIE polymers have been used to explore explosive detection. For example, linear conjugated polymer **119** with TPE units linked together has been explored as an chemosensor.[64] The THF solution and nanoaggregates in THF/water mixtures with 50 and 90 vol % water contents were utilized as probes for comparison in PA detection (Fig. 8A). Hyperbranched polymer **193** prepared from polycyclotrimerization of A_2-type TPE-containing monomer, and hyperbranched polymer **195** prepared through polycyclotrimerization of A_4-type monomer with similar building blocks are expected to possess extended conjugation, more branching sites and migration channels in three dimensional space.[88,89] They have also been studied for PA detection. The Stern-Volmer curves of **119**, **193** and **195** give high quenching constants (K_{sv}) of up to 827 000 M^{-1} (Fig. 8B–C). The nanoaggregates generally have higher K_{sv} values than the corresponding solutions. Compared with hyperbranched polymers **193** and **195**, linear polymer **119** shows better sensitivity in the aggregates, but poorer sensitivity in solution. Moreover, microporous polymer **292** prepared from the same A_4-type monomer but through Hay-Glaser coupling shows even better sensing performance.[37] For hyperbranched AIE polymers **270**–**271**, even without good conjugation, the emission of the polymer nanoaggregates can still be quenched efficiently by PA with large quenching constants up to 207 000 M^{-1}, suggesting that the topological structures greatly contribute to sensitivity.[134] High K_{sv} constant up to 1 090 000 M^{-1} was reported with other AIE polymers.[54,82] Generally, the polymers with better conjugation, more migration channels and decay pathways have higher sensitivity.

A common feature in the Stern-Volmer plots of relative PL intensity (I_0/I) versus PA concentration of many AIE polymers, especially the hyperbranched AIE polymers, show upward-bending curves instead of linear lines, revealing that the fluorescence quenching becomes more efficient at higher quencher concentration. This has been termed as the superamplification effect.[86,87] The superamplification effect is associated with both the AIE feature and topological structure of the polymer. Hyperbranched polymers possess a three dimensional globular structure, which offers more diffusional channels for the excitons to migrate, allowing them to be quickly annihilated by the PA quenchers. The AIE nature keeps its aggregates from suffering the false-positive signal and show enhanced sensing performance. In addition, polymer nanoaggregates offer more cavities for the explosive molecules to enter and further interact with the chromophores. The superamplification effect is associated with both the AIE feature and topological structure of the polymer. When more PA molecules are diffused into the internal cavities, the polymer swells which imparts increased surface area and potential interaction with more analytes. On the other hand, the interior phenyl rings have relatively more space to rotate, which further quench the light emission via nonradiative relaxation channels. Both effects result in higher sensitivity at high quencher concentration (Fig. 9A).

In addition to wet measurement, solid state sensing has also been demonstrated. The AIE polymer **192b** could be adsorbed onto a filter paper and letters of "HKUST" were written by dropping aliquots of a PA solution on the filter paper using a capillary tube. Upon photoexcitation, the letters emitted no light due to the emission quenching by the PA molecules (Fig. 9B).[87,102] Moreover, the polymers could also form a good solid film on a glass substrate by static-casting, whose strong PL will then completely quenched after dipping into dilute aqueous solutions of PA with detection limit down to 10^{-9} M.[103]

Besides PA, there are also other explosive analytes. For example, both 2,4,6-trinitrotoluene (TNT) and PA can cause significant fluorescence quenching of **295**. The spectral overlap between the emission of **295** aggregate and absorption of PA makes PA more sensitive to **295** than TNT in the fluorescence quenching detection.[141] This is also the case in polymer **218**. The main quenching mechanism for PA is long-range energy transfer and for TNT, short-range charge transfer.[99] The attachment of the sensing polymers onto a chromatographic support also allows for simultaneous separation of an explosive mixture, and component identification through the use of multiple sensing polymer **100**.[56] In a 1 mm^2 area solution spotted onto the fluorescent silica plate, the detection limits obtained for the explosives TNT, 2,6-dinitrotoluene (DNT), PA, *N*-methyl-*N*, 2,4,6-trinitroaniline (Tetryl), octahydro-1,3,5,7-tetranitro-1,3,5,7-tetrazocine (HMX), 1,3,5-trinitro-1,3,5-triazacyclohexane (RDX) and 2,4,6,8,10,12-hexanitro-2,4,6,8,10,12-hexaazaisowurtzitane (Cl-20) ranged from 4–750 pg/mm^2.

Selective detection has been achieved in polymers **129**, **131** and **133**.[66] The LUMO of **133** is mainly located on the 2,1,3-benzothiadiazole (BT) units. PA can easily form negative charged anions in aqueous solutions. An electrostatic repulsive interaction between the BT unit and PA will block the efficient electron transfer from the LUMO of **133** to PA, which will not happen in the case of TNT. Therefore, it can selectively detect TNT instead of PA in aqueous solutions. For the film of **133**, the K_{sv} constant of TNT (1.2×10^5 M^{-1}) is almost 2 orders higher than that of PA (1.8×10^3 M^{-1}), thus it can differentiate TNT and PA. **133** exhibits the best sensitivity for TNT with a detection limit of 3 ng/cm^2 (Fig. 9C). In contrast, the donor-only polymers **129** and **131** exhibit higher selectivity toward PA as do most conjugated polymer sensors. For example, the emission of **131** film can be selectively quenched by PA with the K_{sv} constant of 2.8×10^4 M^{-1} and a detection limit of 2 ppb. Moreover, the quenching effect is reversible.

Another example of selective detection of explosives is the nanoparticles of **312** without traditional luminogens.[151] It exhibits high sensitivity and selectivity, as well as fast response to nitroaromatic explosives such as TNT, Tetryl and PA as shown in Fig. 10. No interference from common organic solvents was observed. The nanoscaled size and unique hierarchical porosity makes **312** one of the most sensitive fluorescence-based sensing material.

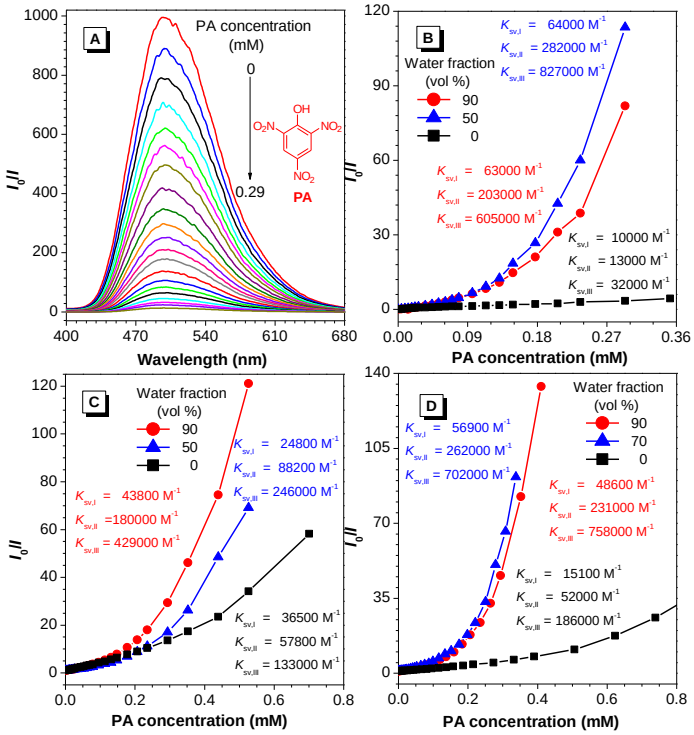

Fig. 8 (A) PL spectra of **119** with different PA concentrations in THF–water mixture with 90% water fraction. Stern–Volmer plots of (I_0/I) value versus [PA] for (B) **119**, (C) **193** and (D) **195** in THF and THF–water mixtures with 50, 70 and 90 vol % water contents. I_0 = intensity at [PA] = 0 mM. Concentration: 10 μM. Adapted with permission from (A–C) Ref. 64 and 88. Copyright 2012 The Royal Society of Chemistry; (D) Ref. 89. Copyright 2013 Wiley-VCH.

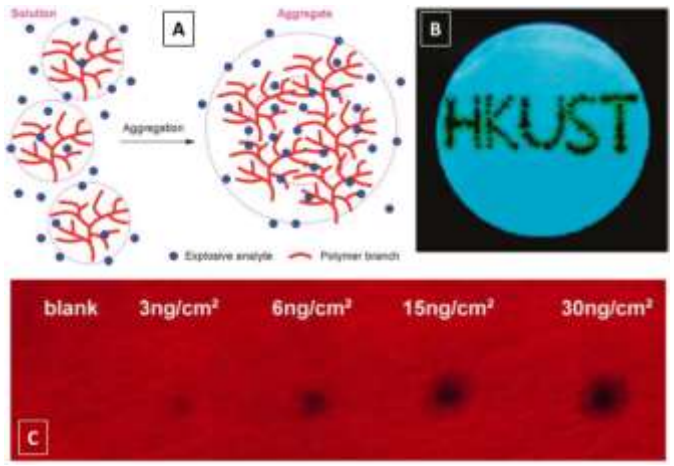

Fig. 9 (A) Illustration of explosive detection by AIE-active hyperbranched polymers in solution and aggregate states. (B) Fluorescent image of **192b** deposited on a filter paper and the letters "HKUST" were written by dropping aliquots of a PA solution on the filter paper using a capillary tube. (C) Fluorescence quenching of the thin-film of **133** coated on filter paper by solid particulates of TNT with various concentrations. Adapted with permission from (A) Ref. 86. Copyright 2010 The Royal Society of Chemistry; (B) Ref. 87. Copyright 2010 American Chemical Society; (C) Ref. 66. Copyright 2011 American Chemical Society.

The fluorescent detection of explosive analytes is mainly based on energy transfer between the fluorescent polymers and the explosive compounds. Although selectivity is demonstrated in some cases, there is still room for further improvement. Enhanced selectivity can be designed through specific chemical structures to achieve one-to-one recognition of analytes. This is of particular importance to the monitor of environment, water, and atmosphere.

Volatile organic chemicals (VOCs) with low chemical reactivity are difficult to detect. However, taking advantage of AIE characteristics, it is easy to detect VOCs by a simple dissolve-evaporate process, where the sensing process is reversible and repeatable. For example, the emission of the polymer **270** spots on the TLC plates can be turned "off" and "on" by wetting and drying processes with organic solvent vapors (Fig. 11A–C).[134] Similar phenomena were also demonstrated with **231–235**[104] and **254–256** (Fig. 11D–F).[124] Poly(fluorene-*o*-carborane) **249** was shown to act as a reversible colorimetric sensor for volatile nitrogen containing molecules based on the various possible photoluminescence pathways of **249**.[119] Exposure to common laboratory solvent vapors led to an emission color change of the films under UV light. The original green emission of the blank polymer shifted to the observed different emission colors. Various emission colors appeared when exposed to different VOCs (Fig. 12). In another example, nanotubes were used to enhance the sensitivity of **210b** towards the VOCs.[158]

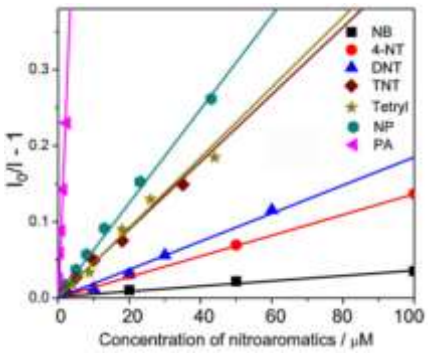

Fig. 10 Stern-Volmer plots of fluorescent quenching of nanoparticles of **312** with various explosive analytes in 2 mL 10% THF aqueous solution. Reproduced with permission from Ref. 151. Copyright 2012 Elsevier Ltd.

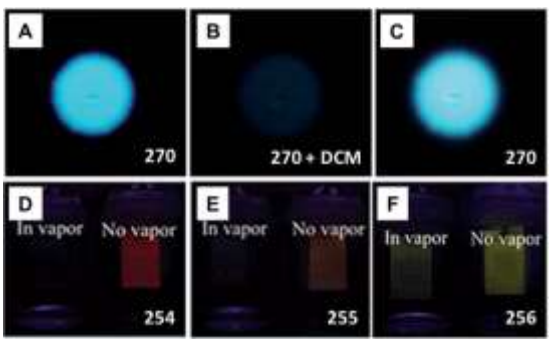

Fig. 11 Fluorescence photographs of spots of hyperbranched polymer **270** deposited on TLC plates (A) before and (B) after exposure to vapour of dichloromethane for 1 min. The photograph in (C) is taken after the organic vapour in (B) had been evaporated. (D-F) On/off fluorescent switching of **254–256**, respectively, on TLC plates in chloroform vapour (left) and without vapour (right). Photos were taken under UV illumination from a hand-held UV lamp. Adapted with permission from (A–C) Ref. 134. Copyright 2013 The Royal Society of Chemistry; (D–F) Ref. 124. Copyright 2011 Wiley-VCH.

MOFs with large porosity also show great advantage in fluorescent chemosensor applications.[159] Interaction of NH_3 with Zn_2(TCPE) **303** causes fluorescence shifts and turn-on luminescence

responses preferentially over a variety of potential interferences such as water, methanol, larger amines, and other gases. Exposure of activated **303** to ammonia, triethylamine, ethylenediamine, *N*, *N*-diethylformamide and water vapors at room temperature shifted its emission maximum by up to 23 nm. Monitoring the effect of these analytes at 100 ^{o}C showed that only ammonia exposure led to a significant shift of the emission maximum from 487 to 511 nm, thus revealing a remarkable selectivity for NH_3 detection at high temperature.

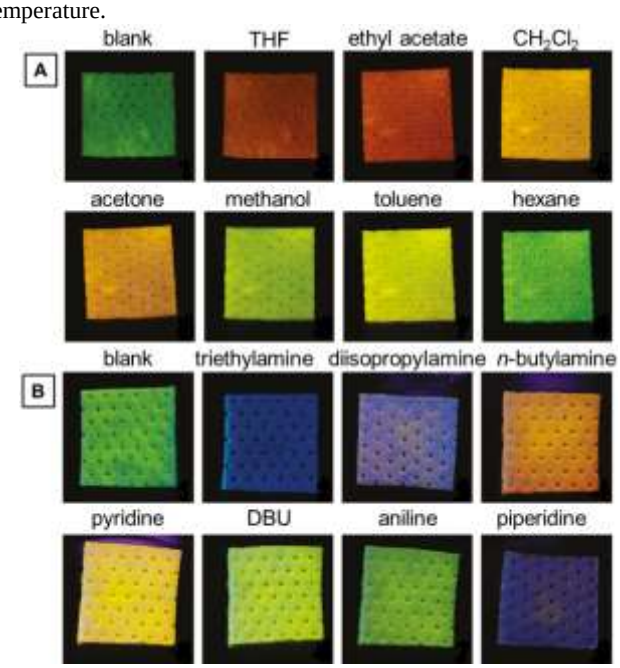

Fig. 12 Optical images under UV light of the pristine polymer **249** coated onto squares of laboratory wipes and (A) in the presence of THF, ethyl acetyate, methylene chloride, acetone, methanol, toluene, and hexanes vapors, and (B) in the presence of triethylamine, diisopropylamine, *n*-butylamine, pyridine, 1,8-Diazabicyclo[5.4.0]undec-7-ene (DBU), aniline, and piperidine. (The blue color is the observed color of the composite wipe under UV light, not an emission from the fluorene segments). Adapted with permission from Ref. 119. Copyright 2011 American Chemical Society.

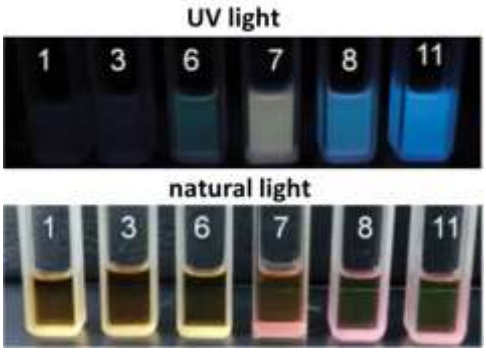

Fig. 13 Images of **313** in ethanol at different pH values under (A) a UV lamp and (B) natural light. The pH values are indicated on each vessel. Adapted with permission from Ref. 152. Copyright 2013 The Royal Society of Chemistry.

Besides gases, the selective sensing can also be conducted in solutions. For example, the polymer **174** can serve as a "light up" probe for the detection of hydrazine to form **176**.[82] Nanoparticles of hyperbranched polymer **313** show different appearance and emission color in different pH environments, suggesting potential pH sensor applications as shown in Fig. 13.[152] Last but not least, the organogel of **257** allows recognition of F^- selectively since the gel can be destroyed in the presence of F^-, accompanied by the emission enhancement.[125] It was difficult for the larger anions to interact with amide groups in **257** on account of steric hindrance of the branched arms.

4.2 Stimuli-responsive materials

Because of the polymers' intrinsic property, various environmental stimuli can result in fluorescent response of AIE polymers, such as light, heat, solvent, etc. For example, an azobenzene-containing block copolymer of PEG_{45}-*block*-poly(dimethylaminoazobenzene)$_{47}$ **331** can undergo reversible photoisomerization from *trans*- to *cis*-isomers (Scheme 39).[160] The block copolymer can self-assemble in water to form unilamellar vesicles with average sizes of about 120 nm, owing to its amphiphilic nature. **331** is non-emissive in THF solution, however, the fluorescence of the resulting vesicular solution at about 550 nm is greatly enhanced by about 130-fold (inset photo, Scheme 39). The observed AIE phenomenon is due to the restriction of the intramolecular motions of dimethylaminoazobenzene groups from the compact stacking in the vesicles. Furthermore, the *trans*-to-*cis* photoisomerization for the vesicular solution is slowed down considerably. The fluorescence spectrum of the vesicular solution of **331** before and after 450 nm irradiation was studied. The PL intensity gradually decreases with increasing irradiation time. After being stirred in the dark, enhanced fluorescence of the vesicular solution is observed. This reversible fluorescence response can be achieved periodically by alternative irradiation of 450 nm light and stirring in the dark.

PNIPAM is a well-known polymer for its thermal sensitivity. One common strategy is to incorporate PNIPAM structures to AIE polymers to achieve thermal-responsive AIE polymers. Polymer **16** with PNIPAM structures show fluorescent response towards temperature change around the biological important temperature range as shown in Fig. 14.[129] When the solution of **16** is heated to 25 ^{o}C, the isopropyl pendants of PNIPAM chains start to dehydrate, which undergo a coil-globule transition. Such a subtle change can hardly be detected by dynamic light scattering (DLS), UV and NMR analyses, but can be sensed by PL as the reduced volume impedes the intramolecular rotation of TPE and enhances its emission. In the temperature range of 29–34 ^{o}C, coil-globule transition becomes active and the whole polymer chains dehydrate, which greatly activates the RIM process of the TPE label and dramatically enhances the emission intensity. When the temperature is beyond 34 ^{o}C, there is minimal further change in the compactness of the aggregates and the heating actives the molecular motions, which make the polymer less emissive.

Similarly, polymer **243a** with tetraphenylthiophene covalently linked to two PNIPAM chains can form core-shell micelles in water at room temperature.[109] The aqueous solution of **243a** is transparent at room temperature but becomes highly opaque when heated to 40 ^{o}C (Fig. 15A). This visual difference can be reversibly manipulated through heating and cooling cycles, which is associated with the average hydrodynamic diameter change in such temperature range. When heated between 20–29 ^{o}C, the aqueous solution of **243a** emitted at 405 nm with constant intensity. However, at elevated temperatures above the lower critical solution temperature (LCST) at 29 ^{o}C, the originally formed micelles underwent structural transformations due to the collapse/aggregation of the PNIPAM segments and the dissociation of the TP aggregates, resulting in the sudden emission slump until the complete emission quench at 34.4

^{o}C. The AIE-active **243a** hence exhibited thermoresponsive PL emission. Besides PNIPAMs, oligo(ethylene glycol)s are commonly integrated into thermosensitive macromolecules. By taking advantage of the AIE properties and thermosensitivity, star-shaped macromolecule **252** is able to sense temperature by showing different emission intensities and turbidity.[122] The temperature-induced fluorescence change is highly reversible.

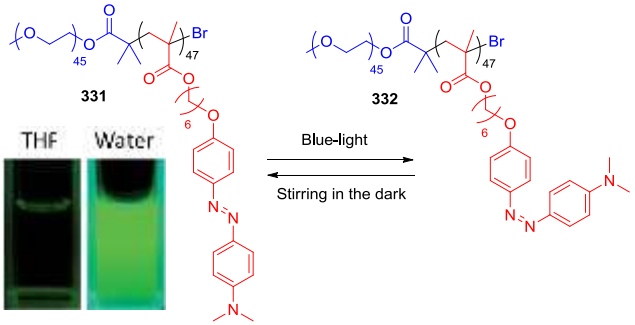

Scheme 39 Schematic representation of the structure of an azobenzene-containing block copolymer **331** and its visible light switchable behavior. Insets: fluorescent images of **331** in THF solution and aqueous medium. Adapted with permission from Ref. 160. Copyright 2013 The Royal Society of Chemistry.

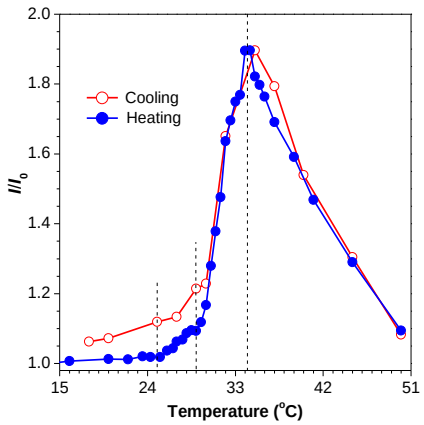

Fig. 14 Effect of temperature on PL intensity at 468 nm of polymer **16**. λ_{ex} = 322 nm; concentration = 1 mg/mL. Adapted with permission from Ref. 129. Copyright 2012 Wiley-VCH.

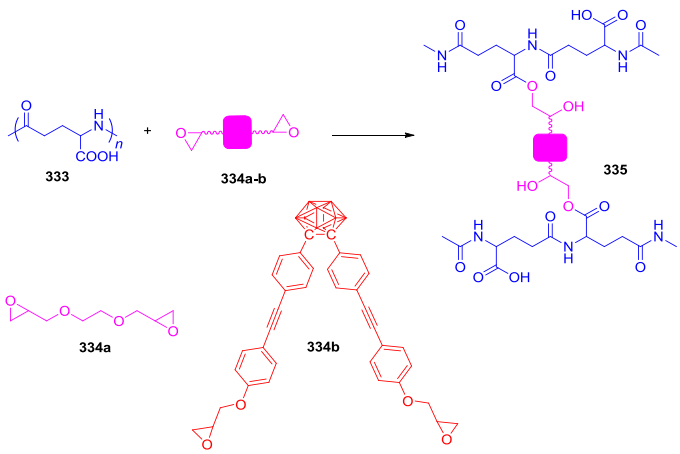

Scheme 40 Preparation of γ-PGA hydrogel **335** using **334a–b** as cross-linkers.

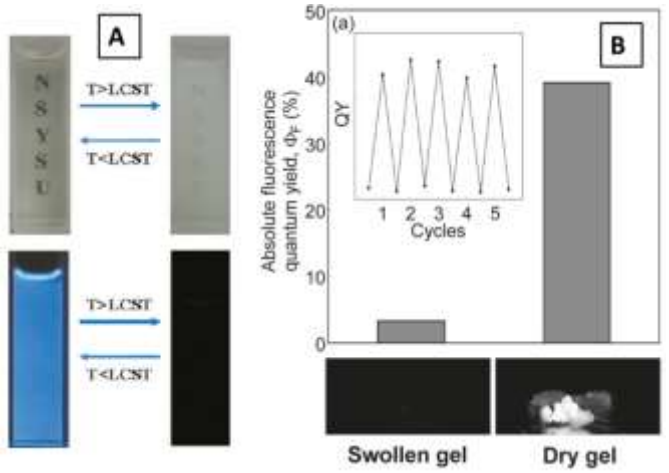

Fig. 15 Photograph showing an aqueous solution of **243a** at room temperature (left) and at 40 ^{o}C (right) under daylight (top) and UV illumination (bottom). (B) Absolute fluorescence quantum yields and the fluorescence images of **335** in swollen and dry state under UV lamp irradiation. Inset: the switching of absolute fluorescence quantum yields of **335** in swollen and dry state. Adapted with permission from (A) Ref. 109. Copyright 2011 American Chemical Society; (B) Ref. 161. Copyright 2010 American Chemical Society.

Besides light and heat-induced PL response, a poly(γ-glutamic acid) (γ-PGA) hydrogel **335** with water-sensitive luminescence derived from AIE of *o*-carborane was reported.[161] γ-PGA **333** was successfully crosslinked with ethylene glycol diglycidyl ether **334a** and *o*-carborane derivative **334b** by stirring at 80 ^{o}C for 2 h (Scheme 40). The ratio of **334a**/**334b** is in the range of 2.0×10^{2}–2.0×10^{4}. Gel formation was observed with more than 5 mol % cross-linker ratio. Hydrogel **335** containing the AIE-dye exhibited effective reversible fluorescence switching between the swollen and dried states (Fig. 15B). The Φ_Fs of the hydrogel **315** in swollen and dried states is 0.03 and 0.39, respectively.

4.3 Biological probes

With their fluorescence response towards biomolecules, AIE polymers are promising candidates for bioprobes. In particular, AIE polyelectrolytes can serve as good biological probes as they can be dissolved in aqueous solutions and still possess AIE property. For example, amphiphilic polymer **30** can be used to detect glucose indirectly through the reaction of glucose oxidase.[33]

Polyelectrolyte **245** with unique dual-channel fluorescence response was applied to detect heparin, a highly sulfated glycosaminoglycan with the highest negative charge density among the known biological molecules.[112] The fluorescence intensity gradually increased upon addition of heparin into the aqueous solution of **245** with a linear response to the concentration of heparin. The fluorescent images of the aqueous solution of **245** without and with heparin are shown in Fig. 16A. Similarly, the PL spectra of **246** changed significantly with the heparin concentration in the solution.[113] With gradual addition of heparin, there was a progressive increase of the yellow emission band around 563 nm and a concomitant decrease of the blue emission band at 419 nm with an isosbestic point at 504 nm. When the heparin concentration reached 1.0 μM, a 7.5-fold PL decrease at 419 nm and a 3.2-fold PL increase at 563 nm were observed. The detection limit was 30 nM. Cationic **246** can form inter-polyelectrolyte complexes with the negatively charged heparin through strong electrostatic attractive interactions, which leads to polymer aggregates. More efficient interchain energy transfer from the polyfluorene segments to the ATPE units as well as

aggregation of ATPE units take place, which quench the original blue emission and enhance the yellow emission from the ATPE units.

In addition to heparin detection, AIE polyelectrolytes have been reported to successfully detect other biomacromolecules, owing to their electrostatic and hydrophobic interactions with biomacromolecules. Polyelectrolyte **64** can bind to bovine serum albumin (BSA) through both electrostatic and hydrophobic interactions to induce emission enhancement, making it a sensitive bioprobe for BSA at ultralow protein concentration (0–0.6 ppm).[42] A fluorescence turn-on biosensor for sensitive DNA detection and quantification was developed by taking advantage of complexation-induced aggregation of **247**, which increases the polymer fluorescence in aqueous solutions.[114] Water soluble fluorescent polyelectrolytes **185** and **188** can be synthesized by means of the quaternization of polymer precursors **184** and **187**.[84] The emission intensity of their aqueous solution can be enhanced up to 7-fold upon binding with biomolecules such as heparin, ctDNA, RNA, BSA and HSA through electrostatic and hydrophobic cooperative interactions.

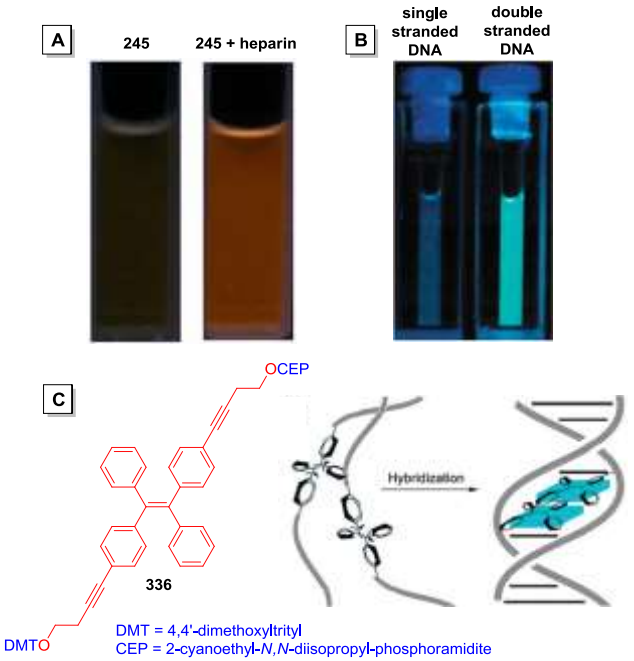

Fig. 16 (A) Fluorescence images of solution of **245** before and after addition of heparin, and (B) single and double stranded DNA incorporated with **336**. (C) Chemical structure of **336** and schematic illustration of using TPE as a building block in single and double stranded DNA. Adapted with permission from (A) Ref. 112. Copyright 2012 Acta Polymerica Sinica; (B–C) Ref. 162. Copyright 2013 The Royal Society of Chemistry.

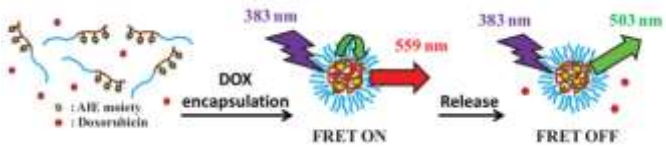

Scheme 41 The schematic illustration of the fluorescent monitoring of the encapsulation and release of Doxorubicin with fluorescent polymeric micelles **25b**. Adapted with permission from Ref. 32. Copyright 2013 Wiley-VCH.

AIEgens can also be covalently linked to biomacromolecules. One such example was to probe the DNA hybridization. For example, TPE-containing phosphoramidite **336** was prepared and then incorporated into the single stranded DNA to form dialkynyl-TPE (DATPE) modified DNA strands, which was then used to monitor the formation of double–stranded DNA (Fig. 16C).[162] The comparison between single stranded DNA and double stranded DNA, each with a total of two DATPE units, shows that the emission is considerably higher in the duplex (Φ_F = 19%) than in the single strand (Φ_F = 7%). Further increasing the number of DATPE units in double stranded DNA, with two DATPE units in each strand, significantly increases the Φ_F to 32%. The AIE effect is illustrated in the fluorescence images of Fig. 16B: the duplex DNA, comprised of single stranded DNA with two DATPE units, exhibits a 10-fold PL enhancement over its single stranded precursor. The aggregates of DATPE units are positively influenced by the well-organized duplex structure compared to the single stranded random coil.

Furthermore, the micelles of amphiphilic polymer **25b** can be simultaneously used as a fluorescent probe and a drug carrier simultaneously.[32] When the micelles of **25b** were loaded with a fluorescent anticancer drug, doxorubicin (DOX), the encapsulation and release of loaded drug can be reflected via PL change (Scheme 41). Energy transfer from pentaphenylsilole units of **25b** to DOX is expected when this donor/acceptor pair is close, owing to the spectral overlap between pentaphenylsilole and DOX. This FRET process was utilized as an indicator for the encapsulation and subsequent release of DOX. The emission peaks of the DOX-loaded **25b** micelles at 503 and 559 nm represent the emission from pentaphenylsilole and DOX, respectively. With higher loading amount of DOX, the relative intensity of I_{559}/I_{503} increases. The quenching of emission at 503 nm, accompanying with the enhancement of PL at 559 nm, suggests the FRET process from pentaphenylsilole to DOX. In the drug release study, the emission spectra of DOX-loaded **25b** micelles with DOX feeding ratio of 20% was studied after release for 24 and 48 h. The green emission at 503 nm recovered and the red emission from DOX decreased with the increasing releasing time. The fluorescent AIE micelles can thus not only act as an anticancer drug carrier, but also can be used to monitor the encapsulation and release of drug via the FRET process.

4.4 Cell imaging

AIE polymers and AIE polymer-based fluorescent organic nanoparticles enjoy superior stability and strong emission efficiency in aqueous media. With structural modification, they can possess good water solubility/dispersibility and good biocompatibility. They thus show great potential in cell imaging applications, especially in long-term cell tracking. In fact, a series of AIE polymers have been successfully used to image a large variety of cells.

For instance, water soluble polymer **188** can serve as fluorescent visualizer for intracellular imaging in HeLa cells with high sensitivity and fast response (Fig. 17A–C).[84] The polymer selectively stains the cytoplasm of living HeLa cells but not their nuclei. Endocytosis is considered to be the major route for polymer **188** to enter the cells, in which **188** was first enclosed by the cell membrane to form small vesicles and then be internalized by the cells.

Various cell lines can be used for imaging. Polymer **20** was endocytosed by two cell lines, human brain glioblastoma U87MG cells and human esophagus premalignant CP-A, with a distribution into the cytoplasm (Fig. 17D–I).[30] The polymer is noncytotoxic to the two cell lines at a concentration of 1 mg/mL. Its analogue polymer **22** is also cell permeable.[31] Cellular uptake of **22** was demonstrated to be through a time and energy-dependent endocytotic mechanism and the fluorescent polymer is located in the cellular cytoplasm area.

AIE polymer-based fluorescent organic nanoparticles (FONs) are quite popular in cell imaging application, owing to their high

brightness, superior stability, non-blinking, etc.[163] The FONs based on conventional dyes normally result in significant decrease of PL intensity when the dyes are aggregated in the nanoparticles because of the aggregation-caused quenching effect. On the other hand, covalently linking the dye and polymer backbones in AIE polymers greatly increase their stability of self-assembled FONs, as compared with AIE small molecule-based FONs. Generally, AIE polymer based FONs are prepared by incorporating AIE dyes into hydrophilic polymer structures. The resulting amphiphilic polymers can then self-assemble to form fluorescent nanoparticles in pure aqueous solution.

The emissive particles of **49** can be used for cellular imaging. The BCap37 cells were incubated with the nanoparticles of **49** as shown in Fig. 17J–L, demonstrating that the particles are accumulated in the cytosol rather than the nucleus.[38] The fluorescent core-shell unimolecular micelles based on hyperbranched AIE polymer was reported as a powerful tool for cell imaging.[133] Through self-assembly of the unimolecular micelles to multi-micelle aggregates, the emission of **267** enhanced. The cellular uptake of **267** by MCF-7 cells was evaluated and strong fluorescence is observed mainly in the cytoplasm of the cells when the cells are cultured in **267** for 2 h.

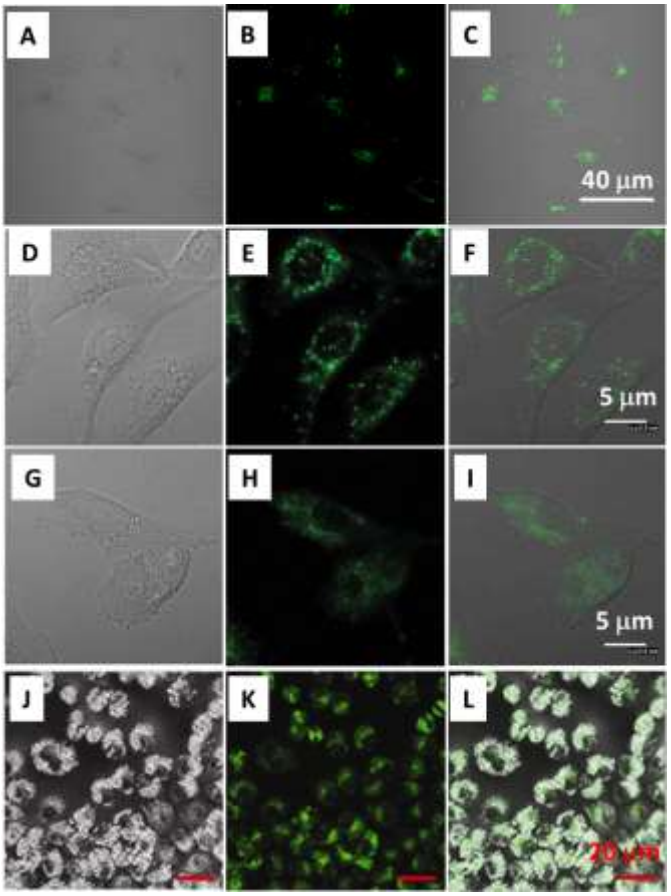

Fig. 17 Confocal fluorescence images of (A–C) HeLa cells stained with **188**, (D–F) CP-A cells and (G–I) U87MG cells stained with **20**, and (J–L) BCap37 cells incubated with the nanoparticles of **49**. (A, D, G, J) Bright field images, (B, E, H, K) fluorescence images, and (C, F, I, L) merged images. Adapted with permission from (A–C) Ref. 84. Copyright 2013 Wiley-VCH; (D–I) Ref. 30. Copyright 2012 Wiley-VCH; (J–L) Ref. 38. Copyright 2012 Springer.

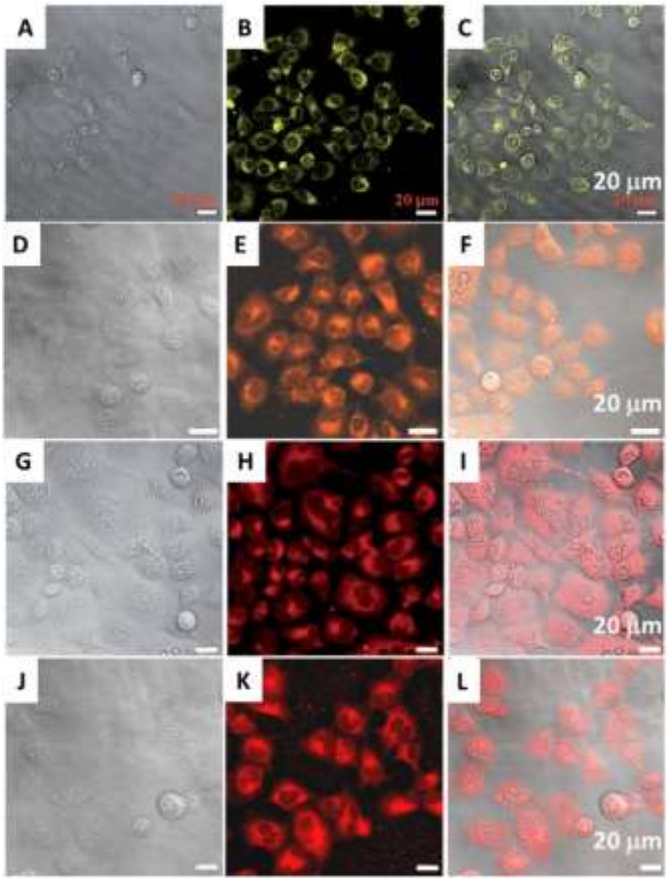

Fig. 18 CLSM images of A549 cells incubated with (A–C) 40 μg/mL of **34**, (D–F) 10 μg/mL of **38**, (G–I) 20 μg/mL of **88**, and (J–L) 10 μg/mL of **89** for 3 h. (A, D, G, J) Bright field images, (B) excited with a 488 nm laser, (E) excited with a 405 nm laser, (H and K) excited with a 543 nm laser, and (C, F, I, L) merged images. Adapted with permission from (A–C) Ref. 34, (D–F) Ref. 35, (G–I) Ref. 49 and (J–L) Ref. 51. Copyright 2014 The Royal Society of Chemistry.

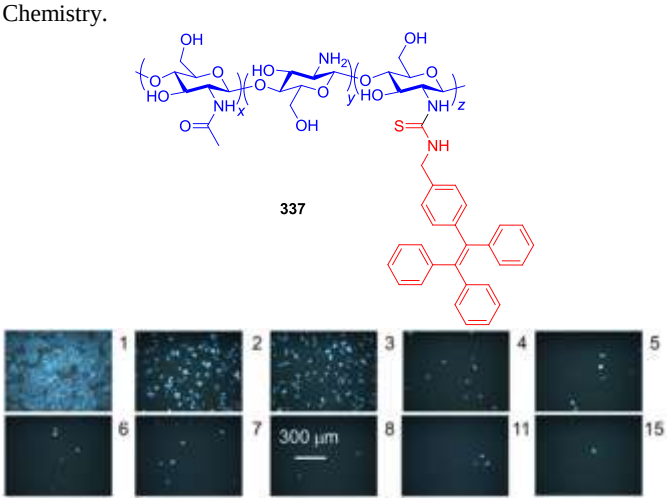

Fig. 19 Chemical structure of TPE-CS bioconjugate **337** and fluorescence images of the HeLa cells stained by the aggregates of **337** with a degree of labelling of 7.86 mol% at different passages taken at magnifications of ×100. Numbers of passages are denoted by the numerals (1–15) on the right sides of the images. Adapted with permission from Ref. 164. Copyright 2013 American Chemical Society.

Cell imaging usually suffers from a severe autofluorescence problem with blue background emission. To mitigate the interference of background noises, fluorescent dyes/particles with different emission color are developed for cell imaging. The AIE polymer-based FONs with various emission colors tuning from yellow to red are thus used for cell imaging. The FONs based on amphiphilic AIE polymers **34**,[34] **38**,[35] **88**,[49] and **89**[51] with yellow to red emission colors are stained with A549 cells and intense emission was observed as shown in Fig. 18.

One major advantage for AIE polymers in cell imaging is their high stability which enables long-term tracking. In a typical work, TPE labels are attached to a chitosan (CS) chain and the resultant TPE-CS bioconjugate **337** is soluble in acidic media.[164] Different from those of their parent forms (TPE and CS), the dilute solution of **337** is fluorescent. When a TPE group is bound to a bulky CS backbone, the intramolecular rotations of its phenyl rings are hindered. With an increasing degree of labelling, the PL intensity of **337** is increased in a nonlinear fashion. The aggregates of **337** can be readily internalized by HeLa cells. Large aggregates are preserved in one cell, instead of distributing in two daughter cells in every cell division cycle. The cellular staining by the aggregates of **337** is so indelible that it enables cell tracing for as long as 15 passages (Fig. 19). Ionic gelation method is also used to fabricate nanoparticles of **337**, which are uniform in size, spherical in shape, monodispersed, and positive in surface charge.[165] The nanoparticles exhibit strong fluorescence and low cytotoxicity, making them well suited for cell imaging. The nanoparticles can be internalized into cytoplasm through an endocytotic pathway, which then retain inside the live cells and enable long-term tracking of 7 passages of cell growth. The nanoparticles are photostable with less than 25% signal loss upon continuous excitation under fluorescence microscope for 30 min. The long retention duration of bioconjugate **337** in a specific preloaded cell line may enable their use as long-term cellular tracers in a variety of unique biomedical applications.

4.5 Electroluminescence devices

Departing from fluorescent sensing and imaging applications, the unique optoelectronic properties of AIE polymers bestow them with a series of potential high-tech applications such electroluminescent (EL) devices.

For example, with their high solid-state photoluminescence, amorphous behaviour and high thermal stabilities, TPE-terminated oligofluorenes **231**–**235** are fabricated into multilayer OLED devices with configuration ITO/poly(3,4-ethylenedioxythiophene) (PEDOT) (40 nm)/dye (~50 nm)/1,3,5-*tris*(N-phenylbenzimidazol-2-yl)benzene (TPBi) (40 nm)/LiF (1 nm)/Al (100 nm) by spin coating deposition processes.[104] The oligomers serves as the light emitting layer, PEDOT functions as the hole-transporting layer and TPBi functions both as the hole-blocking and electron transporting layer. The turn-on voltages and efficiencies can be tuned by the length of the fluorene core and oligomer **231** is the best OLED emitter in the series. The device fabricated from linear oligomer **231** has a maximum luminance, power efficiency, and current efficiency of 1300 cd/m^2, 1 lm/W, and 2.6 cd/A, respectively.

Thanks to its fast electron mobility, silole has been commonly used as an electron-transporting and light-emitting material in the construction of electroluminescent devices.[166] Using silole-substituted polyacetylene **61** as an active layer, a multilayer electroluminescence device with a configuration of ITO/(**61**:PVK) (1:4)/BCP/Alq_3/LiF/Al (PVK = Poly(9-vinylcarbazole), BCP = bathocuproine) emitted a blue light of 496 nm with maximum brightness, currently efficiency, and external quantum yield of 1118 cd/m^2, 1.45 cd/A, and 0.55%, respectively.[41] Polyfluorene is reported to be used as the interfacial layer of the cathode of PLEDs and results in powerful electron injections from air-stable high work-function metals, with device efficiency comparable to those of low-function metals (Ca, Ba).[167] The PLED performances of the fluorene and silole-containing polymers **148a–c** were thus investigated with three different cathode configurations (Al, Ba/Al, and TPBi/Ba/Al).[69] With the device configuration of ITO/PEDOT (50 nm)/**148** (80 nm)/TPBi (30 nm)/Ba/Al, the best result was obtained from **148b** with its maximum brightness, luminance efficiency of 4880 cd/m^2 and 7.96 cd/A, respectively.

The electroluminescence of tetrathiophene-containing linear polymer **240** was also reported. EL devices were fabricated with a configuration of ITO/PEDOT:PSS (100 nm)/**240** (80 nm)/Al (120 nm).[107] The spectrum consists of the main aggregate emission band centred at ~490 nm and the small shoulder-like monomer emission at ~440 nm. The device shows a low operating voltage onset at ~ 5.0V and a high luminance of 1000 cd/m^2.

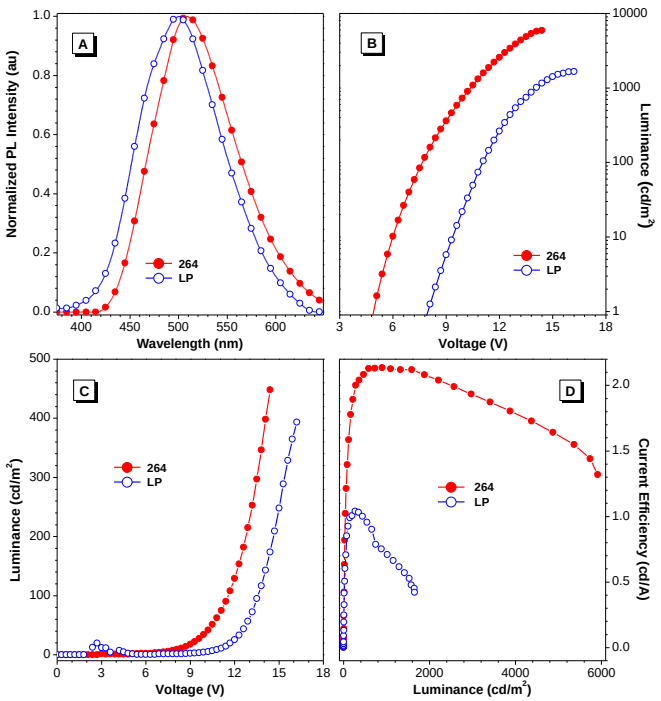

Fig. 20 (A) The EL spectra of **264** and its linear polymer (LP) analogue. (B) Luminance-voltage characteristics of the PLED devices. (C) Current-voltage characteristics of the PLED devices. (D) The luminescence efficiency-current characteristics of the PLED devices. Adapted with permission from Ref. 132. Copyright 2012 The Royal Society of Chemistry.

Carbazoles are famous materials with good hole-transporting and electroluminescent activities and 1,3,4-oxadiazole derivatives are electron deficient materials with good thermal/chemical stabilities and high Φ_F, which are generally used as electron-transporting materials in polymer light-emitting diodes (PLEDs). The incorporation of hole-transporting carbazole units or electron-transporting 1,3,4-oxadiazole units can effectively improve EL performance of the AIE polymer-based PLED devices. PLED devices with a configuration of ITO/PEDOT:PSS (25 nm)/Poly-TPD (25 nm)/**141** or **144** (32 nm)/TPBi (35 nm)/Cs_2CO_3 (8 nm):Ag (100 nm) (PSS = poly(styrenesulfonate), Poly-TPD = poly[*N*,*N*'-bis(4-butylphenyl)-*N*,*N*'-bis(phenyl)-benzidine]) have been fabricated. The EL performance of **141** and **142** was improved dramatically compared with that of their analogues **137** and **139**, owing to the introduced hole-transporting or electron-transporting groups. Carbazole-containing **141** showed the best performance with a

maximum luminance efficiency of 1.17 cd/A and a maximum brightness of 3609 cd/m^2 at 12.9 V in its PLED device.[67] Furthermore, a series of green emission polyfluorene-carbazole-siloles **151a–d** were fabricated into PLED devices with the configuration of ITO/PEDOT (40 nm)/**151** (80 nm)/TPBi (30 nm)/CsF/Al.[71] With **151c** as the emissive layer, a high maximum external quantum efficiency of 2.33%, a maximum luminescence efficiency of 6.62 cd/A, and a maximum brightness of 3857 cd/m^2 were achieved.

The EL behaviour of AIE-active hyperbranched polymers have also been studied. TPE-based hyperbranched polymer **263a–c** have excellent fluorescence stability with stable PL spectra after annealing at 180 and 200 ^{o}C, respectively.[131] The PLED devices with the configuration of ITO/PEDOT:PSS (25 nm)/Poly-TPD (25 nm)/**263** (32 nm)/TPBI (35 nm)/Cs_2CO_3 (8 nm):Ag (100 nm) were fabricated using **263a–c** as the light emitting layer. **263a** demonstrated better EL performance compared to most of conjugative hyperbranched polymers, with the luminescence of 948 cd/m^2 and the luminescence efficiency of 1.15 cd/A.

Hyperbranched polymer **264** with typical AIE characteristics as well as carbazole-based core with potential hole-transport properties, was expected to have outstanding EL performance. The PLED device ITO/PEDOT:PSS (25 nm)/Poly-TPD (25 nm)/**264** (32 nm)/TPBI (35 nm)/Cs_2CO_3 (8 nm):Ag (100 nm) was fabricated.[132] When a bias potential was applied to the electrodes, EL emission at 508 nm could be achieved from the EL device of **264**. The hyperbranched **264** showed much better EL performance than its linear analogue polymer (Fig. 20). The turn-on voltage of the device is only 5.2 V. In addition, the maximum luminescence of **264** is as high as 5914 cd/m^2. Most importantly, **264** exhibited a much higher luminescence efficiency (2.13 cd/A), twice than that of its linear polymer analogue (1.04 cd/A) with a luminescence efficiency of 1654 cd/m^2. This PLED result represents one of the highest values reported so far for conjugated hyperbranched polymers.

4.6 Optical nonlinearities

Materials with nonlinear optical properties have attracted much attention recently, owing to their exceptional utility in three-dimensional microfabrication and storage,[168] optical power limiting,[169] three-dimensional imaging,[170] photodynamic therapy,[171] and two-photon pumped up-converted lasers.[172] Many of the AIE polymers possess large conjugated structure, which may show potential nonlinear optical properties, especially two-photon absorption and two-photon excited fluorescence (TPEF).

For example, TPE-containing linear polymer **154** with C=C bond bridges shows aggregation-induced two-photon absorption enhancement. The two-photon excited fluorescence is similar to its one-photon fluorescence process. When excited with 800 nm light, the THF solution of **154** is faintly emissive at 520 nm, while its nanoaggregates show an 8.6-fold fluorescence enhancement (Fig. 21E). The calculated two-photon absorption cross section (σ_{TPA}) values of solution and nanoaggregates are 107 and 896 GM, respectively.[64] An even higher σ_{TPA} value of 1361 GM was obtained when the nanoaggregates of **154** was excited with 740 nm light.

The two photon absorption of the pyrazoline and 1,8-naphthalimide-containing vinyl monomer **5** and its homopolymer **6** was also studied. Although the σ_{TPA} of **5** is very low in toluene solution (22 GM), that of **6** can reach 983 GM.[27] In addition, in the aggregated state, the σ_{TPA} of **6** in DMF-ethanol is 4.98-fold higher than that in pure DMF solution.

In the star-shaped compounds **254–256**, three electro-donating diphenylamine, phenothiazine, or carbazole groups were connected to the 1,4-positions of the benzene through bis(α-cyano-4-diphenylaminostyryl) conjugation bridges to form three new quadrupolar-type D-π-A-π-A-π-D derivatives. With the highly extended π-conjugation, the appropriate intramolecular charge transfer between their multi-electron-donating triarylamine end-cappers and cyano acceptor groups, together with their AIE features, star-shaped compounds **254–256** are expected to have large two-photon absorption and two-photon excited fluorescence. At an excitation wavelength of 800 nm, the σ_{TPA} values measured by the open-aperture Z-scan technique were determined to be 1016, 1484, and 814 GM for the star-shaped molecules **254**, **255**, and **256**, respectively.[124] The large σ_{TPA} values are attributed to the extended π-system and enhanced intramolecular charge transfer. Because the electron-donating strength of diphenylamine and phenothiazine is larger than carbazole, the σ_{TPA} values of **254** and **255** are much larger than that of **256**. Under the excitation of 800 nm pulse, **254–256** in a mixture of THF/water emit intense red, orange, and deep yellow fluorescence with peaks located at 651, 617, and 573 nm, respectively. Fig. 21A–C shows the two photon excited fluorescence of their THF solutions and nanoaggregates in aqueous media. The spectra overlap between the one- and two-photon excited fluorescence indicates that the emission result from the same excited state, independent with the different excitation sources.

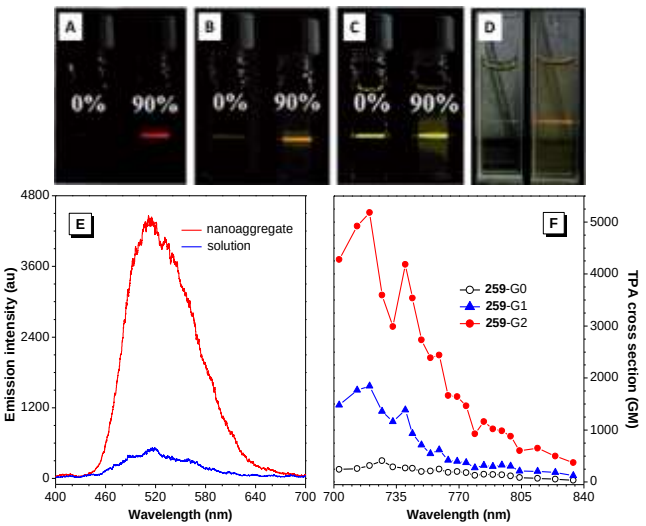

Fig. 21 Two-photon excited fluorescence emission images of (A–C) **254–256** in the THF solution and THF/water mixture with 90 vol % water fraction and (D) **259-G2** in the THF solution and THF/water mixture with 80 vol % water fraction. (E) TPEF spectra of THF solution and nanoaggregates of **154**. (F) Two-photon-induced fluorescence excitation spectra for dendrimers **259-G0~G2** in THF solutions. The TPA cross-sections were determined using the two-photon excited fluorescence method relative to fluorescein. Adapted with permission from (A–C, F) Ref. 124. Copyright 2011 Wiley-VCH; (D) Ref. 127. Copyright 2014 The Royal Society of Chemistry; (E) Ref. 64. Copyright 2012 The Royal Society of Chemistry.

Dendrimer structures were also adopted to enhance the two-photon absorption activity and the amino-branching building blocks were incorporated into dendrimers **259-G0~G2** to serve as dendrons to enhance the σ_{TPA} by effective cooperative effects. Fig. 21F shows the obtained two-photon absorption spectra of **259-G0~G2** in THF solutions at a concentration of 1×10^{-5} mol/L.[127] The maximum σ_{TPA} values of them are 407 GM (**259-G0**), 1850 GM (**259-G1**), and 5180 GM (**259-G2**). The σ_{TPA} values of these dendrimers are enhanced with the increasing generation number, indicating cooperative enhancement through the multi-branched structures.[173] In addition,

the two-photon excited fluorescence was remarkably intensified in the nanoaggregates than that in the THF solution, as shown in Fig. 21D. This enhancement was attributed to the cooperative effects of the high Φ_F and the large σ_{TPA}.

Other nonlinear optical properties were also reported such as optical power limiting. Polymer **107** shows response to harsh laser pulses: the transmitted fluence of the solution increases linearly with the incident fluence but starts to deviate at a limiting threshold; with a further increase of the incident fluence, the transmitted fluence reaches a plateau and becomes saturated .[59]

4.7 Circular polarized luminescence

Circular polarized luminescence (CPL), the emission analogue of circular dichroism, is the selective emission of left- and right-handed circularly polarized light originating from chiral chromophore systems. CPL is commonly used to investigate structural information on the excited state of chiral molecules. The CPL behaviour is evaluated by the luminescence dissymmetry factor (g_{lum}), defined as $g_{lum} = 2(I_L - I_R)/(I_L + I_R)$, where I_L and I_R denote the luminescence intensities of left- and right-handed polarized light.[174] Although most of the CPL studies are focused on chiral lanthanide complex systems,[175] organic compound-based CPL materials have attracted considerable attention in photonic devices such as light-emitting diodes, optical amplifiers, optical information storage, liquid crystal displays and bio-sensing.[176] Compared with small chiral organic molecules, chiral π-extended conjugated polymers can exhibit higher g_{lum} values, which might contribute to the amplification effect of CPL arising from a conjugated polymer backbone.

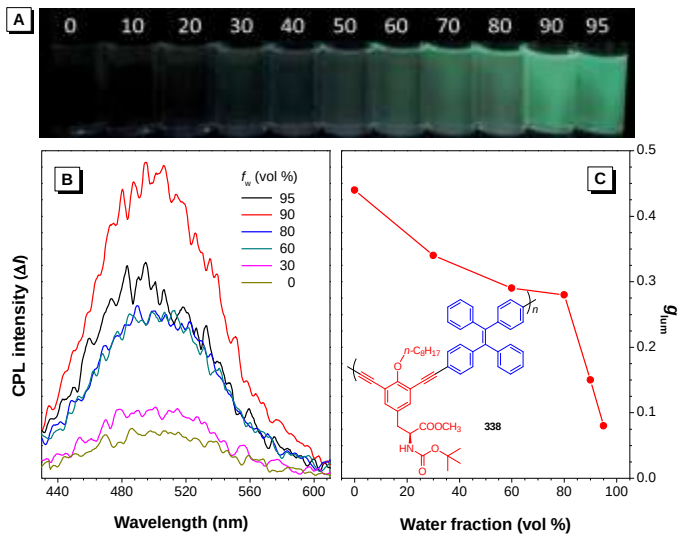

Fig. 22 (A) Fluorescence photographs of **338** in THF-water mixtures with different water fractions taken under 365 nm UV illumination. (B) Circular polarized luminescence spectra of **338** in THF/water mixtures with different water fractions. (C) CPL dissymmetry factor g_{lum} versus water fraction for **338**. Solution concentration: 10 μM. Excitation wavelength: 371 nm. Adapted with permission from Ref. 177. Copyright 2013 The Royal Society of Chemistry.

A TPE-based chiral polymer **338** was thus designed to achieve a high and tunable CPL dissymmetry factor (Fig. 22).[177] Chiral polymer **338** exhibits weak fluorescence emission at 508 nm in THF due to the restriction of the intramolecular rotation of the TPE moieties in the polymer main chain backbone. The fluorescence intensity of **338** at a water fraction of 95 vol % can reach a value 45-fold higher than that in THF solution. The fluorescence photos of **338** in THF/water mixtures with different water content are shown in Fig. 22A. The Φ_F values of **338** in THF solution and 95 vol % aqueous mixtures are 0.4% and 3.6%, respectively. **338** exhibits a moderate Cotton effect at 277 nm in both solution and aggregate states in the CD spectra. As a result of its strong CD signal and aggregate state emission, **338** gives rise to polarized fluorescence emission bands situated at around 500 nm (Fig. 22B). In THF solution, **338** has the largest g_{lum} value as high as 0.44 at 508 nm, which is one of the highest reported g_{lum} values for organic chiral materials, considering that the g_{lum} of small chiral organic molecules is generally less than 0.01.[178] Upon addition of water, g_{lum} values initially drop to 0.28 (f_w = 80 vol %), then dramatically down to 0.08 (f_w = 95 vol %). The decreasing g_{lum} value of **338** is reported to be caused by the local environmental change of the chiral polymer due to the formation of nanoparticles. The CPL g_{lum} value of **338** might mainly originate from the electronic interaction of the isolated molecules rather than the aggregates.

Other chiral polymers have also been reported with both strong CD signal and AIE feature, such as the zigzag-shaped polymer **248d**, which could potentially be developed as CPL materials.[118]

4.8 Photopatterning

The luminescent imaging photolithography technique shows potential applications in photonic and electronic devices and biological sensing and probing chips.[179] Fluorescent conjugated polymers with thin-film formability and photo-response property are promising candidate materials for the construction of high-performance photonic devices. Many of the AIE polymers are highly emissive in the solid state and they can easily form uniform, tough thin film by spin-coating their solutions onto silicon wafers. If the polymer is photo-responsive, fluorescent photopattern can be generated by exposing the thin film to UV irradiation through a negative copper photo mask. Two types of photo-responsive polymers are involved: i) photo-oxidative polymers which will decompose under exposure to UV light and the fluorescence of the exposed region will quench to form two dimensional (2D) positive fluorescent patterns; and ii) photo-crosslinkable polymers which will undergo photo-crosslinking reactions to generate insoluble luminescent crosslinked products. After removal of the soluble unexposed part of the polymer film using solvent as the developing reagent, a 3D negative fluorescent pattern will form. In some special cases, both effects take place, thus they can generate both 2D and 3D fluorescent patterns, respectively.

Linear TPE-TPA polymer **159**,[74] poly(silylenevinylene)s **92a** and **94**,[54] hyperbranched polytriazole **220a**[100] all possess good film-forming ability and strong emission in the solid state, which can be facilely spin-coated onto silicon wafers to form fluorescent thin films. They are photosensitive and can be photo-oxidized. When their thin films are irradiated under UV light through a copper photo mask, 2D fluorescent patterns with high resolutions form. The 2D fluorescent photopattern of **92a** under daylight and UV irradiation is shown in Fig. 23A–B, respectively. The unexposed square parts of the pattern emit bright blue light, while the exposed patterned lines suffer from strong photo-oxidative bleaching and are thus not emissive.

Similarly, AIE-active poly(vinylene sulfide) **107** can undergo photo-oxidative reaction to form 2D fluorescent photopattern under irradiation through copper photomask.[59] In contrast, another poly(vinylene sulfide) **109** with a large number of photosensitive vinyl and ester groups can be readily photo-crosslinked under UV irradiation, attributed to the formation of free radicals under UV light.[61] After the spin-coated thin film of **109** was irradiated in air through a copper photomask, the exposed region is photo-crosslinked. By developing the irradiated polymer film with 1,2-

dichloroethane, a 3D negative photoresist pattern with clear-cut edges is generated.

Because methacrylic/acrylic groups are known to undergo photo-crosslinking reactions, the photopolymerizability of the methacrylic/acrylic pendants of **77a–b** allows their films to be patterned into fluorescent images (Fig. 23C–D).[45] Upon exposure to UV light for 3 min, the (meth)acrylic groups of **77a** and **77b** are photopolymerized to form **78a** and **78b**. The region uncovered by the photo mask is crosslinked, whereas the covered areas remain unchanged. After development by solvent, 3D negative photoresist patterns are obtained. The lines are clearly edged and the patterns emit strong green light under a fluorescent microscope. The cross-linked networks in the photoresists offer the patterned films with high mechanical strength, thermal stability, and etching resistance. Also containing methacrylic groups, the film things of glycogen-like hyperbranched polymers **270** and **271** can be readily crosslinked by UV irradiation to furnish fluorescent 3D negative photoresist patterns with good resolution.[134] Control experiments suggest that radicals are generated under UV irradiation and the vinyl cores of the TPE units in the polymers are involved in the photo-crosslinking reactions.

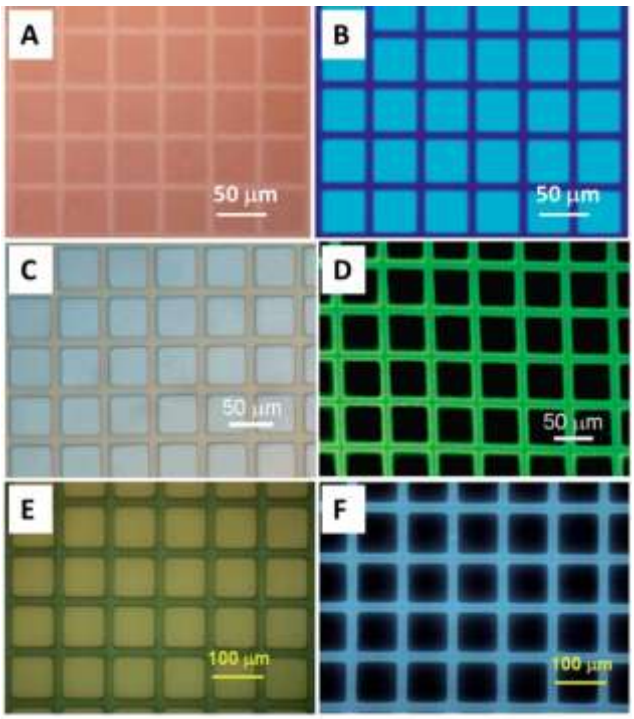

Fig. 23 Two-dimensional photopatterns generated by photo-oxidation of (A–B) **92a** and three-dimensional negative photoresist patterns generated by the photolithography of (C–D) **77b** and (E–F) **193**. The photographs were taken under (A, C, E) normal room light and (B, D, F) UV illumination. Adapted with permission from (A–B) Ref. 54. Copyright 2011 American Chemical Society; (C–D) Ref. 45. Copyright 2007 American Chemical Society; (E–F) Ref. 88. Copyright 2012 The Royal Society of Chemistry.

Besides the free radical-based photo-crosslinking mechanism, hyperbranched polymers with numerous terminal C≡C bonds can also undergo photo-crosslinking. TPE-containing hyperbranched polymer **193** is soluble and can be fabricated into thin films by spin-coating its 1,2-dichloroethane solution onto silicon wafers. After the film had been irradiated by UV light through a copper photomask, the exposed region was crosslinked and became insoluble, while the unexposed region was removed by the development of 1,2-dichloroethane.[88] Its negative 3D photoresist pattern with sharp edges are shown in Fig. 23E and F. Hyperbranched poly(silylenephenylene) **190c** can also form uniform, tough films by spin-coating and be photo-crosslinked to form 3D fluorescent photopatterns.[85]

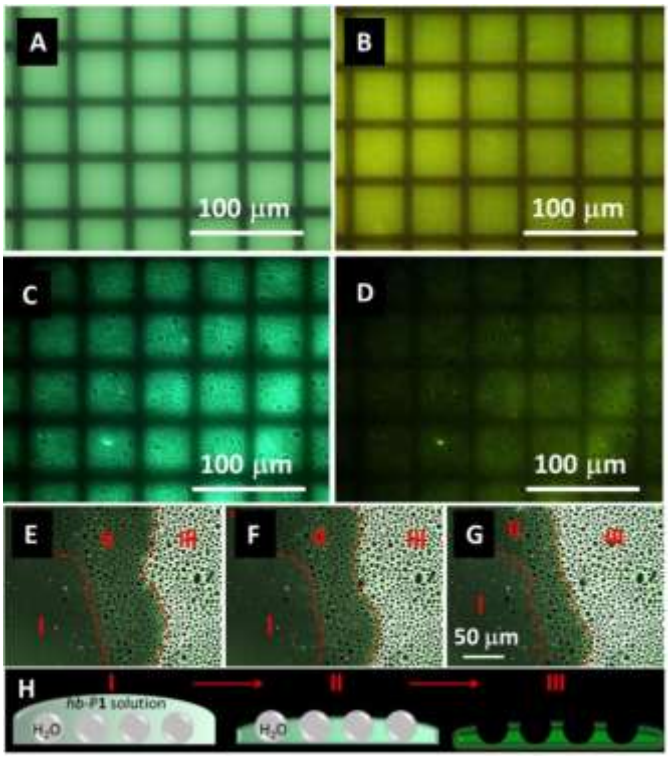

Fig. 24 Fluorescent patterns generated by photo-oxidation of (A–B) uniform thin film and (C–D) microporous thin film of **195** in air at room temperature for 15 min. (E–G) Fluorescence images showing the formation process of microporous film of **195**. (H) Schematic diagram of the formation process of fluorescent microporous film. Photos were taken under UV light illumination. Excitation wavelength: (A, C, E–G) 330–380 nm and (B and D) 460–490 nm. Adapted with permission from Ref. 89. Copyright 2013 Wiley-VCH.

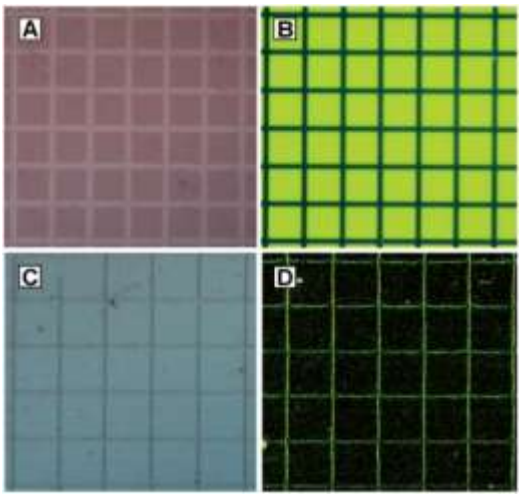

Fig. 25 (A–B) 2D and (C–D) 3D photopatterns generated by photo-oxidation and cross-linking reaction of **172b**. Images were taken under room light (A and C) and UV illumination (B and D). The size of each square is 50 × 50 μm^2. Reproduced with permission from Ref. 80. Copyright 2012 Wiley-VCH.

Although hyperbranched polymer **195** shares a similar chemical structure with **193**, it shows a different photo-responsive behaviour.[89] When the tough uniform thin film of **195** fabricated by spin-coating was UV irradiated through a copper photomask, the emission of the exposed region faded and a 2D fluorescent pattern with sharp edges was thus obtained (Fig. 24A–B). Owing to its large steric hindrance, the photo-crosslinking reaction is less likely to proceed and photo-oxidation is dominant. This is also the case in polymer **192b**.[87] Furthermore, fluorescent microporous film of **195** can be prepared using the breath figure (BF) method. Thanks to the AIE feature of **195**, the real-time BF formation process can be monitored under a fluorescent microscope (Fig. 24E–H). Combining the high photosensitivity and self-assembly property of **195**, photo-oxidation of the honeycomb-patterned film in the presence of UV light through a negative copper photomask furnished a 2D fluorescent pattern with a honeycomb secondary structure (Fig. 24C–D).

Both photo-oxidation and photo-crosslinking can occur under UV irradiation in some polymers, generating 2D and 3D fluorescent patterns without and with solvent development, respectively. The emission was only partially quenched upon exposure to UV light in such polymers. For instance, upon UV irradiation for 15 min, the thin film of hyperbranched polymer **172b** can form 2D fluorescent photopattern without further development (Fig. 25A–B).[80] On the other hand, upon UV irradiation and subsequent development in chloroform, a 3D fluorescent photopattern was obtained (Fig. 25C–D). The exposed crosslinked lines, show only faint emission, probably due to the mismatching with the excitation wavelength, coupled with the oxidation during the patterning process preformed in air. Similarly, UV irradiation of a thin film of polytriazole **208a** through a photomask leads to a bleaching of the exposed area.[95] A 2D fluorescent photopattern is thus generated under 1 min UV irradiation and without the development process, while a 3D photopattern was generated under 3 min UV irradiation and the development in 1,2-dichloroethane.

4.9 Light refractivity

The development of processable materials with high refractive indices (*n*) is of great importance because of their potential applications in photonic and optoelectronic devices. High *n* values can be achieved in organometallic polymers, however, their processability is generally low. Despite good solubility, film-forming capability, as well as structural diversity, organic polymers generally exhibit low refractive indices (*n* = 1.40-1.65). Polarized aromatic rings, ester groups, and heavy atoms are reported to increase the refractive indices.[180]

Polymers **116a–b** consist of polarizable aromatic rings, acetylene units, and heteroatoms thus may show high light refractivity. The *n* values of them are 1.7529–1.6178 (**116a**) and 1.6979–1.6041 (**116b**), in a wide spectral region of 400–1600 nm.[63] These *n* values are much higher than conventional polymers, such as polystyrene (*n* = 1.602–1.589), poly(methyl methacrylate) (*n* = 1.497–1.489), and polycarbonate (*n* = 1.593–1.576).[181] In addition, the chromatic aberrations of these polymers are small. The low optical aberrations of the polymers, coupled with their high light refractivities and optical transparencies, make them good candidates as coating materials in the advanced optical display systems, such as microlens components for charge-coupled devices and high-performance CMOS image sensors.[182]

Highly refractive materials which can undergo large changes in their refractivities with external stimuli is highly desirable for practical applications in optical waveguides, memory and photochromatic and holographic image recording systems.[182] As shown in Fig. 26A, the thin film of **162b** have high refractive indices (1.8360–1.7284) in the wavelength region of 300–1700 nm with low optical dispersions, even though they do not possess metallic species and heavy atoms.[75] Its *n* values can be tuned by UV irradiation. After being exposed to UV light for 20 min, the *n* value dropped to 1.7485–1.6409 in the same wavelength range, due to the structural changes caused by photo-induced reactions. The difference in the refractive index (Δn) at the telecommunication-important wavelength (λ = 1550 nm) was as large as 0.0875, suggesting that it is a promising photonic material.

Hyperbranched polymers comprised of a large amount of densely compacted aromatic rings generally show high refractive indices. Hyperbranched polymers **172a–b** enjoy high *n* of 1.8536–1.7407 (**172a**) and 1.7134–1.6527 (**172b**) in the wavelength region of 600–1700 nm.[80] UV irradiation can modulate the refractivity as can be seen in the photopattern image of **172b** under daylight (Fig. 25A). Upon exposure to 365 nm UV light for 15 min, the *n* values of **172a–b** dropped dramatically, caused by the photo-oxidation-induced structural variations.[183] The refractive index differences for **172a–b** at 1550 nm were 0.0883 and 0.0322, respectively, indicating facile UV modulation. Moreover, hyperbranched polymer **195** with more compacted benzene rings possesses light refractivity of *n* = 1.9288–1.6746 in the wavelength region of 400–1000 nm, which can also be readily tuned by UV-irradiation to 1.6711–1.5862 in the same wavelength range.[89]

Sulfur-rich polymers generally have high refractivity. Indeed, refractivity values of thin film of poly(vinylene sulfide) **107** is 1.7440–1.6848 in the spectral region of 600–1700 nm.[59] Upon UV irradiation, it shows large refractive index value *n* change (Δn = 0.1221) which is very rare in organic polymer systems.

The refractive indices can also be gained through structural modification. For example, poly(vinylene sulfide) **109** displays high refractivities (*n* = 1.7300–1.6569) over 500–1700 nm (Fig. 26B).[61] After metal complexation with $Co_2(CO)_8$ to form organometallic complexes **109**(Co), the *n* values were enhanced and the Δn value at 1550 nm of **109** and **109**(Co) pair is 0.0514.

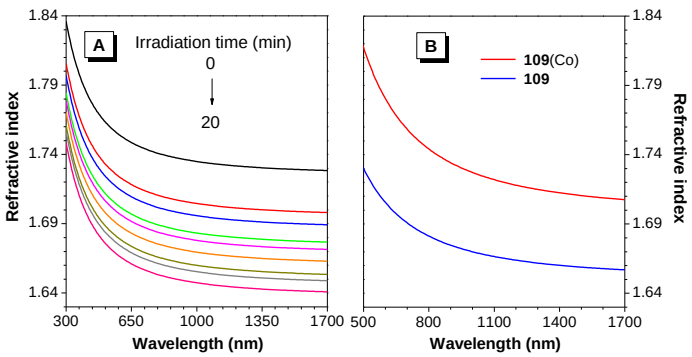

Fig. 26 Wavelength dependence of refractive indices of thin films of (A) **162b** on the irradiation time of 0, 0.5, 1, 2, 3, 4, 5, 10 and 20 min, respectively, and (B) **109** before and after metallization with $Co_2(CO)_8$. Adapted with permission from (A) Ref. 75. Copyright 2012 Wiley-VCH; (B) Ref. 61. Copyright 2010 Wiley-VCH.

4.10 Liquid crystallinities

Fluorescent liquid crystals (LCs), combining the intrinsic light-emitting capability and spontaneous self-organization attribute within a liquid crystalline phase, has received growing attention.[184] Despite their promising prospects in optoelectronic applications such as anisotropic light-emitting diodes and emissive liquid crystal

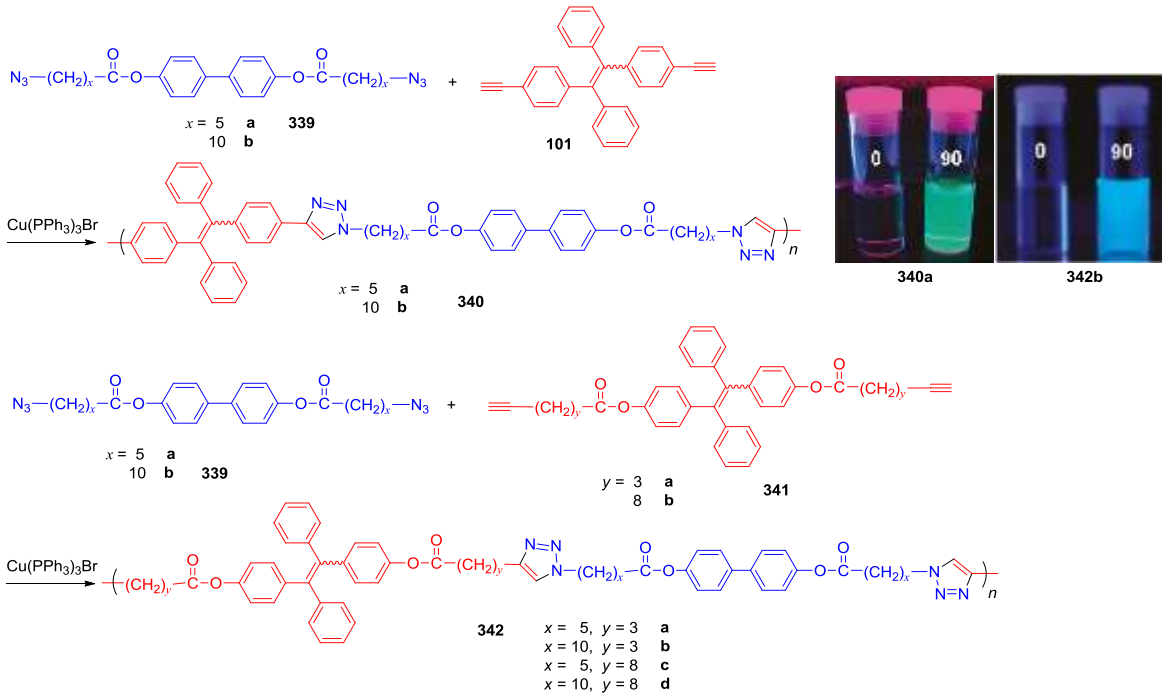

Scheme 42 Synthetic routes of fluorescent main chain liquid crystalline polytriazoles **340a–b** and **342a–d**. Insets: fluorescence photos of **340a** in DMF and DMF/water (1:9 v/v) and **342b** in THF and THF/water (1:9 v/v) taken under UV light. Adapted with permission from Ref. 187. Copyright 2011 American Chemical Society.

displays,[185] their syntheses remain a daunting task, because in the mesophases, the chromophoric mesogens are regularly packed, which often quench their light emissions.[186]

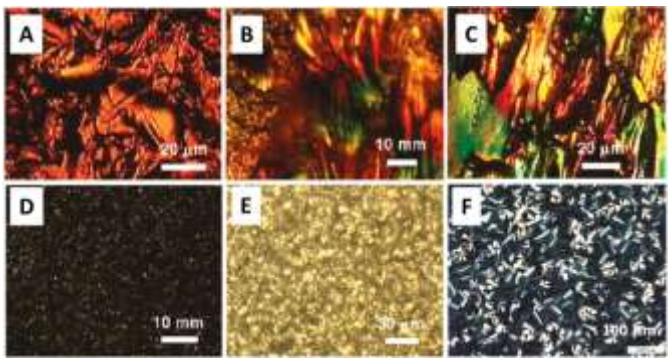

Fig. 27 Mesomorphic textures observed on cooling (A) **340b** to 250.6 °C, (B) **342a** to 89.9 °C, (C) **342b** to 69.8 °C, (D) **342c** to 94.9 °C, and (E) **342d** to 114.9 °C from their melting states at a cooling rate of 1 °C/min. Photos A, C, and D are taken after application of a shearing force. (F) Optical textures of the complex **253**-TNF (1:4 mole ratio) at 120 °C with crossed polarizers. Adapted with permission from (A–E) Ref. 187. Copyright 2011 American Chemical Society; (F) Ref. 123. Copyright 2013 The Royal Society of Chemistry.

The creation of AIE-active liquid crystalline polymers through the copper catalyzed 1,3-dipolar cycloaddition of alkynes with azides was reported.[187] Regioselective 1,3-dipolar polycycloadditions of biphenyl-containing diazides **339a–b** and TPE-carrying diynes **101** and **341a–b** are initiated by $Cu(PPh_3)_3Br$ in THF or DMF generating soluble polytriazoles **340a–b** and **342a–d** in high yields (up to 97%) with narrow M_w distributions (Scheme 42). All the polymers are AIE-active. They emit weakly in solutions with Φ_F values no more than 0.67% and become strong emitters in the aggregated states with Φ_F up to 63.7%. All the polymers are mesomorphic. The liquid crystalline domains of the polymers are generally observed with external stimuli because of the high rigidity of the main chain, which impedes the packing arrangements of the mesogenic units. When a shear force is applied, the small domains merge together and aligned along the shear direction as can be observed under a polarized optical microscope (Fig. 27A–E). While **340a–b** possess rigid main chains and exhibit nematicity, **342a–d** show better mesogenic packing and may form smectic phases. In particular, the relative longer flexible spacers in **342c–d** render the mesogenic units more freedom to pack and small entities emerge from the homotropic dark background when their isotropic liquids are cooled.

The star-shaped macromolecule **253** with four triphenylene discogen exhibits hexagonal columnar mesophase. In order to increase intermolecular interactions and thus induce the mesophase, the electron-donating **253** was doped with electron-accepting 2,4,7-trinitrofluorenone (TNF) in different molar ratios, forming charge-transfer complexes. A typical fan-shaped texture of the columnar mesophase of the complex **253**-TNF (1:4 by molar ratio) was observed from a polarized optical microscopy (Fig. 27F).[123]

4.11 Gas adsorption

Microporous polymers, with their inherent properties of large surface areas, high chemical stabilities, and low skeletal density, have drawn great attention of scientists nowadays. They are widely used in gas adsorption/storage,[188] chemical encapsulation,[189] and heterogeneous catalysis,[190] etc. In a newly developing field of research, the intrinsic fluorescent feature of AIE polymers combined with porosity in various conjugated microporous polymer materials endows the new materials with brand new properties and applications.

Fluorescent CMP **276** was prepared via time-dependent Yamamoto reactions. Field emission scanning electron microscopy (FE-SEM) revealed that **276** consists of platelet-like particles and the size of which increased with reaction time (Fig. 28A and 28C).[138]

High resolution tunnelling electron microscopy (HR-TEM) suggests that the micropores are present homogenously and are similar in size regardless of the reaction time (Fig. 28B and 28D). The Brunauer-Emmett-Teller (BET) surface area increased with increasing reaction time. The BET surface areas of **276** prepared in 2, 12, 36, and 72 h are 753, 1340, 1415, and 1665 m^2/g, respectively (Fig. 29). The pore size of the micropores is about 0.8 nm with similar distributions for the samples synthesized over different reaction times, which fits the calculated results.

The specific surface area of fluorescent CMPs **278**, **280**, **282**, **284**, and **286** enjoy BET specific surface areas ranging from 472 to 810 m^2/g. Copolymer materials **282**, **284**, and **286** prepared by two different core structural monomers generally have higher BET surface areas than those of the respective homopolymers **278** and **280**.[139] For CMPs **278**, **282**, and **284** prepared by the Suzuki coupling polycondensation, pore widths are mainly distributed around 0.58 nm. Meanwhile, CMPs **280** and **286** exhibit a similar pore size distribution with a dominant pore width at 0.67 nm. The SEM and TEM images of **280** and **284** are shown in Fig. 28E-H. Their hydrogen uptake based on the hydrogen physisorption isotherms was measured at 77 K up to a pressure of 1.13 bar as shown in Fig. 30. The total hydrogen capacity is increased with the surface area. The largest hydrogen uptake of 1.07 wt% was achieved in CMP **286** with the highest micropore volume and highest BET specific surface area, demonstrating one of the best results obtained in CMPs with similar surface areas.

The permanent porosities of fluorescent MOF materials are studied by nitrogen adsorption at 77K. Both **303** and **304** are permanently porous with BET apparent surface areas of 317 and 244 m^2/g, respectively, suggesting that they could accommodate small guest molecules to induce fluorescence response.[146]

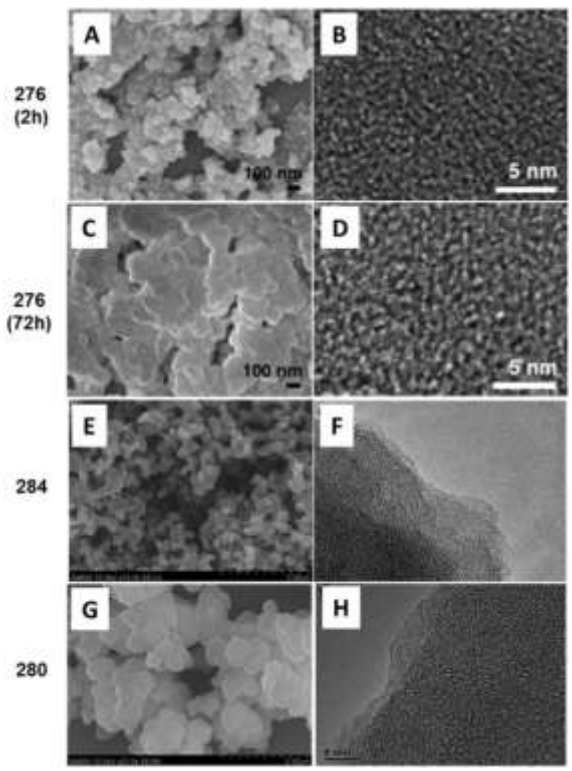

Fig. 28 (A, C, E, and G) FE-SEM and (B, D, F, and H) HR-TEM images of **276** synthesized over (A–B) 2 h and (C–D) 72 h, (E–F) **284**, and (G–H) **280**. Adapted with permission from (A–D) Ref. 138. Copyright 2011 American Chemical Society; (E–H) Ref. 139. Copyright 2011 The Royal Society of Chemistry.

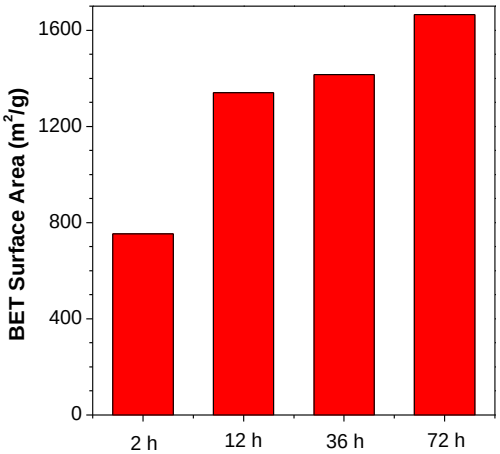

Fig. 29 BET surface areas of **276** synthesized over different reaction times. Adapted with permission from Ref. 138. Copyright 2011 American Chemical Society.

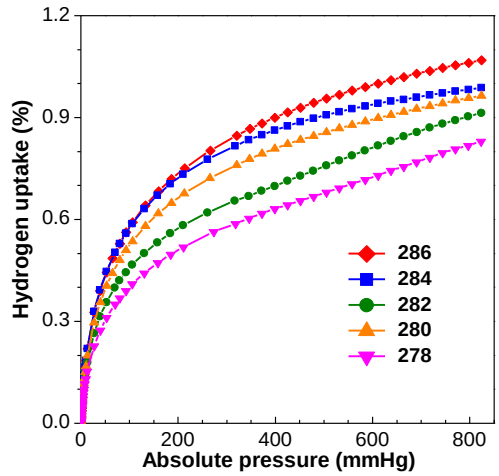

Fig. 30 Gravimetric hydrogen adsorption isotherms for **286**, **284**, **282**, **280**, **278** at 77 K. Adapted with permission from Ref. 139. Copyright 2011 The Royal Society of Chemistry.

Conclusions

AIE macromolecules with their unique features, such as flexible molecular design, diverse building blocks and corresponding properties, along with high emission efficiency in the aggregated states, represent a new class of luminescent materials. This review has summarized most of the developments in this field regarding the design and syntheses, structures and topologies, as well as the functionalities and applications of AIE macromolecules, with the emphasis on the most recent progress.

AIE macromolecules are generally achieved through incorporating AIEgens such as TPE, multiphenyl-substituted silole, and DSA units into the polymer structures, by either directly polymerizing the AIEgen-containing monomers, or modifying AIE-inactive polymers with AIEgens. Chain polymerizations, such as free-radical polymerization and metathesis polymerizations, and step polymerizations, transition-metal catalysed carbon-carbon coupling reactions and polycycloadditions, are used to construct AIE macromolecules. Post modification also allows the generation of AIE macromolecules via the integration of AIE attributes into the repeating units, centre or ends of existing polymers. In addition, the

development of new polymerization approaches is still under investigation, and is promising to generate AIE macromolecules with new structures and functionalities.

Through such versatile polymerization approaches, a vast array of AIE macromolecules with various chemical and topological structures can be easily accessed. Linear or zigzag shaped oligomers and polymers, star-shaped oligomers, dendrimers and hyperbranched polymers, conjugated microporous polymers, crystalline supramolecular polymers, and MOFs, with AIE properties have been reported. The structure-property relationships have been discussed with typical examples, and the restriction of intramolecular motions as well as the structural rigidity of the macromolecules have been correlated with their emission behaviours. It should also be noted that not every AIEgen-containing macromolecule is necessarily AIE-active, and it varies case-by-case depending on structural details. Surprisingly, a series of luminogenic polymers without conventional chromophores, are also reported. These systems generally contain a large number of close heteroatoms with lone pair electrons, and such "heterodox clusters" are proposed to be the luminogens in such polymer systems.

By combining the AIE characteristic with the desired traits of the polymeric materials, a whole new series of materials with the joint advantageous properties have been developed, for example, aggregation-induced emission, stability, solubility, processability, and biocompatibility. Such properties endow the resulting polymers with fascinating functionalities. First, they can exhibit fluorescence response to light, heat, chemical analytes, and biological macromolecules, enabling them to be potential fluorescent sensors. Second, the nanoparticles prepared from the amphiphilic AIE polymers display enhanced emission, stability and biocompatibility, making them promising candidates for long-term cell tracking. Besides sensing and imaging, AIE polymers can possess excellent photophysical properties bestowing them with electroluminescence, nonlinear optical properties, circularly polarized luminescence, light refractivity, photopatternability, and liquid crystallinities, allowing the potential fabrication of multifunctional devices.

AIE macromolecules is still a young research area with numerous possibilities. Indeed, much work can be done to further broaden this field. For example, the development of new polymerization approaches, with the emphasis on controlling the sequence of repeating units and molecular weights, such as living polymerizations, is highly desired and will lead to the exploration of a large variety of new luminescent functional materials. Regarding the chemical structures of AIE macromolecules, although mainly organic polymers have been reported so far, organic/inorganic hybrids and metal-containing materials may open the way to unforeseen properties. Meanwhile, the development of effective new AIEgens with various structures and emission colors covering the full visible spectrum as well as near IR region is highly desired, as are pure organic materials with strong room temperature phosphorescence. Furthermore, AIE macromolecules can bring new opportunities for practical applications. Through external stimuli control from light, electricity, heat, magnetic field, as well as chemicals, the structure, configuration or morphology can be manipulated with fluorescence response. Taking advantage of such signal response, based on the "aggregation-dissociation" process, the development of smart materials is quite promising. Last but not least, AIE polymers without conventional luminogens emitting not just fluorescence but also room temperature phosphorescence are an important clue towards an unexploited territory of molecular luminescence. A deeper understanding into such unexpected luminescent phenomena of systems with heterodox clusters is urgently needed. There is a promising vista within the scope of AIE macromolecules. With such prospects, it is our hope that this review will accelerate the advancement of this promising class of materials, with the new aspects of synthetic methodologies, novel and fascinating structures and properties, as well as innovative high-tech applications.

Acknowledgements

This work was partially supported by the National Basic Research Program of China (973 Program; 2013CB834701), the Research Grants Council of Hong Kong (HKUST2/CRF/10, N_HKUST620/11, 604711 and 604913) and the University Grants Committee of HK (AoE/P-03/08). B.Z.T. thanks the support of the Guangdong Innovative Research Team Program (201101C0105067115).

Notes and references

[a] HKUST-Shenzhen Research Institute, No. 9 Yuexing 1st RD, South Area, Hi-tech Park, Nanshan, Shenzhen 518057, China.
[b] Department of Chemistry, Institute for Advanced Study, Institute of Molecular Functional Materials, Division of Biomedical Engineering, Division of Life Science and State Key Laboratory of Molecular Neuroscience, The Hong Kong University of Science & Technology (HKUST), Clear Water Bay, Kowloon, Hong Kong.
Email: tangbenz@ust.hk
[c] Guangdong Innovative Research Team, SCUT-HKUST Joint Research Laboratory, State Key Laboratory of Luminescent Materials and Devices, South China University of Technology (SCUT), Guangzhou 510640, China.

1 S. Bonacchi, D. Genovese, R. Juris, M. Montalti, L. Prodi, E. Rampazzo and N. Zaccheroni, *Angew. Chem. Int. Ed.*, 2011, **50**, 4056; S. N. Baker and G. A. Baker, *Angew. Chem. Int. Ed.*, 2010, **49**, 6726; Z. Zhao, J. W. Y. Lam and B. Z. Tang, *Soft Matter*, 2013, **9**, 4564; K. M. C. Wong and V. W. W. Yam, *Acc. Chem. Res.*, 2011, **44**, 424; L. Maggini and D. Bonifazi, *Chem. Soc. Rev.*, 2012, **41**, 211; G. Accorsi, A. Listorti, K. Yoosaf and N. Armaroli, *Chem. Soc. Rev*., 2009, **38**, 1690; Y. J. Cui, Y. F. Yue, G. D. Qian and B. L. Chen, *Chem. Rev.*, 2012, **112**, 1126.
2 S. W. Thomas III, G. D. Joly and T. M. Swager, *Chem. Rev*., 2007, **107**, 1339; F. J. M. Hoeben, P. Jonkheijm, E. W. Meijer and A. P. H. J. Schenning, *Chem. Rev*., 2005, **105**, 1491; U. H. F. Bunz, *Chem. Rev*., 2000, **100**, 1605; S. M. Borisov and O. S. Wolfbeis, *Chem. Rev*., 2008, **108**, 423.
3 M Shimizu and T. Hiyama, *Chem. Asian J*. 2010, **5**, 1516.
4 A. Burns, H. Ow and U. Wiesner, *Chem. Soc. Rev*. 2006, **35**, 1028; E. L. Que, D. W. Domaille and C. J. Chang, *Chem. Rev*. 2008, **108**, 1517; X. Feng, L. Liu, S. Wang and D. Zhu, *Chem. Soc. Rev*. 2010, **39**, 2411; M. I. J. Stich, L. H. Fischer and O. S. Wolfbeis, *Chem. Soc. Rev.*, 2010, **39**, 3102; M. Schaferling, *Angew. Chem. Int. Ed.*, 2012, **51**, 3532; Y. Salinas, R. Martinez-Manez, M. D. Marcos, F. Sancenon, A. M. Costero, M. Parra and S. Gil, *Chem. Soc. Rev.*, 2012, **41**, 1261; H. N. Kim, Z. Q. Guo, W. H. Zhu, J. Yoon and H. Tian, *Chem. Soc. Rev*., 2011, **40**, 79; J. S. Wu, W. M. Liu, J. C. Ge, H. Y. Zhang and P. F. Wang, *Chem. Soc. Rev.*, 2011, **40**, 3483.
5 Y. M. Yang, Q. Zhao, W. Feng and F. Y. Li, *Chem. Rev.*, 2013, **113**, 192; H. Mattoussi, G. Palui and H. B. Na, *Adv. Drug Delivery Rev.*, 2012, **64**, 138.
6 H. Yersin, *Highly Efficient OLEDs with Phosphorescent Materials*, Wiley-VCH, Weinheim, 2008; K. Müllen and U. Scherf, *Organic Light-Emitting Devices. Synthesis Properties and Applications*, Wiley-VCH, Weinheim, 2006; W. Y. Wong and C. L. Ho, *J. Mater. Chem.*, 2009, **19**, 4457.
7 J. Zaumseil and H. Sirringhaus, *Chem. Rev*. 2007, **107**, 1296; F. Cicoira and C. Santato, *Adv. Funct. Mater*. 2007, **17**, 3421; I. D. W. Samuel and G. A. Turnbull, *Chem. Rev*. 2007, **107**, 1272; M. D. McGehee and A. J. Heeger, *Adv. Mater*. 2000, **12**, 1655; C. L. Ho and W. Y. Wong, *Coord. Chem. Rev.*, 2011, **255**, 2469.

8 T. L. Andrew and T. M. Swager, *J. Polym. Sci. B: Polym. Phys*., 2011, **49**, 476; J. B. Birks, *Photophysics of Aromatic Molecules*, Wiley, London, 1970; R. Davis, N. S. S. Kumar, S. Abraham, C. H. Suresh, N. P. Rath, N. Tamaoki and S. Das, *J. Phys. Chem. C*, 2008, **112**, 2137.
9 F. Würthner, T. E. Kaiser and C. R. Saha-Möller, *Angew. Chem. Int. Ed.*, 2011, **50**, 3376.
10 Y. Hong, J. W. Y. Lam and B. Z. Tang, *Chem. Soc. Rev*. 2011, **40**, 5361.
11 J. Wang, Y. Zhao, Y. C. Dou, H. Sun, P. Xu, K. Ye, J. Zhang, S. Jiang, F. Li and Y. Wang, *J. Phys. Chem. B*, 2007, **111**, 5082; P. N. Taylor, M. J. O'Connell, L. A. McNeill, M. J. Hall, R. T. Aplin and H. L. Anderson, *Angew. Chem., Int. Ed*., 2000, **39**, 3456.
12 J. Xia, Y. M. Wu, Y. L. Zhang, B. Tong, J. B. Shi, J. G. Zhi and Y. P. Dong, *Imaging Science and Photochemistry* 2012, **30**, 9.
13 J. Luo, J. W. Y. Lam, L. Cheng, H. Chen, C. Qiu, H. S. Kwok, X. Zhan, Y. Liu, D. Zhu and B. Z. Tang, *Chem. Commun*., 2001, 1740.
14 H. Tong, Y. Hong, Y. Dong, Y. Ren, M. Haeussler, J. W. Y. Lam, K. S. Wong and B. Z. Tang, *J. Phys. Chem. B*, 2007, **111**, 2000; H. Tong, Y. Dong, Y. Hong, M. Haeussler, J. W. Y. Lam, H. H. Y. Sung, X. Yu, J. Sun, I. D. Williams, H. S. Kwok and B. Z. Tang, *J. Phys. Chem. C*, 2007, **111**, 2287; Y. Dong, J. W. Y. Lam, A. Qin, J. Liu, Z. Li, B. Z. Tang, J. Sun and H. S. Kwok, *Appl. Phys. Lett.*, 2007, **91**, 011111.
15 M. Shimizu, H. Tatsumi, K. Mochida, K. Shimono and T. Hiyama, *Chem. Asian J*., 2009, **4**, 1289; G. Yui, S. Yin, Y. Liu, J. Chen, X. Xu, X. Sun, D. Ma, X. Zhan, Q. Peng, Z. Shuai, B. Z. Tang, D. Zhu, W. Fang and Y. Luo, *J. Am. Chem. Soc*., 2005, **127**, 6335; Q. Peng, Y. Yi, Z. Shuai and J. Shao, *J. Am. Chem. Soc*., 2007, **129**, 9333; E. P. J. Parrott, N. Y. Tan, R. Hu, J. A. Zeitler, B. Z. Tang and E. Pickwell-MacPherson, *Mater. Horiz.*, 2014, DOI: 10.1039/C3MH00078H.
16 J. W. Y. Lam, J. W. Chen, C. C. W. Law, H. Peng, Z. L. Xie, K. K. L. Cheuk, H. S. Kwok and B. Z. Tang, *Macromol. Symp.* 2003, **196**, 289; B. Z. Tang, *Macromol. Chem. Phys*. 2009, **210**, 900.
17 Y. Chujo, *Macromol. Rapid. Commun.*, 2012, **33**, 1235; Z. Chi, X. Zhang, B. Xu, X. Zhou, C. Ma, Y. Zhang, S. Liu and J. Xu, *Chem. Soc. Rev.*, 2012, **41**, 3878.
18 Y. Hong, J. W. Lam and B. Z. Tang, *Chem. Commun*., 2009, 4332.
19 J. Liu, J. W. Y. Lam and B. Z. Tang, *J. Inorg. Organomet. Polym.*, 2009, **19**, 249.
20 J. Liu, J. W. Y. Lam and B. Z. Tang, *Chem. Rev*. 2009, **109**, 5799.
21 A. Qin, J. W. Lam and B. Z. Tang, *Chem. Soc. Rev.*, 2010, **39**, 2522.
22 R. Hu, J. W. Y. Lam and B. Z. Tang, *Macromol. Chem. Phys.*, 2013, **214**, 175.
23 A. Qin, J. W. Y. Lam and B. Z. Tang, *Prog. Polym. Sci.*, 2012, **37**, 182.
24 T. Huang, Z. Wang, A. Qin, J. Sun and B. Z. Tang, *Acta Chim. Sin.*, 2013, **71**, 979.
25 Z. Yang, T. Yu, M. Chen, X. Zhang, C. Wang, B. Xu, X. Zhou, S. Liu, Y. Zhang, Z. Chi and J. Xu, *Acta Polym. Sin.*, 2009, **6**, 560.
26 J. Shen, B. Tong, J. Shi, S. Sun, J. Zhi and Y. Dong, *Acta Polym. Sin.*, 2010, 765.
27 P. Y. Gu, C. J. Lu, Z. J. Hu, N. J. Li, T. T. Zhao, Q. F. Xu, Q. H. Xu, J. D. Zhang and J. M. Lu, *J. Mater. Chem. C*, 2013, **1**, 2599.
28 P. Y. Gu, C. J. Lu, F. L. Ye, J. F. Ge, Q. F. Xu, Z. J. Hu, N. J. Li and J. M. Lu, *Chem. Commun.*, 2012, **48**, 10234.
29 L. Tang, J. Jin, A. Qin, W. Yuan, Y. Mao, J. Mei, J. Sun and B. Z. Tang, *Chem. Commun.*, 2009, 4974.
30 H. Lu, F. Su, Q. Mei, X. Zhou, Y. Tian, W. Tian, R. H. Johnson and D. R. Meldrum, *J. Polym. Sci. A: Polym. Chem.*, 2012, **50**, 890.
31 H. Lu, F. Su, Q. Mei, Y. Tian, W. Tian, R. H. Johnson and D. R. Meldrum, *J. Mater. Chem.*, 2012, **22**, 9890.
32 J. I. Chen and W. C. Wu, *Macromol. Biosci.*, 2013, **13**, 623.
33 X. Shen, Y. Shi, B. Peng, K. Li, J. Xiang, G. Zhang, Z. Liu, Y. Chen and D. Zhang, *Macromol. Biosci*., 2012, **12**, 1583.
34 X. Zhang, X. Zhang, B. Yang, M. Liu, W. Liu, Y. Chen and Y. Wei, *Polym. Chem.*, 2014, **5**, 356.
35 X. Zhang, X. Zhang, B. Yang, J. Hui, M. Liu, Z. Chi, S. Liu, J. Xu and Y. Wei, *Polym. Chem.*, 2014, **5**, 683.
36 C. A. Chou, R. H. Chien, C. T. Lai and J. L. Hong, *Chem. Phys. Lett.*, 2010, **501**, 80.
37 A. Qin and B. Z. Tang, *Aggregation-Induced Emission: Fundamentals*, John-Wiley & Sons, Ltd., 2014.
38 A. Qin, Y. Zhang, N. Han, J. Mei, J. Sun, W. Fan and B. Z. Tang, *Sci. China Chem*., 2012, **55**, 772.
39 L. Xu, Y. Zhu, J. Shen, J. Shi, B. Tong, J. Zhi and Y. Dong, *Acta Polym. Sin.*, 2011, 740.
40 C. T. Lai and J. L. Hong, *J. Mater. Chem*., 2012, **22**, 9546.
41 J. Chen, Z. Xie, J. W. Y. Lam, C. C. W. Law and B. Z. Tang, *Macromolecules*, 2003, **36**, 1108.
42 W. Yuan, H. Zhao, X. Shen, F. Mahtab, J. W. Y. Lam, J. Sun and B. Z. Tang, *Macromolecules*, 2009, **42**, 9400.
43 A. Qin, C. K. W. Jim, Y. Tang, J. W. Y. Lam, J. Liu, F. Mahtab, P. Gao and B. Z. Tang, *J. Phys. Chem. B*, 2008, **112**, 9281.
44 Y. Li, N. Zhou, W. Zhang, F. Zhang, J. Zhu, Z. Zhang, Z. Cheng, Y. Tu and X. Zhu, *J. Polym. Sci. A: Polym. Chem.*, 2011, **49**, 4911.
45 W. Yuan, A. Qin, J. W. Y. Lam, J. Sun, Y. Dong, M. Häussler, J. Liu, H. Xu, Q. Zheng and B. Z. Tang, *Macromolecules*, 2007, **40**, 3159.
46 H. J. Yen, C. J. Chen and G. S. Liou, *Chem. Commun.*, 2013, **49**, 630.
47 Y. Liu, Y. Zhang, Q. Lan, Z. Qin, S. Liu, C. Zhao, Z. Chi and J. Xu, *J. Polym. Sci. A: Polym. Chem.*, 2013, **51**, 1302.
48 C. W. Chang, H. J. Yen, K. Y. Huang, J. M. Yeh and G. S. Liou, *J. Polym. Sci. Part A: Polym. Chem*. 2008, **46**, 7937; G. S. Liou, S. H. Hsiao and Y. K. Fang, *Eur. Polym. J*. 2006, **42**, 1533.
49 X. Zhang, X. Zhang, B. Yang, J. Hui, M. Liu, Z. Chi, S. Liu, J. Xu and Y. Wei, *Polym. Chem.*, 2014, **5**, 318.
50 X. Zhang, X. Zhang, B. Yang, Y. Zhang, M. Liu, W. Liu, Y. Chen and Y. Wei, *Colloids Surf., B*, 2014, **113**, 435.
51 X. Zhang, X. Zhang, B. Yang, J. Hui, M. Liu, W. Liu, Y. Chen and Y. Wei, *Polym. Chem.*, 2014, **5**, 689.
52 X. Zhang, X. Zhang, S. Wang, M. Liu, L. Tao and Y. Wei, *Nanoscale*, 2013, **5**, 147; X. Zhang, X. Zhang, B. Yang, S. Wang, M. Liu, Y. Zhang and L. Tao, *RSC Adv.*, 2013, **3**, 9633.
53 M. Birot, J. P. Pillot and J. Dunoguès, *Chem. Rev*. 1995, **95**, 1443; I. Manners, *Polyhedron*, 1996, **15**, 4311; M. Bruma and B. Schulz, *J. Macromol. Sci., Polym. Rev*. 2001, **41**, 1; R. J. P. Corriu, *Angew. Chem., Int. Ed*. 2000, **39**, 1376.
54 P. Lu, J. W. Y. Lam, J. Liu, C. K. W. Jim, W. Yuan, C. Y. K. Chan, N. Xie, Q. Hu, K. K. L. Cheuk and B. Z. Tang, *Macromolecules*, 2011, **44**, 5977.
55 Z. Zhao, T. Jiang, Y. Guo, L. Ding, B. He, Z. Chang, J. W. Y. Lam, J. Liu, C. Y. K. Chan, P. Lu, L. Xu, H. Qiu and B. Z. Tang, *J. Polym. Sci. A: Polym. Chem.*, 2012, **50**, 2265.
56 H. P. Martinez, C. D. Grant, J. G. Reynolds and W. C. Trogler, *J. Mater. Chem.*, 2012, **22**, 2908.
57 P. Lu, J. W. Lam, J. Liu, C. K. Jim, W. Yuan, N. Xie, Y. Zhong, Q. Hu, K. S. Wong, K. K. Cheuk and B. Z. Tang, *Macromol. Rapid. Commun.*, 2010, **31**, 834.
58 Z. Zhao, Y. Guo, T. Jiang, Z. Chang, J. W. Lam, L. Xu, H. Qiu and B. Z. Tang, *Macromol. Rapid. Commun.*, 2012, **33**, 1074.
59 J. Liu, J. W. Y. Lam, C. K. W. Jim, J. C. Y. Ng, J. Shi, H. Su, K. F. Yeung, Y. Hong, M. Faisal, Y. Yu, K. S. Wong and B. Z. Tang, *Macromolecules*, 2011, **44**, 68.
60 O. Coulembier, L. Mespouille, J. L. Hedrick, R. M. Waymouth and P. Dubois, *Macromolecules*, 2006, **39**, 4001; B. C. Wilson and C. W. Jones, *Macromolecules*, 2004, **37**, 9709.
61 C. K. W. Jim, A. Qin, J. W. Y. Lam, F. Mahtab, Y. Yu and B. Z. Tang, *Adv. Funct. Mater.*, 2010, **20**, 1319.
62 G. W. Kabalka, M. L. Yao, S. Borella, Z. Wu, Y. H. Ju and T. Quick, *J. Org. Chem.*, 2008, **73**, 2668; M. L. Yao, M. P. Quinn and G. W. Kabalka, *Heterocycles*, 2010, **80**, 779.
63 C. Y. K. Chan, N. W. Tseng, J. W. Y. Lam, J. Liu, R. T. K. Kwok and B. Z. Tang, *Macromolecules*, 2013, **46**, 3246.
64 R. Hu, J. L. Maldonado, M. Rodriguez, C. Deng, C. K. W. Jim, J. W. Y. Lam, M. M. F. Yuen, G. Ramos-Ortiz and B. Z. Tang, *J. Mater. Chem.*, 2012, **22**, 232.
65 J. Shi, Y. Wu, S. Sun, B. Tong, J. Zhi and Y. Dong, *J. Polym. Sci. A: Polym. Chem.*, 2013, **51**, 229.
66 B. Xu, X. Wu, H. Li, H. Tong and L. Wang, *Macromolecules*, 2011, **44**, 5089.
67 W. Wu, S. Ye, R. Tang, L. Huang, Q. Li, G. Yu, Y. Liu, J. Qin and Z. Li, *Polymer*, 2012, **53**, 3163.
68 J. Chen and Y. Cao, *Macromol. Rapid. Commun.*, 2007, **28**, 1714.

69 Z. T. Liu, S. J. Hu, L. H. Zhang, J. W. Chen, J. B. Peng and Y. Cao, *Sci. China Chem*., 2013, **56**, 1129.
70 R. M. Adhikari, R. Mondal, B. K. Shah and D. C. Neckers, *J. Org. Chem*. 2007, **72**, 4727; J. Ding, J. Gao, Y. Cheng, Z. Xie, L. Wang, D. Ma, X. Jing and F. Wang, *Adv. Funct. Mater*. 2006, **16**, 575; S. Grigalevicius, L. Ma, Z. Xie and U. Scheri, *J. Polym. Sci. A Polym. Chem*. 2006, **44**, 5987.
71 Z. Liu, J. Liu, G. Yu, G. Lei and X. Qi, *J. Inorg. Organomet. Polym.*, 2012, **22**, 1350.
72 H. M. Kim and B. R. Cho, *Chem. Commun*., 2009, 153; M. Albota, D. Beljonne, J. L. Bredas, J. E. Ehrlich, J. Y. Fu, A. A. Heikal, S. E. Hess, T. Kogej, M. D. Levin, S. R. Marder, D. McCord-Maughon, J. W. Perry, H. Rockel, M. Rumi, G. Subramaniam, W. W. Webb, X. L. Wu and C. Xu, *Science*, 1998, **281**, 1653; B. A. Reinhardt, L. L. Brott, S. J. Clarson, A. G. Dillard, J. C. Bhatt, R. Kannan, L. X. Yuan, G. S. He and P. N. Prasad, *Chem. Mater*., 1998, **10**, 1863.
73 C.-H. Chen, S.-L. Lee, T.-S. Lim, C.-H. Chen and T.-Y. Luh, *Polym. Chem*., 2011, **2**, 2850.
74 Y. Liu, X. Chen, Y. Lv, S. Chen, J. W. Y. Lam, F. Mahtab, H. S. Kwok, X. Tao and B. Z. Tang, *Chem. Eur. J*., 2012, **18**, 9929.
75 C. K. W. Jim, J. W. Y. Lam, A. Qin, Z. Zhao, J. Liu, Y. Hong and B. Z. Tang, *Macromol. Rapid. Commun.*, 2012, **33**, 568.
76 L. H. Zhang, T. Jiang, L. B. Wu, J. H. Wan, C. H. Chen, Y. B. Pei, H. Lu, Y. Deng, G. F. Bian, H. Y. Qiu and G. Q. Lai, *Chem. Asian J.*, 2012, **7**, 1583.
77 Y. Liu, X. Feng, J. Shi, J. Zhi, B. Tong and Y. Dong, *Chin. J. Polym. Sci*., 2012, **30**, 443.
78 W. Y. Huang, W. Gao, T. K. Kwei and Y. Okamoto, *Macromolecules*, 2001, **34**, 1570.
79 Y. Liu, F. Xie, J. Shi, B. Tong, J. Zhi and Y. Dong, *Acta Polym. Sin.*, 2013, **1**, 50.
80 W. Yuan, R. Hu, J. W. Y. Lam, N. Xie, C. K. W. Jim and B. Z. Tang, *Chem. Eur. J*., 2012, **18**, 2847.
81 D. A. Alonso, C. Najern and M. C. Pacheco, *J. Org. Chem*., 2004, **69**, 1615; L. Chen and C. Li, *Org. Lett*., 2004, **6**, 3151.
82 J. Li, J. Liu, J. W. Y. Lam and B. Z. Tang, *RSC Advances*, 2013, **3**, 8193.
83 J. Liu, C. Deng, N.-W. Tseng, C. Y. K. Chan, Y. Yue, J. C. Y. Ng, J. W. Y. Lam, J. Wang, Y. Hong, H. H. Y. Sung, I. D. Williams and B. Z. Tang, *Chem. Sci.*, 2011, **2**, 1850.
84 R. Hu, R. Ye, J. W. Y. Lam, M. Li, C. W. Leung and B. Z. Tang, *Chem. Asian J*., 2013, **8**, 2436.
85 J. Liu, R. Zheng, Y. Tang, M. Häussler, J. W. Y. Lam, A. Qin, M. Ye, Y. Hong, P. Gao and B. Z. Tang, *Macromolecules*, 2007, **40**, 7473.
86 J. Liu, Y. Zhong, P. Lu, Y. Hong, J. W. Y. Lam, M. Faisal, Y. Yu, K. S. Wong and B. Z. Tang, *Polym. Chem*., 2010, **1**, 426.
87 J. Liu, Y. Zhong, J. W. Y. Lam, P. Lu, Y. Hong, Y. Yu, Y. Yue, M. Faisal, H. H. Y. Sung, I. D. Williams, K. S. Wong and B. Z. Tang, *Macromolecules*, 2010, **43**, 4921.
88 R. Hu, J. W. Y. Lam, J. Liu, H. H. Y. Sung, I. D. Williams, Z. Yue, K. S. Wong, M. M. F. Yuen and B. Z. Tang, *Polym. Chem*., 2012, **3**, 1481.
89 R. Hu, J. W. Y. Lam, M. Li, H. Deng, J. Li and B. Z. Tang, *J. Polym. Sci. A: Polym. Chem*., 2013, **51**, 4752.
90 H. M. Luo, H. Wang, Z. Zeng and H. P. Zeng, *Chin. J. Org. Chem*. 2013, **33**, 915; D. X. Wang, B. Li, Y. H. Zhang, and Z. J. Lu, *J. Appl. Polym. Sci*. 2013, **127**, 516; G. Dominguez and J. Pérez-Castells, *Chem. Soc. Rev*. 2011, **40**, 3430.
91 C. Y. K. Chan, J. W. Y. Lam, C. K. W. Jim, H. H. Y. Sung, I. D. William and B. Z. Tang, *Macromolecules*, 2013, **46**, 9494.
92 A. Qin, J. W. Y. Lam and B. Z. Tang, *Macromolecules*, 2010, **43**, 8693; H. Li, J. Sun, A. Qin and B. Z. Tang, *Chin. J. Polym. Sci*., 2012, **30**, 1.
93 A. Qin, J. W. Y. Lam, L. Tang, C. K. W. Jim, H. Zhao, J. Sun and B. Z. Tang, *Macromolecules*, 2009, **42**, 1421.
94 E. Zhao, H. Li, J. Ling, H. Wu, J. Wang, S. Zhang, J. W. Y. Lam, J. Sun, A. Qin and B. Z. Tang, *Polym. Chem.*, 2014, **5**, 2301.
95 A. Qin, L. Tang, J. W. Y. Lam, C. K. W. Jim, Y. Yu, H. Zhao, J. Sun and B. Z. Tang, *Adv. Funct. Mater.*, 2009, **19**, 1891.
96 H. Li, J. Mei, J. Wang, S. Zhang, Q. Zhao, Q. Wei, A. Qin, J. Sun and B. Z. Tang, *Sci. China Chem.*, 2011, **54**, 611.
97 H. Li, J. Wang, J. Sun, R. Hu, A. Qin and B. Z. Tang, *Polym. Chem*., 2012, **3**, 1075.
98 Q. Wang, M. Chen, B. Yao, J. Wang, J. Mei, J. Sun, A. Qin and B. Z. Tang, *Macromol. Rapid. Commun*., 2013, **34**, 796.
99 J. Wang, J. Mei, W. Yuan, P. Lu, A. Qin, J. Sun, Y. Ma and B. Z. Tang, *J. Mater. Chem*., 2011, **21**, 4056.
100 H. Li, H. Wu, E. Zhao, J. Li, J. Sun, A. Qin and B. Z. Tang, *Macromolecules*, 2013, **46**, 3907.
101 J. Wang, J. Mei, E. Zhao, Z. Song, A. Qin, J. Sun and B. Z. Tang, *Macromolecules*, 2012, **45**, 7692.
102 M. Gao, J. W. Y. Lam, J. Li, C. Y. K. Chan, Y. Chen, N. Zhao, T. Han and B. Z. Tang, *Polym. Chem*., 2013, **4**, 1372.
103 M. Gao, J. W. Y. Lam, Y. Liu, J. Li and B. Z. Tang, *Polym. Chem*., 2013, **4**, 2841.
104 M. P. Aldred, C. Li, G. F. Zhang, W. L. Gong, A. D. Q. Li, Y. Dai, D. Ma and M. Q. Zhu, *J. Mater. Chem*., 2012, **22**, 7515.
105 B. Xu, J. He, Y. Dong, F. Chen, W. Yu and W. Tian, *Chem. Commun*., 2011, **47**, 6602.
106 F. Wang, M. Y. Han, K. Y. Mya, Y. Wang and Y. H. Lai, *J. Am. Chem. Soc*., 2005, **127**, 10350.
107 R. H. Chien, C. T. Lai and J. L. Hong, *J. Phys. Chem. C*, 2011, **115**, 5958.
108 S. T. Li, Y. C. Lin, S. W. Kuo, W. T. Chuang and J. L. Hong, *Polym. Chem*., 2012, **3**, 2393.
109 C. T. Lai, R. H. Chien, S. W. Kuo and J. L. Hong, *Macromolecules*, 2011, **44**, 6546.
110 J. Geng, L. Zhou and B. Liu, *Chem. Commun*., 2013, **49**, 4818.
111 X. Qi, H. Li, J. W. Y. Lam, X. Yuan, J. Wei, B. Z. Tang and H. Zhang, *Adv. Mater*., 2012, **24**, 4191.
112 Y. Wu, J. Shi, B. Tong, J. Zhi and Y. Dong, *Acta Polym. Sin*., 2012, **12**, 1482.
113 B. Xu, X. Wu, H. Li, H. Tong and L. Wang, *Polymer*, 2012, **53**, 490.
114 J. Sun, Y. Lu, L. Wang, D. Cheng, Y. Sun and X. Zeng, *Polym. Chem*., 2013, **4**, 4045.
115 H. Zhang, N. Zhou, X. Zhu, X. Chen, Z. Zhang, W. Zhang, J. Zhu, Z. Hu and X. Zhu, *Macromol. Rapid. Commun.*, 2012, **33**, 1845.
116 M. Lamrani, R. Hamasaki, M. Mitsuishi, T. Miyashita and Y. Yamamoto, *Chem. Commun.*, 2000, 1595; R. Hamasaki, M. Ito, M. Lamrani, M. Mitsuishi, T. Miyashita and Y. Yamamoto, *J. Mater. Chem.*, 2003, **13**, 21; Y. Endo, T. Sawabe and Y. Taoda, *J. Am. Chem. Soc.*, 2000, **122**, 180.
117 K. Kokado and Y. Chujo, *Macromolecules*, 2009, **42**, 1418.
118 K. Kokado, Y. Tokoro and Y. Chujo, *Macromolecules*, 2009, **42**, 9238.
119 J. J. Peterson, A. R. Davis, M. Werre, E. B. Coughlin and K. R. Carter, *ACS Appl. Mater. Interfaces*, 2011, **3**, 1796.
120 Z, Zhao, J. Liu, J. W. Y. Lam, C. Y. K. Chan, H. Qiu and B. Z. Tang, *Dyes and Pigments*, 2011, **91**, 258.
121 D. Jana and B. K. Ghorai, *Tetrahedron Lett*., 2012, **53**, 6838.
122 X. Yin, F. Meng and L. Wang, *J. Mater. Chem. C*, 2013, **1**, 6767.
123 W. H. Yu, C. Chen, P. Hu, B. Q. Wang, C. Redshaw and K. Q. Zhao, *RSC Adv*., 2013, **3**, 14099.
124 B. Wang, Y. Wang, J. Hua, Y. Jiang, J. Huang, S. Qian and H. Tian, *Chem. Eur. J*., 2011, **17**, 2647.
125 D. Xu, X. Liu, R. Lu, P. Xue, X. Zhang, H. Zhou and J. Jia, *Org. Biomol. Chem*., 2011, **9**, 1523.
126 M. Leung, Y. S. Lin, C. C. Lee, C. C. Chang, Y. X. Wang, C. P. Kuo, N. Singh, K. R. Lin, C. W. Hu, C. Y. Tseng and K. C. Ho, *RSC Adv*., 2013, **3**, 22219.
127 B. Xu, J. Zhang, H. Fang, S. Ma, Q. Chen, H. Sun, C. Im and W. Tian, *Polym. Chem*., 2014, **5**, 479.
128 K. Shiraishi, T. Kashiwabara, T. Sanji and M. Tanaka, *New J. Chem.*, 2009, **33**, 1680.
129 G. Huang, B. Ma, J. Chen, Q. Peng, G. Zhang, Q. Fan and D. Zhang, *Chem. Eur. J*., 2012, **18**, 3886.
130 Y. Chen, Y. Lv, Y. Han, B. Zhu, F. Zhang, Z. Bo and C. Y. Liu, *Langmuir*, 2009, **25**, 8548.
131 W. Wu, S. Ye, G. Yu, Y. Liu, J. Qin and Z. Li, *Macromol. Rapid Commun.*, 2012, **33**, 164.
132 W. Wu, S. Ye, L. Huang, L. Xiao, Y. Fu, Q. Huang, G. Yu, Y. Liu, J. Qin, Q. Li and Z. Li, *J. Mater. Chem.*, 2012, **22**, 6374.

133 F. Qiu, C. Tu, R. Wang, L. Zhu, Y. Chen, G. Tong, B. Zhu, L. He, D. Yan and X. Zhu, *Chem. Commun*., 2011, **47**, 9678.
134 R. Hu, J. W. Y. Lam, Y. Yu, H. H. Y. Sung, I. D. Williams, M. M. F. Yuen and B. Z. Tang, *Polym. Chem.*, 2013, **4**, 95.
135 S. Li and C. Gao, *Polym. Chem*., 2013, **4**, 4450.
136 A. Patra and U. Scherf, *Chemistry*, 2012, **18**, 10074; Y. Xu, S. Jin, H. Xu, A. Nagai and D. Jiang, *Chem. Soc. Rev.*, 2013, **42**, 8012.
137 S. Yuan, B. Dorney, D. White, S. Kirklin, P. Zapol, L. Yu and D. J. Liu, *Chem. Commun*., 2010, **46**, 4547.
138 Y. Xu, L. Chen, Z. Guo, A. Nagai and D. Jiang, *J. Am. Chem. Soc*., 2011, **133**, 17622.
139 Q. Chen, J. X. Wang, F. Yang, D. Zhou, N. Bian, X. J. Zhang, C. G. Yan and B. H. Han, *J. Mater. Chem*., 2011, **21**, 13554.
140 Y. Xu, A. Nagai and D. Jiang, *Chem. Commun*., 2013, **49**, 1591.
141 X. M. Hu, Q. Chen, D. Zhou, J. Cao, Y. J. He and B. H. Han, *Polym. Chem.*, 2011, **2**, 1124.
142 P. P. Kapadia, L. R. Ditzler, J. Baltrusaitis, D. C. Swenson, A. V. Tivanski and F. C. Pigge, *J. Am. Chem. Soc*. 2011, **133**, 8490.
143 P. P. Kapadia, J. C. Widen, M. A. Magnus, D. C. Swenson and F. C. Pigge, *Tetrahedron Letters*, 2011, **52**, 2519.
144 P. P. Kapadia, M. A. Magnus, D. C. Swenson and F. C. Pigge, *J. Mol. Struct.*, 2011, **1003**, 82.
145 P. P. Kapadia, D. C. Swenson and F. C. Pigge, *Cryst. Growth Des.*, 2012, **12**, 698.
146 N. B. Shustova, B. D. McCarthy and M. Dincă, *J. Am. Chem. Soc.*, 2011, **133**, 20126.
147 H. L. Sun, R. Jiang, Z. Li, Y. Q. Dong and M. Du, *CrystEngComm*, 2013, **15**, 1669.
148 N. B. Shustova, A. F. Cozzolino and M. Dincă, *J. Am. Chem. Soc.*, 2012, **134**, 19596.
149 M. Wang, Y. R. Zheng, K. Ghosh and P. J. Stang, *J. Am. Chem. Soc*., 2010, **132**, 6282.
150 W. I. Lee, Y. Bae and A. J. Bard, *J. Am. Chem. Soc.*, 2004, **126**, 8358; D. Wang and T. Imae, *J. Am. Chem. Soc.*, 2004, **126**, 13204; C. C. Chu and T. Imae, *Macromol. Rapid Commun.*, 2009, **30**, 89; L. Pastor-Pérez, Y. Chen, Z. Shen, A. Lahoz and S.-E. Stiriba, *Macromol. Rapid Commun*., 2007, **28**, 1404; W. Yang, C.-Y. Pan, M.-D. Luo and H.-B. Zhang, *Biomacromolecules*, 2010, **11**, 1840; Y. Shen, X. Ma, B. Zhang, Z. Zhou, Q. Sun, E. Jin, M. Sui, J. Tang, J. Wang and M. Fan, *Chem. Eur. J*., 2011, **17**, 5319.
151 W. Zhang, L. G. Qiu, Y. P. Yuan, A. J. Xie, Y. H. Shen and J. F. Zhu, *J. Hazard. Mater.*, 2012, **221**, 147.
152 T. Liu, Y. Meng, X. Wang, H. Wang and X. Li, *RSC Advances*, 2013, **3**, 8269.
153 Y. Ruff, E. Buhler, S. J. Candau, E. Kesselman, Y. Talmon and J. M. Lehn, *J. Am. Chem. Soc*., 2010, **132**, 2573; Y. Ruff and J. M. Lehn, *Angew. Chem. Int. Ed*, 2008, **47**, 3556.
154 Y. Gong, Y. Tan, J. Mei, Y. Zhang, W. Yuan, Y. Zhang, J. Sun and B. Z. Tang, *Sci. China Chem.*, 2013, **56**, 1178.
155 C. M. Xing and W. T. Yang, *Macromol. Rapid. Commun.*, 2004, **25**, 1568.
156 C. M. Xing, J. W. Y. Lam, A. Qin, Y. Dong, M. Häuβler, W. T. Yang and B. Z. Tang, *Polym. Mater. Sci. Eng.*, 2007, **96**, 418.
157 A. Pucci, R. Rausa and F. Ciardelli, *Macromol. Chem. Phys.*, 2008, **209**, 900.
158 G. Xu, Q. Xu, A. Qin, J. Cheng, N. Wang, J. Wei, C. Zhang, Z. Yang and B. Z. Tang, *J. Mater. Chem. C*, 2013, **1**, 1717.
159 N. B. Shustova, A. F. Cozzolino, S. Reineke, M. Baldo and M. Dincă, *J. Am. Chem. Soc.*, 2013, **135**, 13326.
160 R. Dong, B. Zhu, Y. Zhou, D. Yan and X. Zhu, *Polym. Chem.*, 2013, **4**, 912.
161 K. Kokado, A. Nagai and Y. Chujo, *Macromolecules*, 2010, **43**, 6463.
162 S. Li, S. M. Langenegger and R. Haner, *Chem. Commun.*, 2013, **49**, 5835.
163 D. Ding, K. Li, B. Liu and B. Z. Tang, *Acc. Chem. Res*., 2013, **46**, 2441.
164 Z. Wang, S. Chen, J. W. Y. Lam, W. Qin, R. T. Kwok, N. Xie, Q. Hu and B. Z. Tang, *J. Am. Chem. Soc.*, 2013, **135**, 8238.
165 M. Li, Y. Hong, Z. Wang, S. Chen, M. Gao, R. T. Kwok, W. Qin, J. W. Y. Lam, Q. Zheng and B. Z. Tang, *Macromol. Rapid. Commun.*, 2013, **34**, 767.
166 H. Murata, G. G. Malliaras, M. Uchida, Y. Shen and Z. H. Kafafi, *Chem. Phys. Lett.* 2001, **339**, 161; H. Murata, Z. H. Kafafi and M. Uchida, *Appl. Phys. Lett.* 2002, **80**, 189.
167 H. B. Wu, F. Huang, J. B. Peng, Y. Cao. *Org Electron*, 2005, **6**, 118.
168 G. S. He, T. S. Tan, Q. D. Zheng and P. N. Prasad, *Chem. Rev*., 2008, **108**, 1245; S. Kawata and Y. Kawata, *Chem. Rev*., 2000, **100**, 1777; A. S. Dvornikov, E. P. Walker and P. M. Rentzepis, *J. Phys. Chem. A*, 2009, **113**, 13633.
169 P.-A. Bouit, G. Wetzel, G. Berginc, B. Loiseaux, L. Toupet, P. Feneyrou, Y. Bretonnière, K. Kamada, O. Maury and C. Andraud, *Chem. Mater*., 2007, **19**, 5325; N. Venkatram, D. N. Rao and M. A. Akundi, *Opt. Express*, 2005, **13**, 867.
170 W. Denk, J. H. Strickler and W. W. Webb, *Science*, 1990, **248**, 73; D. R. Larson, W. R. Zipfel, R. M. Williams, S. W. Clark, M. P. Bruchez, F. W. Wise and W. W. Webb, *Science*, 2003, **300**, 1434; D. J. Bharali, D. W. Lucey, H. Jayakumar, H. E. Pudavar and P. N. Prasad, *J. Am. Chem. Soc*., 2005, **127**, 11364.
171 J. P. Celli, B. Q. Spring, I. Rizvi, C. L. Evans, K. S. Samkoe, S. Verma, B. W. Pogue and T. Hasan, *Chem. Rev*., 2010, **110**, 2795; H. Stiel, K. Teuchner, A. Paul, W. Freyer and D. Leupold, *J. Photochem. Photobiol., A*, 1994, **80**, 289.
172 A. Mukherjee, *Appl. Phys. Lett*., 1993, **62**, 3423.
173 M. Drobizhev, A. Karotki, Y. Dzenis, A. Rebane, Z. Suo and C. W. Spangler, *J. Phys. Chem. B*, 2003, **107**, 7540.
174 F. S. Richardson and J. P. Riehl, *Chem. Rev*., 1977, **77**, 773; J. P. Riehl and F. S. Richardson, *Chem. Rev*., 1986, **86**, 1.
175 A. Moussa, C. Pham, S. Bommireddy and G. Muller, *Chirality*, 2009, **21**, 497; M. Iwamura, Y. Kimura, R. Miyamoto and K. Nozaki, *Inorg. Chem*., 2012, **51**, 4094; J. L. Lunkley, D. Shirotani, K. Yamanari, S. Kaizaki and G. Muller, *J. Am. Chem. Soc*., 2008, **130**, 13814.
176 E. Peeters, M. P. T. Christiaans, R. A. J. Janssen, H. F. M. Schoo, H. P. J. M. Dekkers and E. W. Meijer, *J. Am. Chem. Soc*., 1997, **119**, 9909; M. Grell and D. D. C. Bradley, *Adv. Mater*., 1999, **11**, 895; J. Liu, H. Su, L. Meng, Y. Zhao, C. Deng, J. C. Y. Ng, P. Lu, M. Faisal, J. W. Y. Lam, X. H. Huang, H. K. Wu, K. S. Wong and B. Z. Tang, *Chem. Sci*., 2012, **3**, 2737.
177 X. Liu, J. Jiao, X. Jiang, J. Li, Y. Cheng and C. Zhu, *J. Mater. Chem. C*, 2013, **1**, 4713.
178 R. Carr, N. H. Evans and D. Parker, *Chem. Soc. Rev*., 2012, **41**, 7673.
179 L. Campbell, D. N. Sharp, M. T. Harrison, R. G. Denning and A. J. Turberfield, *Nature* 2000, **404**, 53; J. M. Kim, *Macromol. Rapid Commun*. 2007, **28**, 1191.
180 R. Okutsu, Y. Suzuki, S. Ando and M. Ueda, *Macromolecules* 2008, **41**, 6165.
181 N. J. Mills, *Concise Encyclopedia of Polymer Science & Engineering*, J. I. Kroschwitz, Ed. Wiley: New York, 1990.
182 J. Liu and M. Ueda, *J. Mater. Chem*. 2009, **19**, 8907.
183 C. K. W. Jim, A. Qin, J. W. Y. Lam, M. Häussler, J. Liu, M. M. F. Yuen, J. K. Kim, K. M. Ng and B. Z. Tang, *Macromolecules* 2009, **42**, 4099; M. Häußler, J. W. Y. Lam, A. Qin, K. K. C. Tse, M. K. S. Li, J. Liu, C. K. W. Jim, P. Gao and B. Z. Tang, *Chem. Commun*. 2007, 2584.
184 R. K. Vijayaraghavan, S. Abraham, H. Akiyama, S. Furumi, N. Tamaoki and S. Das, *Adv. Funct. Mater*. 2008, **18**, 2510; J. Seo, S. Kim, S. H. Gihm, C. R. Park and S. Y. Park, *J. Mater. Chem*. 2007, **17**, 5052.
185 H. Hayasaka, T. Miyashita, K. Tamura and K. Akagi, *Adv. Func. Mater*. 2010, **20**, 1243; Y. S. Jeong and K. Akagi, *J. Mater. Chem*. 2011, **21**, 10472; B. A. San Jose, S. Matsushita, Y. Moroishi and K. Akagi, *Macromolecules* 2011, **44**, 6288.
186 C. H. Ting, J. T. Chen, C. S. Hsu, *Macromolecules* 2002, **35**, 1180; S. A. Jenekhe, J. A. Osaheni, *Science* 1994, **265**, 765.
187 W. Z. Yuan, Z. Q. Yu, Y. Tang, J. W. Y. Lam, N. Xie, P. Lu, E.-Q. Chen and B. Z. Tang, *Macromolecules*, 2011, **44**, 9618.
188 C. J. Doonan, D. J. Tranchemontagne, T. G. Glover, J. R. Hunt and O. M. Yaghi, *Nat. Chem*., 2010, **2**, 235; J. H. Choi, K. M. Choi, H. J. Jeon, Y. J. Choi, Y. Lee and J. K. Kang, *Macromolecules*, 2010, **43**, 5508.
189 A. Li, H. X. Sun, D. Z. Tan, W. J. Fan, S. H. Wen, X. J. Qing, G. X. Li, S. Y. Li and W. Q. Deng, *Energy Environ. Sci*., 2011, **4**, 2062.
190 L. Chen, Y. Yang and D. Jiang, *J. Am. Chem. Soc*., 2010, **132**, 9138; X. Du, Y. Sun, B. Tan, Q. Teng, X. Yao, C. Su and W. Wang, *Chem. Commun*., 2010, **46**, 970.

AIE Macromolecules: Syntheses, Structures and Functionalities

Rongrong Hu, Nelson L. C. Leung and Ben Zhong Tang*

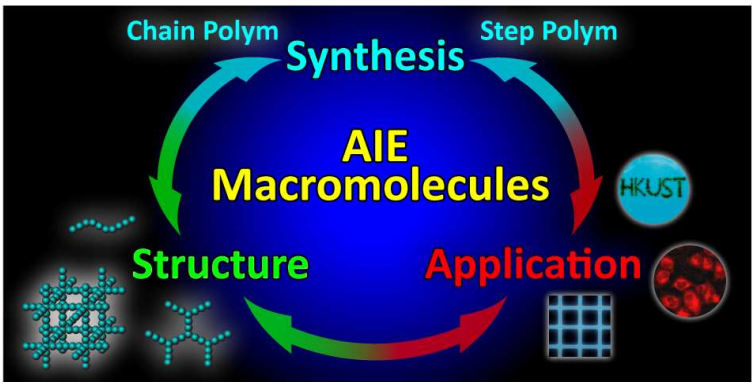

A comprehensive review of macromolecules with aggregation-induced emission attributes is presented, covering the frontiers of syntheses, structures, functionalities and applications.

Rongrong Hu received her B.S. degree from Peking University in 2007 and Ph.D. degree from HKUST in 2011 under the supervision of Prof. Tang. She is now conducting her postdoctoral work on the development of functional luminescent materials and acetylenic polymers in Tang's group.

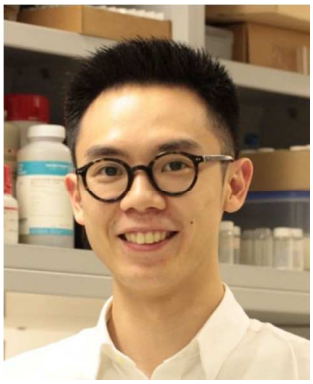

Nelson L. C. Leung received his B.S. degree from HKUST in 2013 and is currently a Ph.D. candidate under the supervision of Prof. Tang. He is currently conducting research on luminescent materials with aggregation-induced emission characteristics.

Ben Zhong Tang received his Ph.D. degree from Kyoto University and conducted his postdoctoral work at University of Toronto. He is Chair Professor in the Department of

Chemistry and Division of Biomedical Engineering, Stephen K. C. Cheong Professor of Science at HKUST, and also honorary professor at SCUT. He was elected to the Chinese Academy of Sciences in 2009. His research interest lies in the creation of new molecules with novel structures and unique properties with implications for high-tech applications. He is currently Associate Editor of *Polymer Chemistry* and sits in the editorial boards of a dozen journals.